DISSERTATION

Dye sensitization of low-index atomically flat TiO_2 surfaces

Submitted By

Yunfeng Lu

Department of Chemistry

In Partial fulfillment of the requirements

for the Degree of Doctor of Philosophy

Colorado State University

Fort Collins, Colorado

Spring 2007

COLORADO STATE UNIVERSITY

January 08, 2007

WE HEREBY RECOMMEND THAT THE DISSERTATION PREPARED UNDER OUR SUPERVISION BY **YUNFENG LU** ENTITLED "*DYE SENSITIZATION OF LOW-INDEX ATOMICALLY FLAT TIO_2 SURFACES*" BE ACCEPTED AS FULLFILING IN PART REQUIREMENTS FOR THE DEGREE OF DOCTOR OF PHILOSOPHY.

Committee on Graduate Work

Peter Dorhout

Gary Maciel

Simon Tavener

Charles Henry

Adviser – Bruce Parkinson

Department Head

ABSTRACT OF DISSERTATION

DYE SENSITIZATION OF LOW-INDEX ATOMICALLY FLAT TIO_2 SURFACES

Dye-sensitization of large band-gap semiconductors has been known for over a century since this is the process used in silver halide photography. There has been a renewed interest in this topic following Grätzel's invention of an efficient dye sensitized solar cell. A solar-to-electric energy conversion efficiency of over 10% has been obtained for this system. However, due to the large surface area and irregular structure of the nanocrystalline titanium dioxide (TiO_2), there is still little fundamental information about the interface between the semiconductor and the adsorbed dye layer. We use atomically flat single crystal surfaces to help understand the binding of dye molecules to various TiO_2 surfaces.

Atomically flat surfaces of anatase (101), (001) and rutile (100), (001) single crystals were successfully prepared and their surface flatness verified with atomic force microscopy (AFM).

Dye sensitization with the ruthenium complex dye N3 (cis-di(thiocyanato)-bis(2,2'-bipyridyl -4,4'- dicarboxylate) ruthenium(II)) was studied on these surfaces. The adsorption isotherms were measured on all four surfaces. Rutile (100) and anatase (101) gave higher incident photon to current conversion efficiency (IPCE) values than the other two surfaces. Study of adsorption kinetics revealed a two-step adsorption process and the slow adsorption step was fit with a Langmuir kinetic model. The adsorption and desorption rate constants for each surface were derived by fitting the adsorption data. Differences in IPCE were explained based on the structure of N3 and the geometry and reactivity of the binding sites on the four surfaces.

A structurally similar series of carboxylated thiacyanine dyes were also employed in exploring the fundamentals of dye sensitized solar cells as an attempt to understand the interaction of organic dye molecules and TiO_2 surfaces. A simple method for measuring the surface coverage of these adsorbed dyes onto TiO_2 surfaces was developed. Quantum yields for sensitized photocurrent generation were studied and dimer and extended H-aggregates formation of some dye molecules were resolved. We attempt to understand these experimental results with structural models of the TiO_2 surfaces.

Yunfeng Lu
Department of Chemistry
Colorado State University
Fort Collins, CO 80523
Spring 2007

Acknowledgements

My way toward obtaining a Ph. D would be a lot more difficult without the help I have constantly received from others. My adviser, Bruce A Parkinson, is the first one I need to thank. His knowledgeable guidance is always my lighthouse during my study, without which a lot more efforts would be required to get today. Dr. Mark T Spitler is thanked for offering us the dye molecules for my research project, training me on the dye synthesis and lots of valuable discussions. I want to thank Anna Chick for her warmth and willingness to help all the time. Bengt Jaeckel, our postdoc from Germany, is thanked for his help on LEED measurements and a lot other inputs. I need to thank Dae-jin Choi for collecting with me some of the data presented here. The rest of the Parkinson group is acknowledged for their endless help during everyday of my graduate study at Colorado State University.

My wife, Ming Yu, who is also a graduate student here at Colorado State University, accompanied me to pursue my Ph. D in the US. She has always been my support whenever I am happy or not. Without her support and encourage, I would not succeed in continuing my education.

I would like to thank my parents for their emotional support and understanding of my continuous education abroad.

Table of Contents

Index of Figures

Index of Tables

Preface

Development of the modern world relies on energy. Between 1850 and 1970, the population on Earth more than tripled—yet the energy consumed was 12 times higher. By 2002, human numbers had grown another 68 percent and fossil fuel consumption, which accounts for 85% of the total energy use today, was up another 73 percent. We humans today collectively consume an average of 13 terawatts (TW) of power. Thanks to global population growth and economic development and the tendency of energy consumption to grow with development, most energy experts predict by year 2050 we will need about an additional 30 TW of power. Unfortunately, oil production, a major component of fossil fuel, has almost peaked and the world will begin to run out of fossil fuels within 50 years. [1]

To meet the need of energy consumption and reduce the greenhouse effect, we have to turn to other energy alternatives, especially renewable energy. Energy can be produced from nuclear power plants, wind, biomass, geothermal and ocean waves. These energy alternatives have both potential and drawbacks. Even if we could build enough nuclear plants to meet the rising need, there are concerns of waste disposal, safety, nuclear proliferation, and terrorism. Wind energy has already demonstrated cost-effectness but it is predicted that the maximum power we can produce from wind is only 2 to 6 TW. Biomass's potential is limited by the need to use arable land to grow food; geothermal energy's potential is limited by high drilling costs and limited geographic availability; and ocean power has been stalled in part by high construction costs and again limited availability.

Solar energy is the only large scale alternative. Every moment there is 170,000 TW of solar energy striking Earth, a number well beyond the projected human need. Solar cells have been designed to convert solar energy into electricity. Solid state semiconductor junction cells were first developed in 1950s and they are widely used to power satellites, spacecraft, and villages in third-world countries to produce power for buildings. These photovoltaic solar cells are still costly compared to traditional sources of electricity.

One interesting new method of converting solar energy is the dye-sensitized solar cell, where a dye is used to sensitize a large band-gap semiconductor. The advantage of this type solar cell, over traditional junction solar cells, is the separation of the light absorption and charge collection events. However, only a very small portion of the visible light can be absorbed due to the small number of adsorbed molecules and therefore the total energy conversion efficiency is very low.

The breakthrough for dye-sensitized solar cells came in 1991 when a nanocrystalline thin film of TiO_2 on a conductive glass as the supporting substrate was used for the adsorption of the dye sensitizers. [2] The 1000-fold enhanced surface area greatly improved the cell efficiency. The use of inexpensive, low-purity material reduces the manufacturing costs when compared to other solar cells. Together with the long term stability of TiO_2, this type of dye-sensitized solar cell has become a promising candidate for future solar cells. An energy conversion efficiency of over 10% has already been achieved on laboratory scale cells and further efficiency increases are possible by improvements in sensitizing dyes, regenerating agents, electrolytes and cell morphologies.[3]

Despite the development of dye-sensitized solar cells in both their energy conversion efficiency and stability, many aspects of the metal oxide/dye interfaces are largely unknown because the large surface area and defect structure of nanocrystalline TiO_2 thin film make the interface difficult to study. In this thesis, I use atomically flat surfaces of various polymorphs of single crystal TiO_2 to understand the adsorption, desorption and sensitization behavior of the widely studied N3 dye and a variety of other organic dye molecules. We are hoping that this study will elucidate the interfacial structure of the dye-sensitized solar cell and provide some guidance on building more efficient solar cells in the future.

References:

1. Service, R.F., *SOLAR ENERGY: Is It Time to Shoot for the Sun? 10.1126/science.309.5734.548.* Science, 2005. **309**(5734): p. 548-551.

2. Oregan, B. and Gratzel, M., *A Low-Cost, High-Efficiency Solar-Cell Based on Dye-Sensitized Colloidal TiO_2 Films.* Nature, 1991. **353**(6346): p. 737-740.

3. Nazeeruddin, M.K., Kay, A., Rodicio, I., Humphrybaker, R., Muller, E., Liska, P., Vlachopoulos, N., and Gratzel, M., *Conversion of Light to Electricity by Cis-X2bis(2,2'-Bipyridyl-4,4'-Dicarboxylate)Ruthenium(Ii) Charge-Transfer Sensitizers (X = Cl-, Br-, I-, Cn-, and Scn-) on Nanocrystalline TiO_2 Electrodes.* Journal of the American Chemical Society, 1993. **115**(14): p. 6382-6390.

Chapter 1:

Background and Development of Dye-Sensitized Solar Cells

1.1 Photovoltaic Effects

The photovoltaic effect was first discovered in 1839 by a French scientist Edmond Becquerel when he observed a current and voltage while illuminating a silver electrode immersed in a chloride electrolyte.[1] Thirty-four years after the discovery of the photovoltaic effect, Willoughby Smith reported the photoconductivity of selenium and this inspired W. G. Adams and R. E. Day to make the first selenium cell in 1877.[1] Subsequent work on selenium and copper oxide led to the development of the selenium solar cell and its wide use in photographic exposure meters. Modern solar cells were first developed in 1954 at Bell Labs by D. M. Chapman and C. S. Fuller using a solid-state semiconductor junction. These early silicon cells were similar to those of today in the working mechanism but the efficiency was much less. Today's PV solar cells are widely

used to power satellites, spacecraft and in remote villages in the third-world countries and hold the promise of carbon-free power for future energy demands.[2]

1.2 Silicon Solar Cells

At the present time, photovoltaic technology is based on the elemental semiconductor silicon, either single crystalline or multicrystalline. There is an abundance of silicon in the Earth's crust, therefore the silicon supply is practically endless. Both the energy input (about 50 kWh/kg) and cost (about $2/kg) are relatively low for the production of low purity silicon (98-99%), but the purification process is much more costly to produce solar-grade feedstock. When used for solar cells, silicon is able to absorb photons with a wavelength smaller than 1128 nm, which corresponds to about 75% of solar spectrum while the other 25% of long wavelength photons are unused. However, many of the high-energy photons are absorbed near the crystal surface and there is a high percentage lost by recombination of photogenerated charge carriers in the surface region. This electron-hole pair recombination brings the efficiency down by about another 40%. There is also 10-20% reflection of the incident light at the surface even with an antireflection coating. Together with the limitations of the photovoltaic action itself, an upper limit of about 24-26% can be obtained at room temperature when a single crystal of Si is used for a photovoltaic solar cell. Commercial modules usually produce an efficiency in the range of 10-15%.

Figure 1.1 shows the solar spectrum, indicating that most of solar energy is located in the visible range. Therefore an efficient solar cell should be able to absorb visible light and convert it into electricity. Crystalline silicon has a band-gap energy of

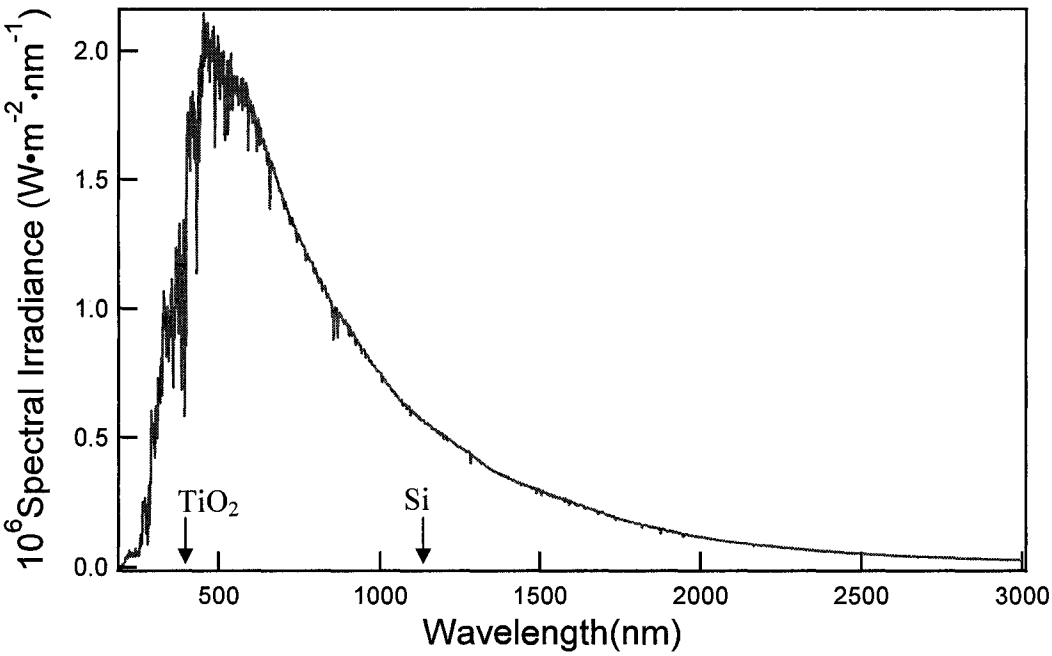

Figure 1.1 Solar spectrum. The arrows indicate wavelengths corresponding to the band-gap energy of TiO_2 and Si, repectively.

1.1 eV and is able to absorb photons with a wavelength of smaller than 1128 nm. Although Si's band-gap meets the criteria for an efficient solar cell, there are other drawbacks. The semiconductor performs two processes simultaneously: absorption of light and the separation of the charges. To avoid the premature recombination of electrons and holes, the semiconductors employed must be highly pure and defect-free.

1.3 Dye-Sensitization of Large Band-Gap Semiconductors

Solid-state junction devices have been dominating the commercial production of photovoltaic devices. Recently, however, they have been challenged by a new generation of photovoltaic devices including dye sensitized solar cells, which may someday overtake Si in both production cost and efficiency.

Fujishima and Honda reported in 1972 the photoelectrolysis of water at a titanium dioxide (TiO_2) electrode surface[3] and the photocurrent generation with TiO_2 encouraged people to explore its use in solar cell devices. However, due to its large band-gap of 3.2 eV, only a small portion of light can be absorbed and converted into electricity and therefore the total energy conversion efficiency is very low.

In the late 19^{th} century certain organic dyes were found to be able to extend the response of silver-halide-based photographic film to visible wavelengths.[2] This is caused by electron transfer from the organic dye molecules to the semiconducting silver-halide grain. This sensitization effect is the basis of film photography. In a similar mechanism, sensitizing dyes have been attached to wide band-gap metal oxides such as TiO_2, SnO_2 ,ZnO and $SrTiO_3$.[4-9] Upon irradiation, photocurrent can be produced through electron transfer from the excited dye into the conduction band of the

semiconductor and subsequent reduction of the photooxidized dye by a redox couple present in the solution. At the surface of a counter electrode, the oxidized regenerator is reduced, resulting in no net change in the electrolyte. In this way, light absorption leads to a photovoltage and the absorption edge can be adjusted by choosing different dyes. These are the prototype of dye-sensitized solar cells. Figure 1.2 shows operating principles and energy levels of the dye-sensitized solar cell.

1.4 Dye-Sensitized nanocrystalline TiO_2 solar cell

Despite the efforts to develop a dye-sensitized solar cell, the efficiency of the original prototypes was very low. The biggest problem was poor light harvesting efficiency. On a smooth surface, less than 1% of the incident light can be absorbed by a monolayer of dye sensitizer. Attempts to put multilayers of dye molecules on a semiconductor surface were unsuccessful due to recombination within the thick dye layers where carrier (exciton) mobilities are low.[10] A major breakthrough came in 1991 when O'Regan and Grätzel reported that a thin layer of nanocrystalline TiO_2 particles sensitized by cis-di(thiocyanato)- bis(2,2'-bipyridyl -4,4'- dicarboxylate) ruthenium(II) (referred to as N3) could achieve respectable power conversion efficiencies.[11]

The main reason for success of the new architecture was the 2000-fold increase in the surface area of the nanocrystalline thin film which resulted in a greatly improved amount of adsorbed dye. With this configuration, 46% of the solar energy flux was harvested and an overall light to electric conversion efficiency of 7.1-7.9% was obtained in simulated solar light and 12% was obtained in diffuse light. The cost of electricity

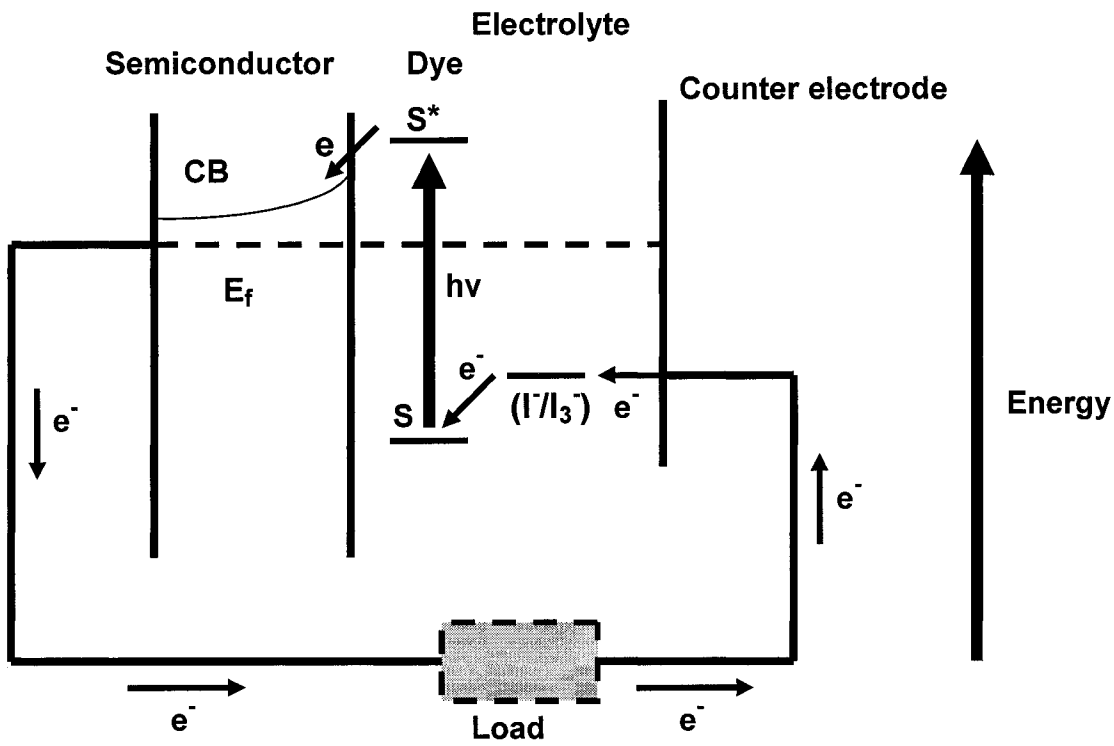

Figure 1.2 Operating principles and energy level diagram of dye-sensitized solar cell. A photon is absorbed by a dye molecule which excites the dye from its ground state into the excited state, followed by electron injection into the conduction band of the semiconductor. On the surface of a counter electrode, a redox couple is reduced, which in turn reduces the oxidized dye molecule, resulting in no net change in the electrolyte.

generation could be greatly reduced since low-to-medium purity materials were used to produce TiO_2 nanoparticles and the cell displayed excellent long-term stability operating for five million turnovers of the dye without decomposition. The exciting potential for low cost and high efficiency solar energy conversion sparked a renewed interest to electrochemists for many researchers who now study dye-sensitized solar cells.

1.5 Efficient Sensitizer

The original sensitizing dye used in the Grätzel cell was the ruthenium complex called N3, named by the synthetic chemist M. K. Nazeeruddin. N3 has four carboxylate groups that can bind to the TiO_2 surface. The absorption coefficients of the absorption maxima for a N3/ethanol solution are reported to be 1.42×10^4 M^{-1} cm^{-1} at 534 nm, 1.40×10^4 M^{-1} cm^{-1} at 396 nm, and 3.12×10^4 M^{-1} cm^{-1} at 313 nm.[12] The molecular structure of N3 is shown in Figure 1.3.

N3 dye binds to a flat surface with one or two of its carboxylate groups.[13,14] There are three ways a carboxylate group can coordinate to the TiO_2 surface: as a unidentate mode, as a chelating mode, and as a bridging bidentate mode (Figure 1.4). Adsorption of N3 dye on a flat anatase (101) surface was systematically studied by Fillinger et al.[15] ATR-FTIR spectroscopy was also applied to study the interaction of the sensitizers with nanocrystalline TiO_2 film and data show that the complexes are anchored onto the TiO_2 surface in bridging coordination mode using two out of their four carboxylic acid groups.[13] Density functional theory (DFT) has been applied to investigate the interfactial structure and significant structural adjustments of both the dye and the nanocrystal are predicted to be induced by the strain imposed by the simultaneous

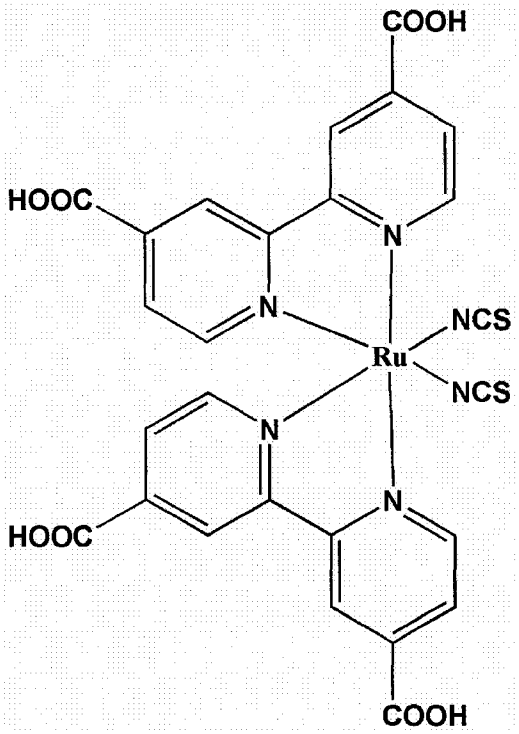

Figure 1.3 Molecular structure of the N3 dye.

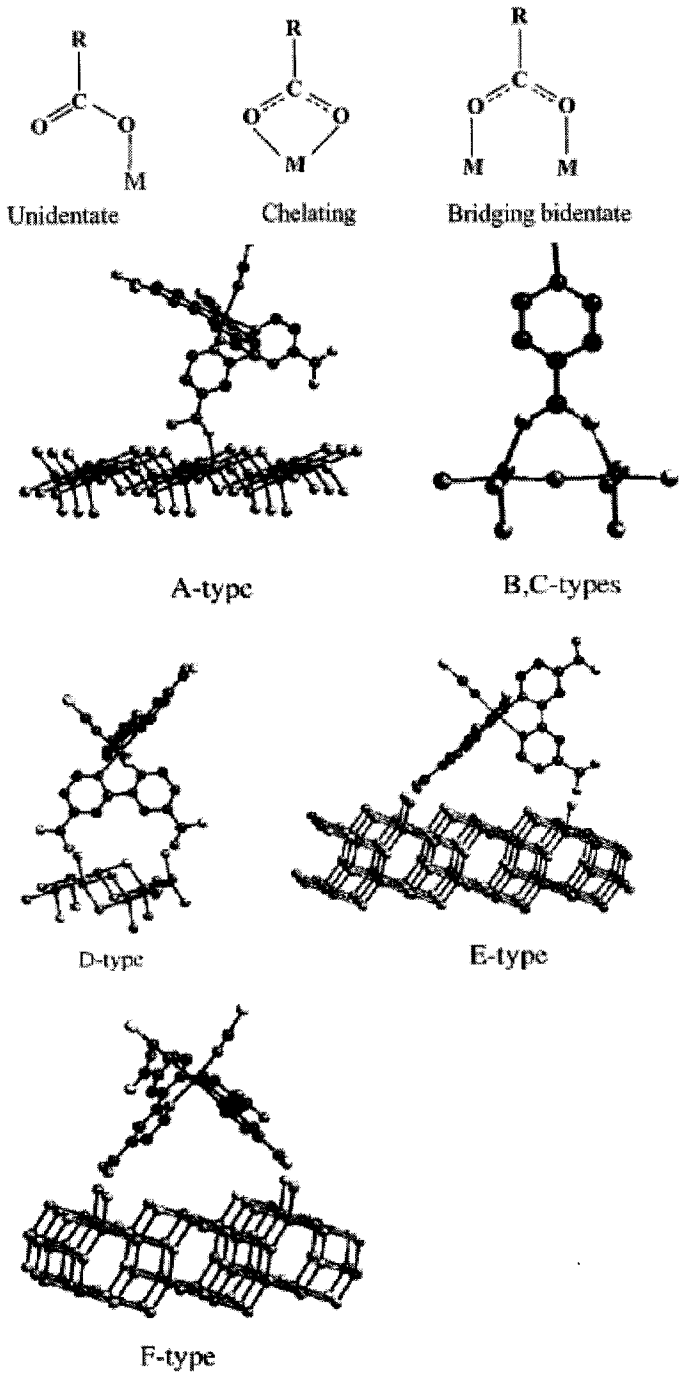

Figure 1.4 Possible anchoring modes for N3 sensitizer using carboxylic acid functional groups.[13]

formation of multiple dye-surface bonds.[16] Experimental details of the dye structure on the TiO_2 surfaces are lacking and one goal of this thesis research is an understanding of this dye semiconductor interface.

1.6 Semiconductor/Electrolyte Interface

One significant difference of bulk single crystals from nanocrystalline films is the existence of a space charge layer. Nanocrystalline thin films are made up of particles that are too small to support a depletion layer. Therefore the Grätzel cell operates under different principles than convertional solar cells or when sensitizating a single crystal.

When a semiconductor is placed in contact with an electrolyte, electric current initially flows across the junction until electronic equilibrium is reached, where the Fermi energy of the electrons in the solid (E_f) equilibrates to the redox potential of the electrolyte (E_{redox}). The transfer of electric charge produces a region on each side of the junction where the charge distribution differs from the bulk material, and this is known as the space-charge layer. On the electrolyte side, this corresponds to the familiar electrolytic double layer, that is, the compact (Helmholtz) layer followed by the diffuse (Gouy–Chapman) layer. On the semiconductor side of the junction the nature of the band bending depends on the position of the Fermi level in the solid. If the Fermi level of the electrode is equal to the flat band potential, there is no excess charge on either side of the junction and the bands are flat. If electrons accumulate at the semiconductor side one obtains an accumulation layer. If, however, they move from the solid into the solution, a depletion layer is formed, leaving behind a positive excess charge formed by immobile

ionized donor states when an n-type semiconductor is used. An energy level diagram is shown in Figure 1.5.

The flat band potential is a very useful quantity in photoelectrochemistry as it reveals the location of the energetic position of the valence and conduction band edge of a given semiconductor material relative to the redox levels in solution. It is obtained by measuring the capacity of the semiconductor–electrolyte junction. The semiconductor is subjected to reverse bias — that is, a voltage is applied to increase the potential drop across the junction — and the differential capacity is determined as a function of the applied potential, V. The space charge capacity of the semiconductor (C_{sc}) is in series with that of the Helmholtz layer (C_H) present at the electrolyte side of the interface. In the depletion regime the condition $C_H > C_{sc}$ applies, so the measured capacity is that of the space-charge layer.[17] This depends on the applied bias voltage according to the Mott–Schottky equation:

$$\frac{1}{C^2_{sc}} = \frac{2}{\varepsilon_s \varepsilon_0 e N_0}\left(V - V_{fb} - \frac{kT}{e}\right)$$

where C_{sc} is the space charge capacitance, ε_s is the dielectric constant of the semiconductor, ε_0 is permittivity of vacuum, N_0 is the dopant concentration, k is the Boltzmann constant and T is temperature in Kelvin. From the Mott-Schottky plots, the flat band potential and doping density of the semiconductor can be derived. These are important parameters in dye sensitization since it allows the calculation of the electric field gradient at the surface and predicts what dyes can inject electrons into the conduction band from their excited states.

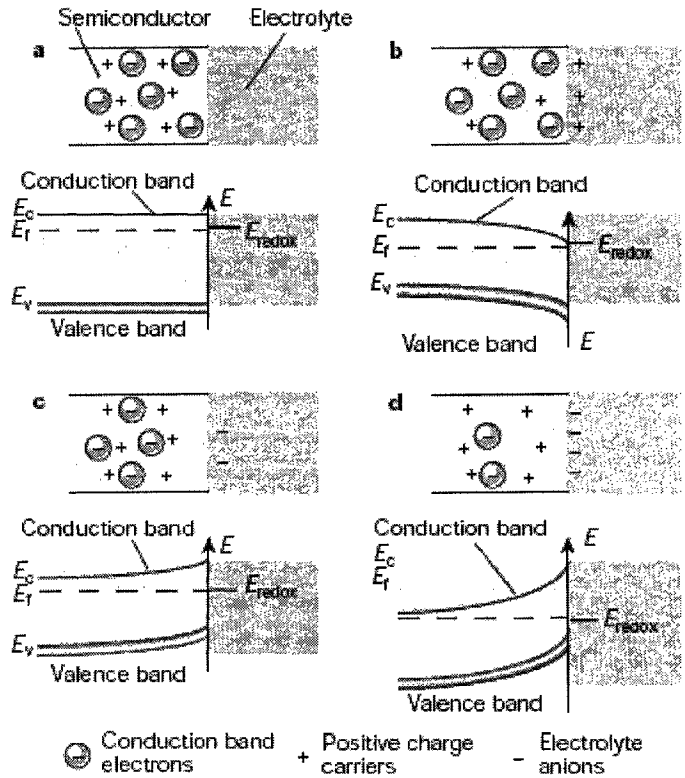

Figure 1.5 Schematic showing the electronic energy levels at the interface between an n-type semiconductor and an electrolyte containing a redox couple. The four cases indicated are: **a**, flat band potential, where no space-charge layer exists in the semiconductor; **b**, accumulation layer, where excess electrons have been injected into the solid producing a downward bending of the conduction and valence band towards the interface; **c**, depletion layer, where electrons have moved from the semiconductor to the electrolyte, producing an upward bending of the bands; and **d**, inversion layer where the electrons have been depleted below their intrinsic level, enhancing the upward band bending and rendering the semiconductor p-type at the surface.[17]

1.7 Electron Injection and Charge Transport

The electron transfer mechanism and rates for photoinjection into the conduction band of TiO_2 by photoexcited N3 is of interest since N3 is one of the most promising sensitizers for dye-sensitized solar cells. The electron transfer from the excited-state of N3 dye adsorbed onto a TiO_2 nanoparticle to the conduction band of TiO_2 is one of the fastest process in chemistry.[20, 21] The measurement of charge carrier dynamics in photoelectrochemical cells has been improved over the years to measure rise times in the picosecond time domain[22] down to femtoseconds[23-24]. The carboxylated complexes exhibit two $\pi \rightarrow \pi^*$ intraligand transitions in the UV and two $t_2 \rightarrow \pi^*$ MLCT bands in the visible and near UV.[12] N3 adsorbed on nanocrystalline TiO_2 exhibits a slightly blue-shifted absorbance maximum and resonance raman spectroscopy indicated that the excited-state dynamics of N3 molecules were independent of the number of N3 molecules adsorbed per TiO_2 nanoparticle.[25] Upon absorbing a photon of proper energy, a metal 3d electron is excited into the ^{1}MLCT and transferred into the ligand π^* state (Figure 1.6), and the excited electron is essentially localized on one of the ligand bipyridine groups. This rate is significantly faster than those of the homogeneous intramolecular electron-transfer rates with comparable donor-acceptor separation distances, indicating that the TiO_2 nanoparticle has a strong effect on the dynamics of electron transfer. Experimental evidence of charge transfer time of less than 3 fs was observed with resonant photoemission spectroscopy.[26] Density functional theory (DFT) calculations predict that injection times are on the order of 10 fs for MLCT excitations to the ligand π^* levels that interact most strongly with the TiO_2 conduction band, and

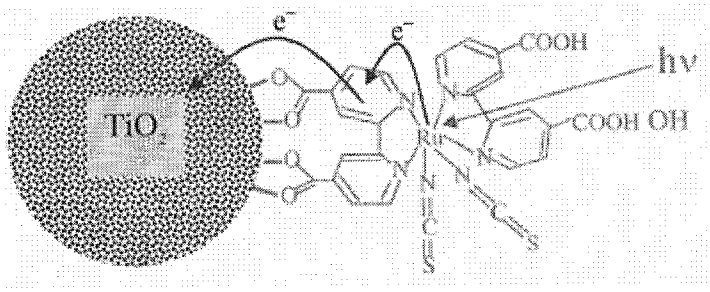

Figure 1.6 N3 dye adsorbed onto a nanocrystalline TiO_2 particle and electron transfer from the dye to TiO_2.

predicts an order of magnitude increase in the injection times for excitations to dye levels with poor spatial or energetic overlaps with the substrate conduction band,[16, 27] which is in agreement with the experimental results. However, Haque et al. concluded that such ultrafast dynamics are not required or desirable for efficient photovoltaic energy conversion; electron injection kinetics with a half time of 150 ps can allow a high injection yield while minimizing interfacial charge recombination losses.[28] Therefore electron transfer dynamics need to be understood and optimized for efficient energy conversion devices.[29]

Different rates of charge injection have been observed for the kinetics of electron transfer from N3 to TiO_2. Benkö et al. reported that the charge injection process took place with a biphasic kinetics.[30] The first ultrafast component was estimated to have a rise time of 28 fs and the second multiexponential part to occur within the 1 – 50 ps time range. This behavior was rationalized in terms of a two–state mechanism, the fast and slow components being attributed to the injection from the singlet and triplet excited states of the ruthenium complex, respectively. However, based on their transient absorbance measurements at 860 nm upon ultrashort laser pulse excitation, Wenger et al. concluded that the slow component of electron injection arises from sensitizer molecules that are loosely attached onto the surface or are present in an aggregated form.[31]

The efficiency of the nanocrystalline device also critically depends on the charge recombination rate, and for the N3/TiO_2 system, this occurs in the microsecond to millisecond time scale.[25] Surface photovoltage transients study indicated that at low temperatures (100 – 250 K), the dynamics are governed exclusively by spatially dependent tunneling recombination. For higher temperatures (250 – 540K), the thickness

dependence of the decays indicates that the dynamics of surface recombination are retarded by the diffusion of electrons toward the interior of the film (see Figure 1.7).[32]

1.8 Efforts on Increasing Cell Efficiency

Over the years since the emergence of the Grätzel cell, there have been constant efforts in trying to optimize its performance and increase the overall efficiency. Many other sensitizing dyes have been synthesized and some of them offer comparable or better yields. The ruthenium complexes $(Bu_4N)_2[Ru(dcbpyH)_2(NCS)_2]$ (N719) and $(Bu_4N)_4[Ru(dcbpy)_2(NCS)_2]$ (N712) are of the same family as N3 with two carboxylic/two carboxylate groups and zero carboxylic/four carboxylate groups, respectively and give a slightly higher efficiency than the N3 dye.[13] Efficient panchromatic sensitizers (black dyes) were reported in 2001 that produced an overall conversion efficiency of 10.4%, which is the best sensitizer so far.[33] A series of zinc metalloporphyrins, which are attractive from the standpoint of cost, were also able to function as sensitizing dyes with an efficiency of 5.6%, making them the most efficient porphyrin-based sensitized solar cells.[34] Although Ru complex sensitizers are efficient for solar energy conversion, there are concerns that the scare metal is expensive and can cause environmental problems. Efforts have been made to synthesize efficient metal-free sensitizing dyes to replace the metal complex. Spitler et al. [35] and Horiuchi et al.[36] reported the synthesis and characterization of organic dyes for use in a dye-sensitized solar cell. After synthesizing and investigating a number of organic dyes, a novel indoline dye exhibiting very good performance was found to give a solar-to-electric conversion efficiency of 6.1%, compared to 6.3% for N3 dye under the same

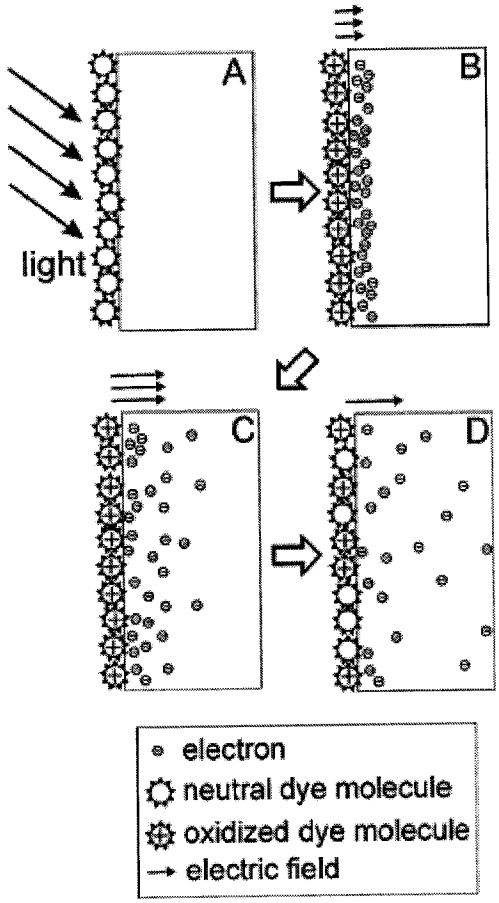

Figure 1.7 Scheme of elementary processes in the investigated model system consisting of a thin TiO_2 layer sensitized with dye molecules at the surface. The photovoltage is given by the amount of separated charge and by the effective charge separation length. (A) Laser excitation. (B) Initial charge separation. (C) Diffusion. (D) Recombination.[32]

experimental conditions. These dyes are easily prepared, exhibit high efficiencies and are relatively cheap due to the simple preparation procedures. Another indoline dye sensitizer was also synthesized with an efficiency as high as 8% in 2004.[37] Two years later, Thomas et al. successfully synthesized organic dyes containing thienylfluorene conjugation for solar cells that gave a 5.5% efficiency.[38] Oligothiophene-containing coumarin dyes were also able to sensitize nanocrystalline TiO_2 yielding a 7.4% efficiency.[39] The molecular structures of the three organic dyes that offer higher energy conversion efficiencies are shown in Figure 1.8. In addition to high efficiencies, these dyes were also found to be highly stable. The appearance of these dyes will make practical application of dye-sensitized solar cells more feasible by further reducing their electricity generation costs.

In addition to synthesis of various sensitizers, many other refinements have been developed, a few of which will be summarized. By illuminating the assembled dye-sensitized solar cell with ultraviolet (UV) light from a xemon arc lamp, photocurrents were dramatically increased, especially for cells with very poor initial quantum yiels.[40] This was explained as to cause a positive shift in the conduction band edge of the nanocrystalline TiO_2. The increase in the overall conversion efficiency of up to 45 times for some dyes was observed. To increase light absorption by the nanocrystalline thin film, additional light scattering layers were introduced in the fabrication of the TiO_2 film.[41] Upon protonation of the TiO_2 films through HCl pretreatment, the efficiency of the black dye-sensitized solar cell was increased.[42] A network structure of single-crystal-like anatase TiO_2 nanowires was developed to be used in dye-sensitized solar cells and high conversion yield of 9.3% was obtained.[43] Likewise, a dye-sensitized solar

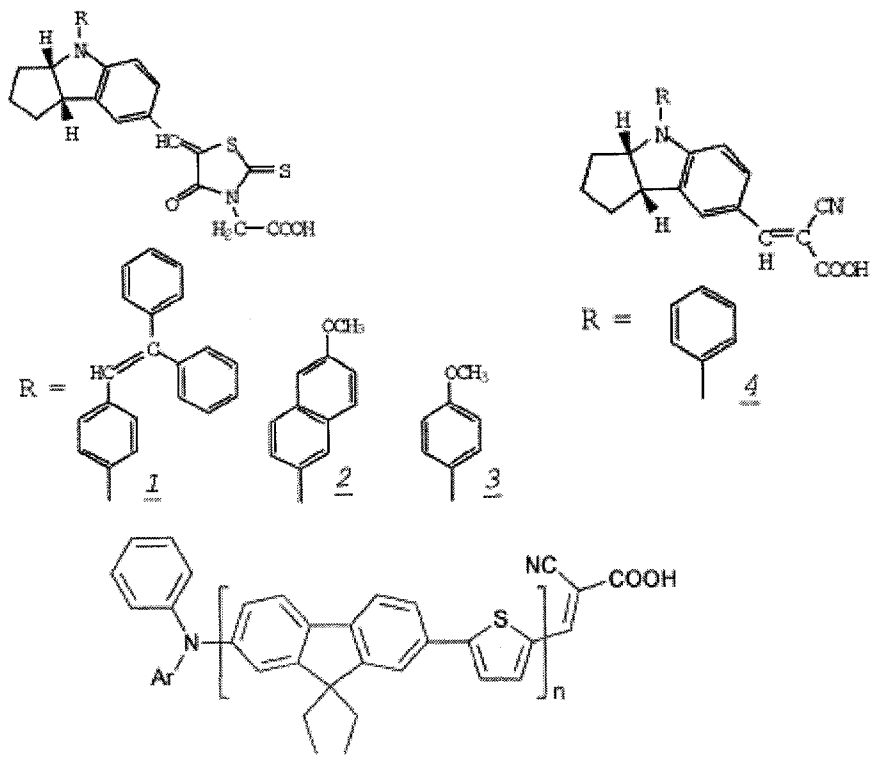

	R_1	R_2	R_3
Indoline Dye **1**	$-CH_2COOH$	$-CH_2CH_3$	$=S$
2	$-CH_2COOH$	$-CH_2COOH$	$=S$
3	$-CH_2CH_2COOH$	$-CH_2CH_3$	$=S$
4	$-CH_2COOH$	$-CH_2CH_3$	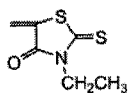

Figure 1.8 Efficient metal-free organic dyes for dye-sensitized solar cells.[36-38]

cell based on single-crystalline TiO_2 nanorods has been successfully fabricated and has achieved a high efficiency of 7.29%.[44]

Coadsorbants have been introduced to dye-sensitized nanocrystalline TiO_2 solar cell in an attempt to increase the conversion efficiency. Zhipan Zhang et al. reported the use of 4-guanidinobutyric acid (GBA) as a coadsorbant together with the K-19 dye resulting in an increase of 50 mV in open circuit voltage without a loss of current.[45] While Neale et al. reported that with the coadsorbant chenodeoxycholate, dye loading was reduced by as much as 60% while having a relatively small effect on the short-circuit photocurrent.[46] This was explained by displacement of the weakly adsorbed dyes by the coadsorbant. A nitrogen-doped nanocrystalline TiO_2 electrode was prepared and higher efficiencies in the range of 380 – 520 nm and 550 – 750 nm were observed.[47] Interestingly, spherical voids of diameter 400 nm can be introduced into the nanocrystalline TiO_2 film and increase the device performance by 25%.[48] The films have further potential of being used in high-viscosity electrolytes, which are interesting from the standpoint of using a nonvolatile electrolyte to reduce leakage from constructed solar cell modules.

1.9 Open Questions for Dye-Sensitized Solar Cells

Dye-sensitized nanocrystalline TiO_2 solar cells have made great progress in both efficiency and stability, but there is still little known about the structure of the organic dye/metal oxide interface due to the large surface area, the heterogeneous surface structure and the nanoporous nature of the nanocrystalline films. The atomic structure of the interface is highly important, since it can directly influence the electron transfer. The

possibly important structural aspects are: (1) ordering if any of the sensitizer molecules on the semiconductor surface, (2) the surface packing density of the sensitizers, and (3) the number of bonds between the sensitizer molecule and semiconductor surface.[14]

By preparing well-terraced, atomically flat single crystal surfaces and dye-sensitizing these surfaces, we can explore the dye/semiconductor interfacial structures and understand the binding of organic dye molecules to these metal oxide surfaces at the molecular level. A complete understanding of the dye/semiconductor interface will guide the construction of more efficient DSSCs with organic dyes since the light absorption and electron injection efficiencies can be optimized.

References:

1. Randall, J.F., *Designing Indoor Solar Products.* 2005.

2. Smestad, G.P., *Optoelectronics of Solar Cells.* 2002.

3. Fujishima, A. and Honda, K., *electrochemical photolysis of water at a semiconductor electrode.* Nature, 1972. **238**: p. 37-38.

4. Moses, P.R. and Murray, R.W., *Chemically Modified Electrodes .3. SnO_2 and TiO_2 Electrodes Bearing an Electroactive Reagent.* Journal of the American Chemical Society, 1976. **98**(23): p. 7435-7436.

5. Fox, M.A., Nobs, F.J., and Voynick, T.A., *Chemically Modified Electrodes in Dye-Sensitized Photogalvanic Cells.* Journal of the American Chemical Society, 1980. **102**(12): p. 4036-4039.

6. Fujihira, M., Ohishi, N., and Osa, T., *Photocell Using Covalently-Bound Dyes on Semiconductor Surfaces.* Nature, 1977. **268**(5617): p. 226-228.

7. Fujihira, M., Kubota, T., and Osa, T., *Organo-Modified Metal-Oxide Electrode .5. Efficiency of Electron Injection into Conduction-Band from Photo-Excited Dye Molecule Covalently Attached to an SnO_2 Surface.* Journal of Electroanalytical Chemistry, 1981. **119**(2): p. 379-387.

8. Spitler, M.T. and Calvin, M., *Electron-Transfer at Sensitized TiO_2 Electrodes.* Journal of Chemical Physics, 1977. **66**(10): p. 4294-4305.

9. Matsumura, M., Matsudaira, S., Tsubomura, H., Takata, M., and Yanagida, H., *Dye Sensitization and Surface-Structures of Semiconductor Electrodes.* Industrial & Engineering Chemistry Product Research and Development, 1980. **19**(3): p. 415-421.

10. Splan, K.E., Massari, A.M., and Hupp, J.T., *A Porous Multilayer Dye-Based Photoelectrochemical Cell That Unexpectedly Runs in Reverse.* The Journal of Physical Chemistry B, 2004. **108**(13): p. 4111-4115.

11. Oregan, B. and Grätzel, M., *A Low-Cost, High-Efficiency Solar-Cell Based on Dye-Sensitized Colloidal TiO_2 Films.* Nature, 1991. **353**(6346): p. 737-740.

12. Nazeeruddin, M.K., Kay, A., Rodicio, I., Humphrybaker, R., Muller, E., Liska, P., Vlachopoulos, N., and Grätzel, M., *Conversion of Light to Electricity by Cis-X2bis(2,2'-Bipyridyl-4,4'-Dicarboxylate)Ruthenium(II) Charge-Transfer Sensitizers (X = Cl^-, Br^-, I^-, CN^-, and SCN^-) on Nanocrystalline TiO_2 Electrodes.* Journal of the American Chemical Society, 1993. **115**(14): p. 6382-6390.

13. Nazeeruddin, M.K., Humphry-Baker, R., Liska, P., and Grätzel, M., *Investigation of Sensitizer Adsorption and the Influence of Protons on Current and Voltage of a Dye-Sensitized Nanocrystalline TiO_2 Solar Cell.* The Journal of Physical Chemistry B, 2003. **107**(34): p. 8981-8987.

14. Shklover, V., Ovchinnikov, Y.E., Braginsky, L.S., Zakeeruddin, S.M., and Grätzel, M., *Structure of Organic/Inorganic Interface in Assembled Materials Comprising Molecular Components. Crystal Structure of the Sensitizer Bis (4,4 '-carboxy-2,2 '-bipyridine)(thiocyanato) Ruthenium(II).* Chemistry of Materials, 1998. **10**(9): p. 2533-2541.

15. Fillinger, A., Soltz, D., and Parkinson, B.A., *Dye Sensitization of Natural Anatase Crystals with a Ruthenium-Based Dye.* Journal of the Electrochemical Society, 2002. **149**(9): p. A1146-A1156.

16. Persson, P. and Lundqvist, M.J., *Calculated Structural and Electronic Interactions of the Ruthenium Dye N3 with a Titanium Dioxide Nanocrystal.* The Journal of Physical Chemistry B, 2005. **109**(24): p. 11918-11924.

17. Grätzel, M., *Photoelectrochemical Cells.* 2001. **414**(6861): p. 338-344.

18. Deford, J.W. and Johnson, O.W., *Electron-Transport Properties in Rutile from 6-K to 40-K.* Journal of Applied Physics, 1983. **54**(2): p. 889-897.

19. Nowotny, J., Radecka, M., and Rekas, M., *Semiconducting Properties of Undoped TiO_2.* Journal of Physics and Chemistry of Solids, 1997. **58**(6): p. 927-937.

20. Zewail, A.H., *Femtochemistry: Atomic-Scale Dynamics of the Chemical Bond Using Ultrafast Lasers - (Nobel lecture).* Angewandte Chemie-International Edition, 2000. **39**(15): p. 2587-2631.

21. Miller, S.E., Zhao, Y.Y., Schaller, R., Mulloni, V., Just, E.M., Johnson, R.C., and Wasielewski, M.R., *Ultrafast Electron Transfer Reactions Initiated by Excited CT States of Push-Pull Perylenes.* Chemical Physics, 2002. **275**(1-3): p. 167-183.

22. Bitterling, K. and Willig, F., *Charge Carrier Dynamics in the Picosecond Time Domain in Photoelectrochemical Cells.* Journal of Electroanalytical Chemistry, 1986. **204**(1-2): p. 211-224.

23. Hannappel, T., Burfeindt, B., Storck, W., and Willig, F., *Measurement of Ultrafast Photoinduced Electron Transfer from Chemically Anchored Ru-Dye Molecules into Empty Electronic States in a Colloidal Anatase TiO_2 Film.* The Journal of Physical Chemistry B, 1997. **101**(35): p. 6799-6802.

24. Asbury, J.B., Ellingson, R.J., Ghosh, H.N., Ferrere, S., Nozik, A.J., and Lian, T.Q., *Femtosecond IR Study of Excited-State Relaxation and Electron-Injection Dynamics of $Ru(dcbpy)_2(NCS)_2$ in Solution and on Nanocrystalline TiO_2 and Al_2O_3 Thin Films.* The Journal of Physical Chemistry B, 1999. **103**(16): p. 3110-3119.

25. Shoute, L.C.T. and Loppnow, G.R., *Excited-State Metal-to-Ligand Charge Transfer Dynamics of a Ruthenium(II) Dye in Solution and Adsorbed on TiO_2 Nanoparticles from Resonance Raman Spectroscopy.* Journal of the American Chemical Society, 2003. **125**(50): p. 15636-15646.

26. Schnadt, J., Bruhwiler, P.A., Patthey, L., O'Shea, J.N., Sodergren, S., Odelius, M., Ahuja, R., Karis, O., Bassler, M., Persson, P., Siegbahn, H., Lunell, S., and Martensson, N., *Experimental Evidence for Sub-3-fs Charge Transfer from An Aromatic Adsorbate to a Semiconductor.* Nature, 2002. **418**(6898): p. 620-623.

27. Rego, L.G.C. and Batista, V.S., *Quantum Dynamics Simulations of Interfacial Electron Transfer in Sensitized TiO_2 Semiconductors.* Journal of the American Chemical Society, 2003. **125**(26): p. 7989-7997.

28. Haque, S.A., Palomares, E., Cho, B.M., Green, A.N.M., Hirata, N., Klug, D.R., and Durrant, J.R., *Charge Separation versus Recombination in Dye-Sensitized Nanocrystalline Solar Cells: the Minimization of Kinetic Redundancy.* Journal of the American Chemical Society, 2005. **127**(10): p. 3456-3462.

29. Durrant, J.R., Haque, S.A., and Palomares, E., *Towards Optimisation of Electron Transfer Processes in Dye Sensitised Solar Cells.* Coordination Chemistry Reviews, 2004. **248**(13-14): p. 1247-1257.

30. Benko, G., Kallioinen, J., Korppi-Tommola, J.E.I., Yartsev, A.P., and Sundstrom, V., *Photoinduced Ultrafast Dye-to-Semiconductor Electron Injection from Nonthermalized and Thermalized Donor States.* Journal of the American Chemical Society, 2002. **124**(3): p. 489-493.

31. Wenger, B., Grätzel, M., and Moser, J.E., *Rationale for Kinetic Heterogeneity of Ultrafast Light-Induced Electron Transfer from Ru(II) Complex Sensitizers to Nanocrystalline TiO_2.* Journal of the American Chemical Society, 2005. **127**(35): p. 12150-12151.

32. Mora-Sero, I., Dittrich, T., Belaidi, A., Garcia-Belmonte, G., and Bisquert, J., *Observation of Diffusion and Tunneling Recombination of Dye-Photoinjected Electrons in Ultrathin TiO_2 Layers by Surface Photovoltage Transients.* The Journal of Physical Chemistry B, 2005. **109**(31): p. 14932-14938.

33. Nazeeruddin, M.K., Pechy, P., Renouard, T., Zakeeruddin, S.M., Humphry-Baker, R., Comte, P., Liska, P., Cevey, L., Costa, E., Shklover, V., Spiccia, L., Deacon,

G.B., Bignozzi, C.A., and Grätzel, M., *Engineering of Efficient Panchromatic Sensitizers for Nanocrystalline TiO_2-Based Solar Cells.* Journal of the American Chemical Society, 2001. **123**(8): p. 1613-1624.

34. Wang, Q., Campbell, W.M., Bonfantani, E.E., Jolley, K.W., Officer, D.L., Walsh, P.J., Gordon, K., Humphry-Baker, R., Nazeeruddin, M.K., and Grätzel, M., *Efficient Light Harvesting by Using Green Zn-Porphyrin-Sensitized Nanocrystalline TiO_2 Films.* The Journal of Physical Chemistry B, 2005. **109**(32): p. 15397-15409.

35. Ehret, A., Stuhl, L., and Spitler, M.T., *Spectral Sensitization of TiO_2 Nanocrystalline Electrodes with Aggregated Cyanine Dyes.* The Journal of Physical Chemistry B, 2001. **105**(41): p. 9960-9965.

36. Horiuchi, T., Miura, H., and Uchida, S., *Highly-Efficient Metal-Free Organic Dyes for Dye-Sensitized Solar Cells.* Chemical Communications, 2003(24): p. 3036-3037.

37. Horiuchi, T., Miura, H., Sumioka, K., and Uchida, S., *High Efficiency of Dye-Sensitized Solar Cells Based on Metal-Free Indoline Dyes.* Journal of the American Chemical Society, 2004. **126**(39): p. 12218-12219.

38. Thomas, K.R.J., Lin, J.T., Hsu, Y.C., and Ho, K.C., *Organic Dyes Containing Thienylfluorene Conjugation for Solar Cells.* Chemical Communications, 2005(32): p. 4098-4100.

39. Hara, K., Wang, Z.S., Sato, T., Furube, A., Katoh, R., Sugihara, H., Dan-Oh, Y., Kasada, C., Shinpo, A., and Suga, S., *Oligothiophene-Containing Coumarin Dyes for Efficient Dye-Sensitized Solar Cells.* The Journal of Physical Chemistry B, 2005. **109**(32): p. 15476-15482.

40. Ferrere, S. and Gregg, B.A., *Large Increases in Photocurrents and Solar Conversion Efficiencies by UV Illumination of Dye Sensitized Solar Cells.* The Journal of Physical Chemistry B, 2001. **105**(32): p. 7602-7605.

41. Kavan, L., Oregan, B., Kay, A., and Grätzel, M., *Preparation of TiO_2 (Anatase) Films on Electrodes by Anodic Oxidative Hydrolysis of TiCl3.* Journal of Electroanalytical Chemistry, 1993. **346**(1-2): p. 291-307.

42. Wang, Z.S., Yamaguchi, T., Sugihara, H., and Arakawa, H., *Significant Efficiency Improvement of the Black Dye-Sensitized Solar Cell through Protonation of TiO_2 Films.* Langmuir, 2005. **21**(10): p. 4272-4276.

43. Adachi, M., Murata, Y., Takao, J., Jiu, J.T., Sakamoto, M., and Wang, F.M., *Highly Efficient Dye-Sensitized Solar Cells with a Titania Thin-Film Electrode Composed of a Network Structure of Single-Crystal-Like TiO_2 Nanowires Made*

by the "Oriented Attachment" Mechanism. Journal of the American Chemical Society, 2004. **126**(45): p. 14943-14949.

44. Jiu, J., Isoda, S., Wang, F., and Adachi, M., *Dye-Sensitized Solar Cells Based on a Single-Crystalline TiO_2 Nanorod Film.* The Journal of Physical Chemistry B, 2006. **110**(5): p. 2087-2092.

45. Zhang, Z., Zakeeruddin, S.M., O'Regan, B.C., Humphry-Baker, R., and Grätzel, M., *Influence of 4-Guanidinobutyric Acid as Coadsorbent in Reducing Recombination in Dye-Sensitized Solar Cells.* The Journal of Physical Chemistry B, 2005. **109**(46): p. 21818-21824.

46. Neale, N.R., Kopidakis, N., vandeLagemaat, J., Grätzel, M., and Frank, A.J., *Effect of a Coadsorbent on the Performance of Dye-Sensitized TiO_2 Solar Cells: Shielding versus Band-Edge Movement.* The Journal of Physical Chemistry B, 2005. **109**(49): p. 23183-23189.

47. Ma, T.L., Akiyama, M., Abe, E., and Imai, I., *High-Efficiency Dye-Sensitized Solar Cell Based on a Nitrogen-Doped Nanostructured Titania Electrode.* Nano Letters, 2005. **5**(12): p. 2543-2547.

48. Hore, S., Nitz, P., Vetter, C., Prahl, C., Niggemann, M., and Kern, R., *Scattering Spherical Voids in Nanocrystalline TiO_2 - Enhancement of Efficiency in Dye-Sensitized Solar Cells.* Chemical Communications, 2005(15): p. 2011-2013.

Preface to Chapter 2

This Chapter consists of a paper published in Langmuir, 2006, 22, 4472-4475. All data was obtained by me except the LEED patterns of the different TiO_2 polymorphs were measured by Dr. Bengt Jaeckel. The ability to obtain clean, atomically flat and reproducible surfaces is the key for the studies presented later in this dissertation.

Chapter 2: Preparation and Characterization of Terraced Surfaces of Low Index Faces of Anatase, Rutile and Brookite

2.1 Abstract

Simple polishing and low temperature annealing procedures for preparing atomically flat terraced surfaces of various single-crystal TiO_2 polymorphs are described. Anatase (101), anatase (001), rutile (100), rutile (110) and brookite (111) surfaces could all be prepared to show a terraced surface structure in AFM images. The rutile (100), (110) and anatase (101) surfaces were also shown to produce acceptable LEED patterns immediately upon insertion into a UHV system even without sputter and anneal cycles.

2.2 Introduction

Metal oxides have many applications in catalysis, energy conversion, consumer products and ceramics. Titanium dioxide (TiO_2) is prototypical among the metal oxides since TiO_2 can be a photocatalyst[1, 2] component of a solar cell[3, 4] as well as a component of sunscreen, toothpaste and many other consumer products. Single crystal TiO_2 surfaces have also been studied as a model for dye sensitized solar cells and catalyst supports[5, 6]. Although rutile is the high temperature polymorph of TiO_2, it is kinetically stable under ambient conditions. The anatase to rutile transformation occurs in the temperature range of 700 – 1000°C, depending on the crystallite size and impurity content[5]. Brookite, another polymorph of TiO_2, usually contains small amounts of Fe substituted for Ti and is converted into rutile by heating to temperatures above 700°C[7].

There has been a lot of research on the surface structure and reactivity of TiO_2[8-10] in ultrahigh vacuum (UHV)[11, 12]. The achievement of clean atomically flat surfaces usually takes many cycles of sputtering and annealing, which can be time consuming and costly[13, 14]. The surfaces prepared with this method were found to be unstable after exposure to aqueous solutions[15]. Recently, Nakato et al.[16, 17] reported a chemical etching method to prepare atomically flat rutile surfaces by immersing the rutile single crystals in 20% HF for 10 minutes, followed by washing, drying in nitrogen and annealing at 600°C in air. Chemical etching is a good way to prepare atomically flat surfaces for stable crystal surface planes. However, for surfaces with a higher surface energy, they can be selectively etched, forming channels or pits along certain crystallographic directions[18, 19]. Herein we report simple procedures for obtaining atomically flat surfaces for various surface orientations of all three common polymorphs

of TiO_2 (anatase, rutile and brookite) by polishing, ultrasonic cleaning and annealing in air. The surfaces are characterized by atomic force microscopy (AFM) operated in air[i] and low energy electron diffraction (LEED)[ii] in ultrahigh vacuum (UHV).

2.3 Experimental, Results and Discussion

A mechanically polished single crystal of rutile (100) was obtained from Commercial Crystal Laboratories, LTD. The as-received polished rutile (100) revealed no terraces in AFM images and a surface roughness was measured to be about 0.32 nm. The crystal was then manually polished[iii] with a soft polishing cloth (CHEMOMET) using 0.02 μm colloidal silica for about 3 minutes. After rinsing with H_2O, the sample was ultrasonically cleaned for 8 minutes in 18 M-Ω Millipore H_2O to remove the polishing particles. In order to heal the polishing damage and form smooth terraces, the sample was then heated to 700°C for 7.5 hours in air in a Lindberg furnace, and slowly cooled (~ 2°C/minute) to room temperature by turning off the power. After surface treatments the rutile (100) surface was imaged with AFM. The images show very uniform terraces with an average width of about 50 nm corresponding to a miscut angle of 0.4° (Figure 2.1A). From the section analysis, the average height of a single step is shown to be 0.50 nm (Figure 2.1B), within experimental error of the calculated terrace height of 0.459 nm. It is noteworthy that the annealing is usually required only once to obtain the terraced surface. For further cleaning, polishing and sonication are enough.

---

[i] Topographic images were recorded from a Nanoscope IIIa Multimode SPM (from Digital Instruments) operating in tapping mode. Rectangular silicon cantilevers with a spring constant of 40 N/m and resonant frequencies of about 170 KHz, purchased from Mikromasch, were used.

[ii] LEED patterns were obtained with a commercial Omicron Spectraleed optic with various electron energies. The atomic distance calibration was done by using graphite and $MoTe_2$ single crystals.

[iii] The polishing cloth, fine alumina particles and colloidal silica were obtained from Buehler Inc.

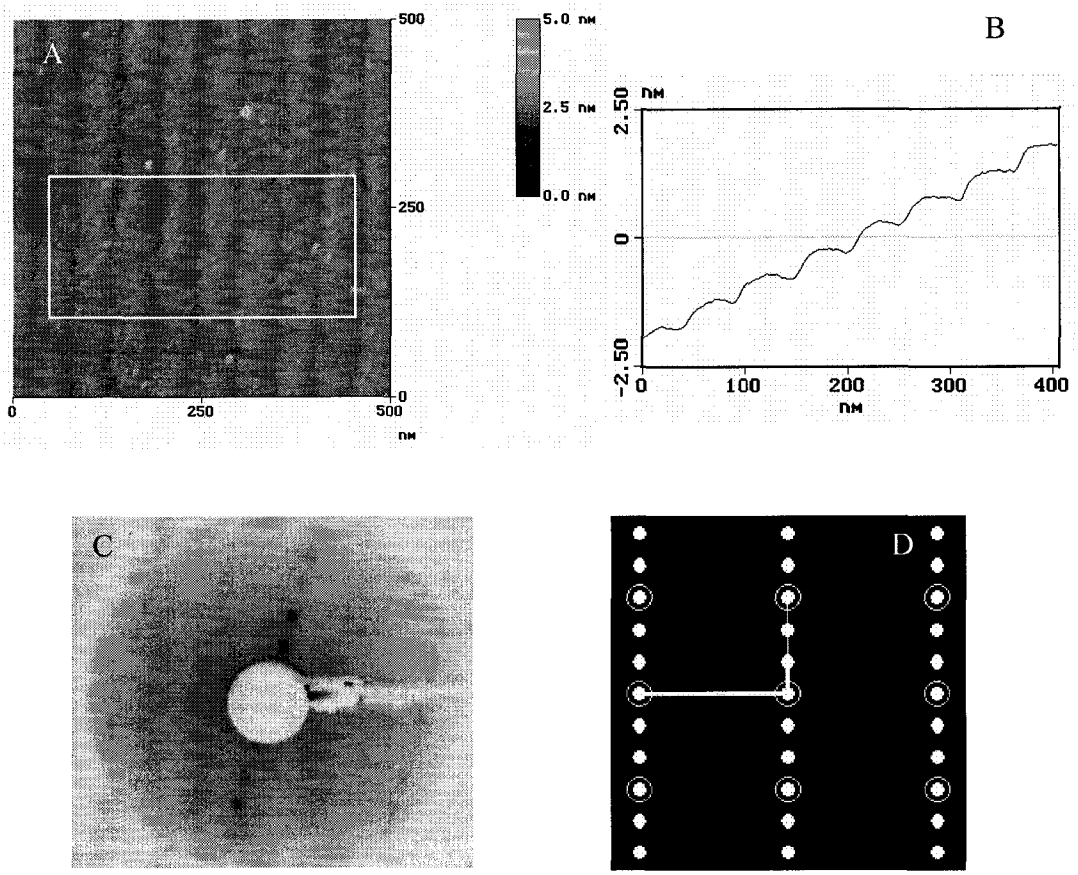

Figure 2.1. (A) Topographic AFM image and (B) section average of the rutile (100) surface. The average step height is 0.50 nm. (C) Observed LEED pattern (46 eV) of the as-prepared surface showing a 1 x 3 reconstruction. A calculated LEED pattern is given in (D).

A LEED pattern of the rutile (100) surface was obtained after insertion into the UHV system without any additional surface treatments. Figure 2.1C shows a LEED pattern obtained with an electron beam energy of 46 eV. The pattern matches the rutile (100) symmetry and lattice parameters of: a = 0.459 nm, b = 0.295 nm and α = 90°. Evaluation of the spot distances leads to the conclusion that the prepared TiO_2 (100) surface has a 1 x 3 reconstruction. A schematic representation of the LEED pattern is shown in Figure 1D by using the lattice parameters of rutile (100) with a software called LEEDpat[iv]. This type of reconstruction is usually found under UHV conditions by sputter-annealing cycles in a more reductive atmosphere. As shown by Muryn et al.[20], this surface can be oxidized in a high oxygen partial pressure into a 1 x 1 stoichiometry. The physical and chemical reason why the polishing and sonication procedures lead to a 1 x 3 reconstruction is still unclear. Further XPS/UPS/STM studies to investigate the surface properties in detail are in progress.

The rutile (110) crystal was also commercially grown and was polished in an identical fashion to the (100) surface. The topographic AFM image of this surface is shown in Figure 2.2A and revealed an average terrace height of 0.33 nm (shown in Figure 2.2B), matching the calculated single TiO_2 layer step height of 0.325 nm. The LEED pattern obtained at 55 eV indicated an unreconstructed 1 x 1 surface (Figure 2.2C) identical to the simulated pattern shown in Figure 2.2D.

The anatase samples were naturally occurring mineral crystals that were mined in Hargvidda, Tyssedal in Norway. These bi-pyramidal crystals exhibited low-energy growth surfaces with large wedge shaped (101) faces and (001) end caps. The (101) crystal faces were dark grey metallic and shiny. They were cut along the (101) plane

[iv] http://w3.rz-berlin.mpg.de/~hermann/LEEDpat/

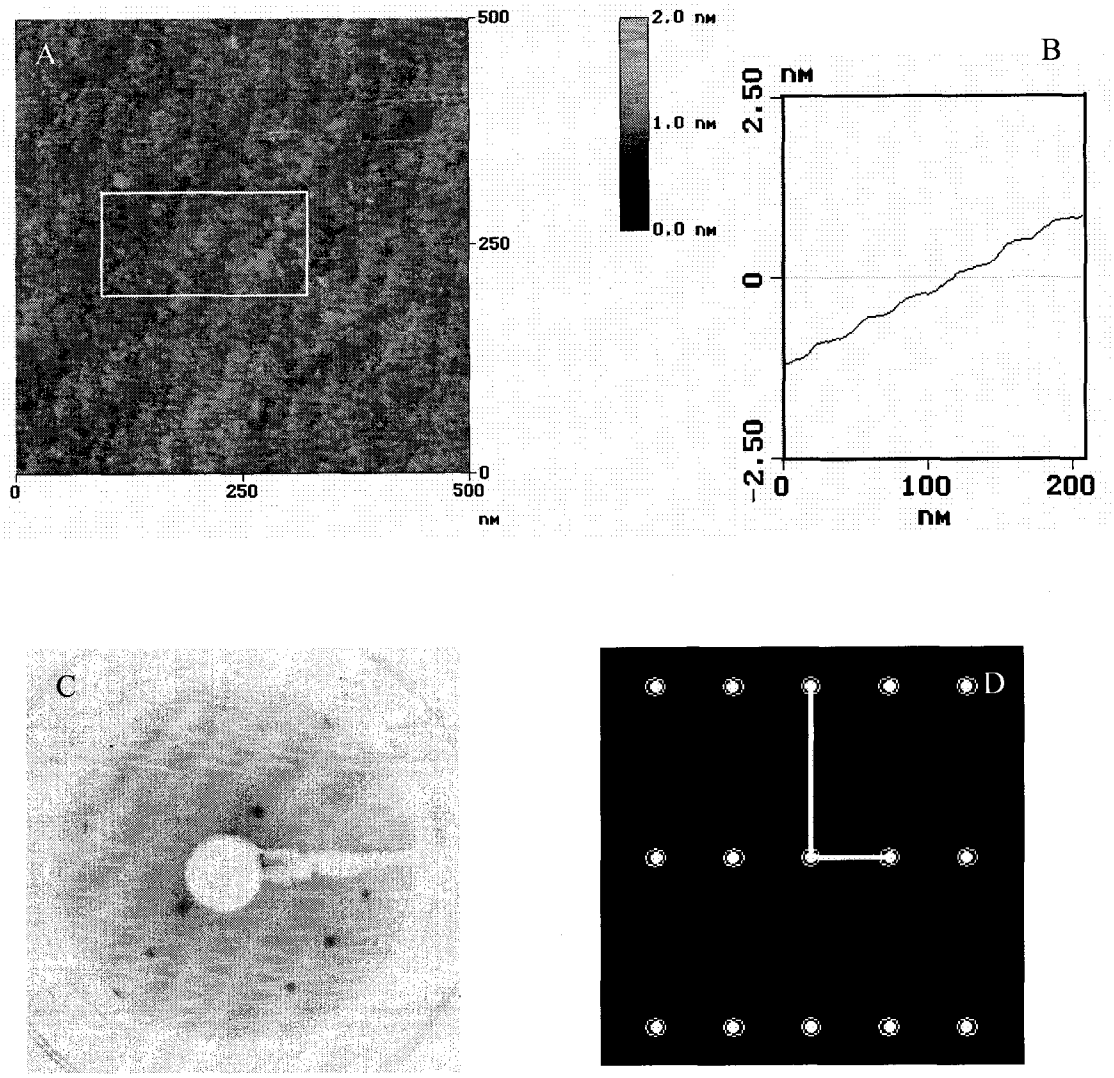

Figure 2.2. (A) Topographic AFM image and (B) section average of the rutile (110) surface. The average step height is 0.33 nm. (C) Observed LEED pattern (55 eV) of the as-prepared surface. A calculated LEED pattern is given in (D).

using a slow speed diamond saw or the entire crystals were used. The natural anatase (101) surfaces were initially quite rough. To prepare them the crystal face was first ground flat with fine (600 grit) sand paper for 30 seconds, followed by successive polishing steps with 0.3μm and 0.05μm alumina each for 3 minutes. The next step was polishing with 0.02 μm colloidal silica for 2 to 5 minutes followed by ultrasonic agitation for 8 minutes. The surface was then characterized with tapping mode AFM. After about 4 cycles of polishing and ultrasonic agitation (total polishing time about 11 minutes), the AFM images indicated that the surfaces were very flat (rms roughness of 0.17 nm) but no distinct terrace structures were evident. The anatase (101) was then gently annealed in the furnace at 350°C for 2 hours. Finally the surfaces were polished for about 5 minutes with 0.02 μm colloidal silica, followed again by ultrasonic agitation. Figure 2.3A and 2.3B show the surface topography and section analysis of the anatase (101) surface, respectively. Unlike the commercial rutile single crystal, the AFM images of the natural anatase single crystal show terraces with irregular widths and edges over the entire surface. Section analysis of the image gives an average step height of 0.36 nm matching one monolayer step height (0.35 nm). The LEED pattern of this sample was obtained at 100 eV (Figure 2.3C) and showed both first and second order spots. The measured reflection distances and angles are in agreement with parameters of anatase (101) surface (centered rectangular: a = 1.02 nm, b = 0.378 nm and $\alpha = 90°$). A simulated LEED pattern for this surface is shown in Figure 2.3D.

The anatase (001) surface was polished in an identical fashion to the anatase (101) surface. After the series of surface treatments and annealing at 275°C for 10 hours, AFM images revealed terraces with an average step height of about 0.28 nm, corresponding to

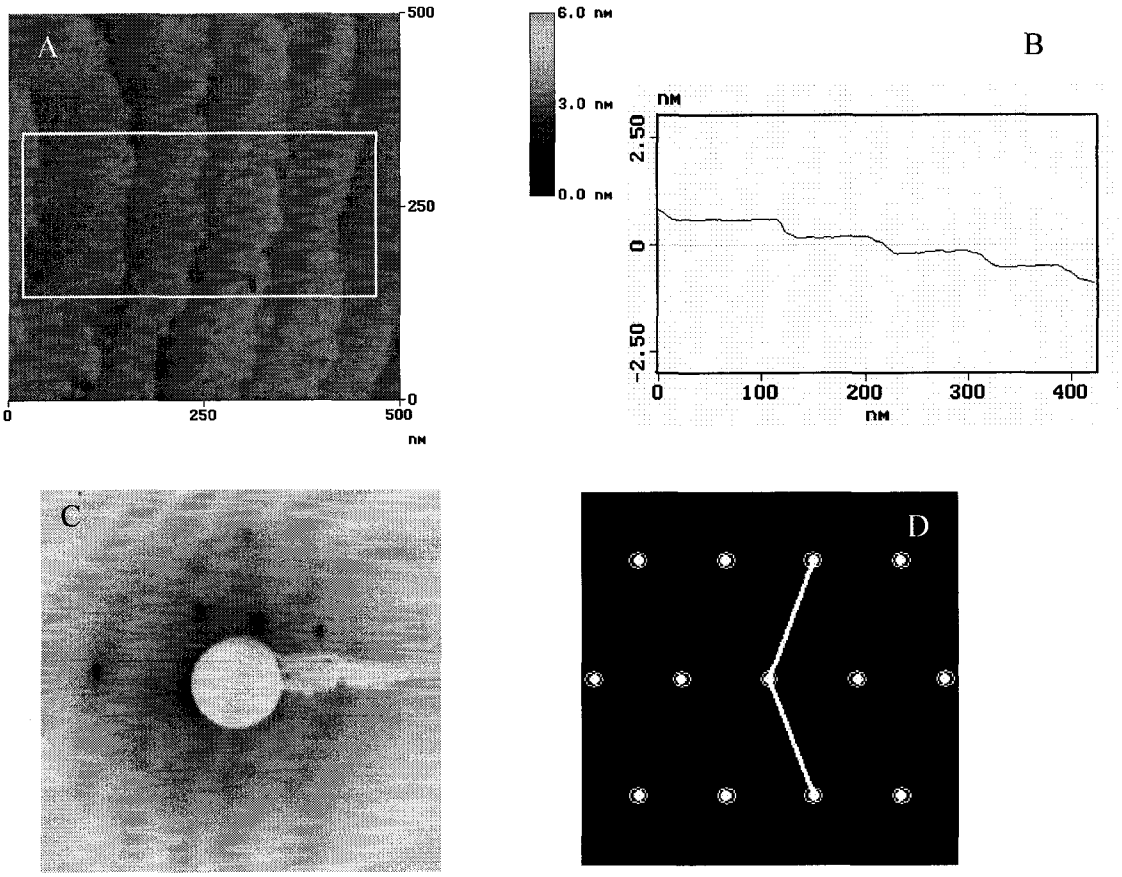

Figure 2.3. (A) Topographic AFM image and (B) section average of the anatase (101) surface. The average step height is 0.36 nm. (C) Observed LEED pattern (100 eV) of the as-prepared surface. A calculated LEED pattern is given in (D).

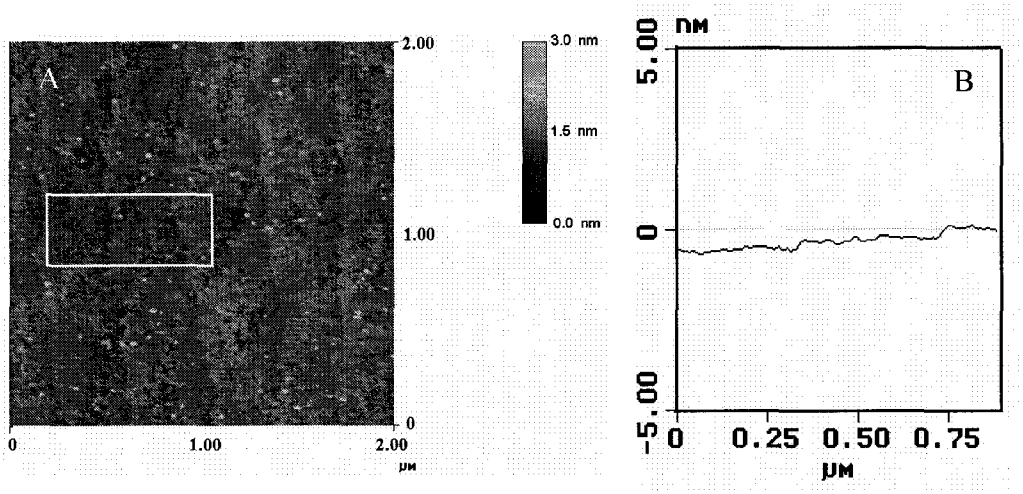

Figure 2.4. (A) Topographic AFM image and (B) section average of the anatase (001) surface. The average step height is 0.28nm.

¼ of a unit cell height along [001] direction. Figure 2.4A and 2.4B show the topographic image and section analysis for this surface, respectively.

The brookite (111) crystal is also a natural mineral crystal from Arkansas. The natural brookite (111) surface was the roughest of the crystals we studied and so extensive polishing was necessary. The polishing revealed some inclusions in the crystal and so that the entire surface could not be polished as smooth as the surfaces of the other polymorphs. The polishing procedures used for anatase, from sand paper to 0.02 μm colloidal silica, were also applied to the brookite crystal. After a total polishing time of about 15 minutes the crystal was gently annealed in the furnace at 250°C for 16 hours. It was then given a final polish for 5 minutes with 0.02 μm colloidal silica followed by ultrasonic cleaning as described above. Figure 2.5A shows the topographic image of a typical area of the brookite (111) surface and the corresponding section analysis is shown in Figure 2.5B. Again irregular terraces are observed. The average terrace height is calculated to be 0.31 nm, matching the single unit cell step height along the [111] direction (0.35 nm). Due to small size of the anatase (001) and brookite (111) crystal sections we were unable to mount them onto a UHV sample holder so no LEED patterns were obtained.

2.4 Summary

In summary we have shown that simple physical polishing and low temperature annealing in air can produce surfaces with atomically flat terraces for five low index surfaces of three TiO_2 polymorphs. The LEED patterns demonstrate that the surfaces have long-range order and the observed flat terraces with defined steps are not unusually ordered areas. We have used these procedures, coupled with a final ultraviolet

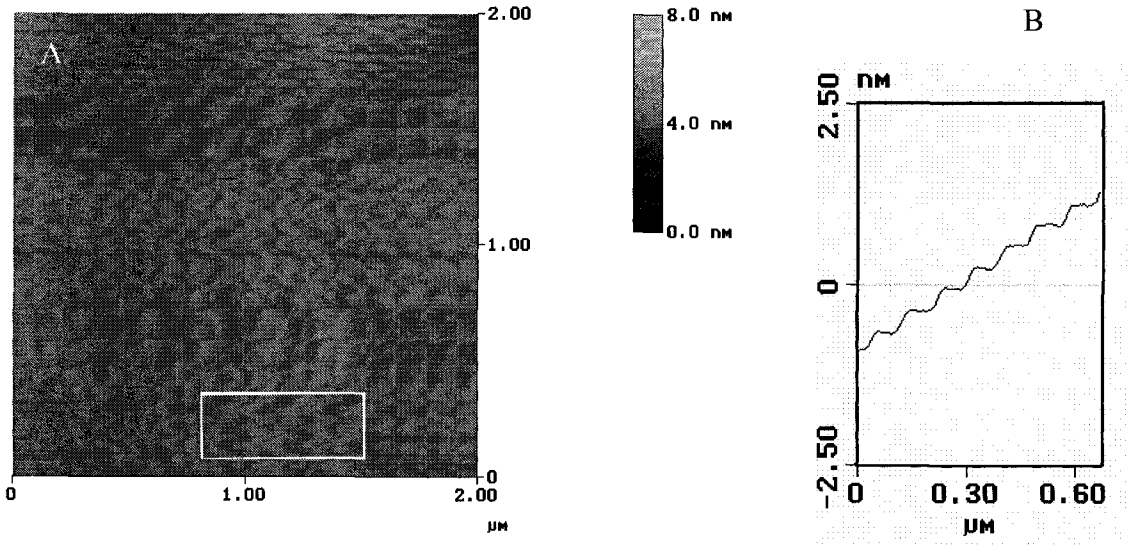

Figure 2.5. (A) Topographic AFM image and (B) section average of brookite (111) surface. The average step height is 0.31nm.

photooxidation step to remove any organic contaminants, to prepare reproducible surfaces for studying dye sensitization of these oxide semiconductors[21]. In one case greatly improved dye coverages were obtained when compared to previous work where the surface pretreatments were not done[6]. We anticipate that performing these procedures prior to inserting the oxide crystal into the UHV system will substantially reduce the sputter and annealing time and cycles usually necessary to produce such well-terraced surfaces since, on the three surfaces where LEED was done, acceptable LEED patterns were obtained simply by inserting them into the UHV system.

6. Acknowledgement

This work was supported by the Department of Energy Office of Basic Energy Sciences under contract # DE-F603-96ER14625.

References:

1. Fujishima, A. and Honda, K., Nature, 1972. 238: p. 37.

2. Linsebigler, A.L., Lu, G., and Yates, J.T., Chem. Rev., 1995. 95: p. 735.

3. O'Regan, B. and Gratzel, M., Nature, 1991. 353: p. 737.

4. Fillinger, A. and Parkinson, B.A., Journal of the Electrochemical Society, 1999. 146(12): p. 4559.

5. Kavan, L., Gratzel, M., Gilbert, S.E., Klemenz, C., and Scheel, H.J., *Electrochemical and photoelectrochemical investigation of single-crystal anatase.* Journal of the American Chemical Society, 1996. 118(28): p. 6716-6723.

6. Fillinger, A., Soltz, D., and Parkinson, B.A., Journal of The Electrochemical Society, 2002. 149(9): p. A1146.

7. Palache, C., Berman, H., and Frondel, C., *The System of Mineralogy.* 1944.

8. Liang, Y., Gan, S.P., Chambers, S.A., and Altman, E.I., *Surface structure of anatase $TiO_2(001)$: Reconstruction, atomic steps, and domains.* Physical Review B, 2001. 63(23): p. 235402.

9. Hebenstreit, W., Ruzycki, N., Herman, G.S., Gao, Y., and Diebold, U., *Scanning tunneling microscopy investigation of the TiO_2 anatase (101) surface.* Physical Review B, 2000. 62(24): p. R16334-R16336.

10. Berko, A. and Solymosi, F., *Study of clean $TiO_2(110)$ surface by scanning tunneling microscopy and spectroscopy.* Langmuir, 1996. 12(5): p. 1257-1261.

11. Fukui, K., Onishi, H., and Iwasawa, Y., *Imaging of atomic-scale structure of oxide surfaces and adsorbed molecules by noncontact atomic force microscopy.* Applied Surface Science, 1999. 140(3-4): p. 259-264.

12. Diebold, U., *The surface science of titanium dioxide.* Surface Science Reports, 2003. 48(5-8): p. 53-229.

13. Hengerer, R., Bolliger, B., Erbudak, M., and Gratzel, M., *Structure and stability of the anatase TiO_2 (101) and (001) surfaces.* Surface Science, 2000. 460(1-3): p. 162-169.

14. Fukui, K., Tero, R., and Iwasawa, Y., *Atom-resolved structures of $TiO_2(001)$ surface by scanning tunneling microscopy.* Japanese Journal of Applied Physics Part 1-Regular Papers Short Notes & Review Papers, 2001. 40(6B): p. 4331-4333.

15. Uetsuka, H., Sasahara, A., and Onishi, H., *Topography of the rutile TiO_2(110) surface exposed to water and organic solvents.* Langmuir, 2004. 20(11): p. 4782-4783.

16. Nakamura, R., Okamura, T., Ohashi, N., Imanishi, A., and Nakato, Y., *Molecular mechanisms of photoinduced oxygen evolution, PL emission, and surface roughening at atomically smooth (110) and (100) n-TiO_2 (rutile) surfaces in aqueous acidic solutions.* Journal of the American Chemical Society, 2005. 127(37): p. 12975-12983.

17. Nakamura, R., Ohashi, N., Imanishi, A., Osawa, T., Matsumoto, Y., Koinuma, H., and Nakato, Y., *Crystal-face dependences of surface band edges and hole reactivity, revealed by preparation of essentially atomically smooth and stable (110) and (100) n-TiO_2 (rutile) surfaces.* Journal of Physical Chemistry B, 2005. 109(5): p. 1648-1651.

18. Kisumi, T., Tsujiko, A., Murakoshi, K., and Nakato, Y., *Crystal-face and illumination intensity dependences of the quantum efficiency of photoelectrochemical etching, in relation to those of water photooxidation, at n-TiO_2 (rutile) semiconductor electrodes.* Journal of Electroanalytical Chemistry, 2003. 545: p. 99-107.

19. Tsujiko, A., Kisumi, T., Magari, Y., Murakoshi, K., and Nakato, Y., *Selective formation of nanoholes with (100)-face walls by photoetching of n-TiO_2 (rutile) electrodes, accompanied by increases in water-oxidation photocurrent.* Journal of Physical Chemistry B, 2000. 104(20): p. 4873-4879.

20. Muryn, C.A., Hardman, P.J., Crouch, J.J., Raiker, G.N., Thornton, G., and Law, D.S.L., *Step and Point-Defect Effects on TiO_2 (100) Reactivity.* Surface Science, 1991. 251: p. 747-752.

21. Ushiroda, S., Ruzycki, N., Lu, Y., Spitler, M.T., and Parkinson, B.A., J. Am. Chem. Soc., 2005. 127: p. 5158.

Preface to Chapter 3

This chapter consists of a paper published in the Journal of the Electrochemical Society 2006, 153(8), E131-E137. In this Chapter, Dae-Jin Choi helped collect the N3 isotherms with the four different TiO_2 surfaces and contributed to the adsorption kinetics study. Jimmy Nelson and O-Bong Yang contributed to the data analysis, discussion and editing of the manuscript.

Chapter 3: Adsorption, Desorption and Sensitization of Low Index Anatase and Rutile Surfaces by the Ruthenium Complex Dye N3

3.1 Abstract

Single crystal anatase (101), (001) and rutile (100), (001) surfaces with atomically flat terraces were prepared and their structure verified with atomic force microscopy (AFM). A ruthenium complex dye, cis-di(thiocyanato)- bis(2,2'-bipyridyl - 4,4'- dicarboxylate) ruthenium(II) (usually known as N3), was used to sensitize these surfaces. The N3 coverage dependence of the incident photon to current efficiencies (IPCE) was measured for all four surfaces. IPCE values were much higher on anatase (101) and rutile (100) than on the other two surfaces. The kinetics of N3 adsorption and was also studied on the four surfaces. The adsorption kinetics for a slow adsorption step could be fit with a Langmuir kinetic model. The differences in the adsorption of N3 and the IPCE values are discussed based on the structure of the N3 and the geometry and reactivity of the binding sites on the four surfaces.

3.2 Introduction

Titanium dioxide (TiO_2) is one of the most intensively studied wide band gap metal oxide semiconductors. Nanocrystalline TiO_2 has been used in the dye-sensitized solar cell discovered by Grätzel[1]. The nanocrystalline dye sensitized cell is promising due to its respectable solar conversion efficiency (>10% in laboratory cells), ease of manufacture and relatively low costs[2]. The most highly studied sensitizing dye in the nanocrystalline system is the ruthenium complex, cis-di(thiocyanato)-bis(2,2'-bipyridyl-4,4'-dicarboxylate) ruthenium(II), usually referred to as N3. N3 has several advantages when used as a sensitizing dye including a broad range of visible light absorption and demonstrated stability over many hours of cell operations[2]. Despite its widespread use in prototype solar cells, there has been relatively little work on the fundamental aspects of the adsorption of this dye on metal oxide surfaces. Grätzel et al have reported the adsorption on synthetic anatase crystals[3] and have also published some speculative surface structures on the anatase (101) surface[4]. We have previously reported the adsorption of N3 on natural anatase crystals and measured isotherms for N3 on nanocrystalline TiO_2[5, 6].

Studying dye adsorption on well-ordered single crystals can provide fundamental information concerning adsorption sites, surface structure and the degree of aggregation that are important for optimizing the nanocrystalline cells. However despite the long history of studies on single crystal rutile[7-13], most of the early work concerned dyes that were not covalently linked to the surface as is the case in the Grätzel cell, and used

surfaces that were not well characterized.

There have been extensive studies on the photoelectrochemical properties of single crystal rutile (001) surface[8-11] and the dye sensitization effect on vacuum deposited thin film of organic dyes was reported[9, 11]. Natural anatase crystals were used to study the sensitization by N3 and a series of thiacyanine dyes[6, 14] but only the (101) orientation was studied. Atomically flat single crystal rutile (100) and (110) surfaces were prepared and their surface band edges and hole reactivity were revealed[15]. ZnO was also studied on dye-sensitized solar cells as a comparison to TiO_2[16, 17].

Charge transfer processes at the TiO_2/electrolyte interface should be sensitive to the crystal orientation[3], therefore it is useful to study dye sensitization on different polymorphs and different crystal orientations of TiO_2. In this study, natural anatase crystals with (101) and (001) orientations and single crystal rutile (100) and (001) surfaces were sensitized with N3 to both better understand the mechanism of interfacial electron transfer and to correlate the sensitization behavior of TiO_2 with its surface structure.

3.3 Experimental Section

A mechanically polished single crystal of rutile (100) was supplied by Commercial Crystal Laboratories, LTD. The rutile (001) sample was grown at DuPont Central Research. The anatase samples were natural anatase crystals that were mined in Hargvidda, Tyssedal in Norway. These bi-pyramidal crystals exhibited low-energy

growth surfaces with the large wedge shaped (101) faces and the (001) end caps. The (101) crystal faces were dark blue metallic and shiny and were sometimes cut along the (101) plane using a diamond saw, and in other cases entire crystals were used. The crystals were polished and annealed to obtain atomically flat surfaces as was described earlier[14]. Atomic Force Microscopy (AFM) (Digital Instruments Nanoscope IIIA controller and a multimode SPM) was used to characterize the polished surface. Silicon tips from MikroMasch with a 40 N/m force constant and resonant frequency around 170 KHz were used.

The crystal was mounted to the electrode using epoxy (Dexter Epoxy Patch) with Ga/In eutectic applied to the back of the electrode for an ohmic contact. After the epoxy set, the electrode was sealed with silicone rubber (RTV) and allowed to dry for a few hours. Before photoelectrochemical experiments the crystal was polished with a soft polishing cloth using 20 nm colloidal silica (Buehler, inc) and cleaned with 0.2 M NaOH, followed by a MilliQ (18 MΩ) water rinse. The electrodes were then illuminated at 0.6 V vs Ag/AgCl in 1 M HCl (for anatase) or 10 mM $NaClO_4$ (for rutile) for 5 minutes using an Oriel 150 W Xe lamp followed by an ethanol (Pharmaco, ACS grade) rinse. To allow the UV illumination to reach the sample surface a quartz cell was used. After UV treatment the electrodes were immediately sensitized by immersing in solutions of various concentrations of cis-di(thiocyanato) -bis(2,2'-bipyridyl- 4,4'-dicarboxylate) ruthenium(II) (N3: obtained from Dr. C. Michael Elliot) dissolved in ethanol. High and quite reproducible dye coverages were obtained with this method. Subsequent to dye

adsorption the electrode was rinsed with ethanol and then used in photoelectrochemical measurements. For isotherm measurements the electrodes were dipped in solutions of the lowest N3 concentrations then moving to the highest concentrations. The single crystal electrodes were cleaned and UV treated between each concentration.

Electrochemical measurements were made in a three-electrode configuration with platinum (Pt) counter and Pt pseudo-reference electrode. Acetonitrile (Fisher, optima grade) electrolyte containing 10 mM tetrabutylammonium perchlorate (Fluka, electrochemical grade) was used as a supporting electrolyte with 4.5 mM hydroquinone added as supersensitizer or regenerator. The electrolyte was deoxygenated with nitrogen gas. Photocurrent/voltage measurements were carried out using a potentiostat (EG&G, 174A) and a lock-in amplifier (Stanford Research, SR830) under PC control. Photocurrent spectroscopy was done using an apparatus that has been described previously[6].

Mott-Schottky analysis used a EG&G PAR173 polarographic analyzer, a Stanford Research SR830 Lock-in amplifier and a Standford Research DS345 function generator under PC control. The same electrolyte as described above was used. An Ag/AgCl reference electrode in acetonitrile solution saturated with tetramethylammonium chloride (TMAC) was used as a reference electrode. The frequency used was 500 Hz for both with and without N3 dye. For the Mott-Schottky plots with adsorbed N3 dye, the electrodes were dipped in 62 μM solution of N3 for 10 minutes after UV treatment. Photocurrent/voltage curves were measured with a 2.25 mW, 532 nm diode laser after

exposing the crystal to a dye concentration of 62 μM, a concentration on the plateau region of the isotherm.

3.4 Results and Discussion

Polishing and annealing were done for all crystals and orientations until AFM imaging showed atomically flat terraces[14]. Figure 3.1 shows AFM images of polished and annealed rutile (100), anatase (101), anatase (001) and rutile (001) surfaces. AFM images of anatase crystals showed terraces on most parts of the surface but the terrace widths varied from place to place as may be expected with natural crystals. The terraces of the rutile (100) crystal were quite uniform across the surface showing an average width of 50 nm. The rutile (001) surface showed smaller less uniform terraces. As in our previous work[14] we verified with AFM that the UV treatment, used to clean the electrodes before and between all experiments, did not etch or pit the surfaces. However, after extended use the crystals were renewed by demounting them from the electrodes, repolishing and reanealing them to produce clean terraced surfaces.

Mott-Schottky analysis was performed by measuring the capacitance of the various TiO_2 crystal surfaces in electrolytes with and without adsorbed N3. Mott- Schottky plots provide the band positions of the various TiO_2 polytypes and reveal any band shifts that might be induced by the adsorption of N3. We carried out the measurements at three different frequencies: 200 Hz, 500 Hz and 1000 Hz. Very little frequency dispersion was observed so only the measurements done at 500 Hz are shown in Figure 3.2. After the

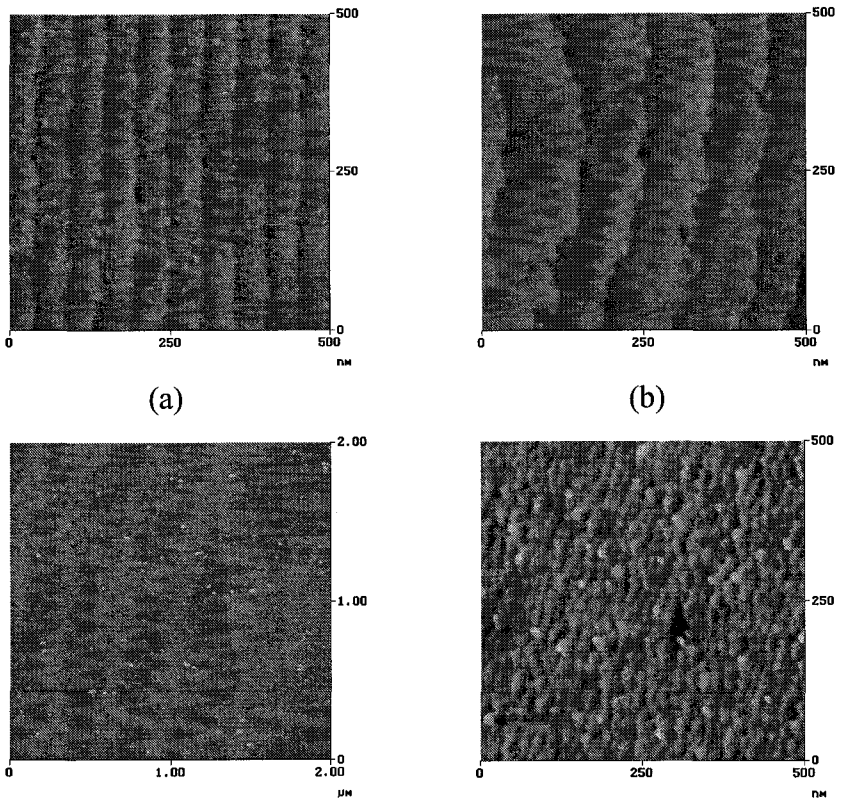

Figure 3.1. AFM images of (a) rutile (100), (b) anatase (101), (c) anatase (001), and (d) rutile (001) surfaces used in this study. Z scale full range for the images: (a) 3 nm; (b) 6 nm; (c) 10 nm (d) 5 nm. For surface preparation procedures see the experimental section.

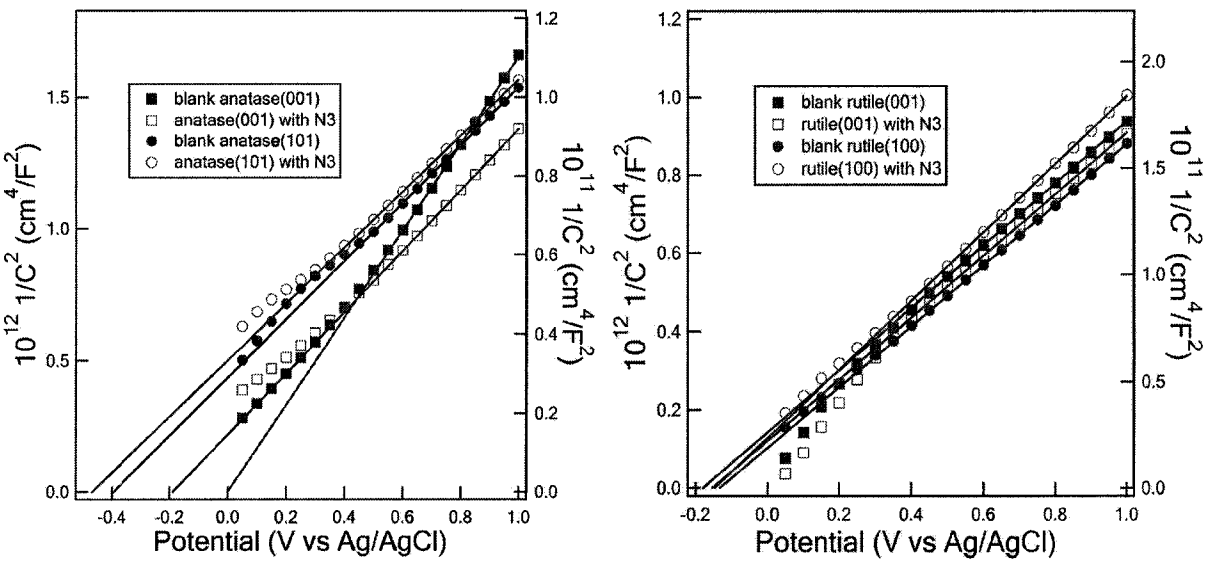

Figure 3.2. Mott-Schottky plots for (a): two anatase electrodes. Left axis for anatase (001) and right axis for anatase (101). (b): two rutile electrodes. Left axis for rutile (001) and right axis for rutile (100). Solid lines are linear least squares fitting results. Potentials are relative to Ag/AgCl electrode in acetonitrile solution saturated with TMAC.

N3 dye was adsorbed the flat band potentials for the two anatase surfaces shifted to slightly more negative potentials, indicating that some of the adsorbed dyes carried negative charges since a much larger shift (~3V) would be observed if each N3 adsorbed as a singly charged anion. There was almost no shift in the flat band potential with N3 adsorption for the two rutile surfaces. The anatase (101) electrode showed a plateau in the capacitance characteristic of the presence of surface states at around 0.4 V. The charge associated with these states was calculated to be about 3.7×10^{-7} C/cm^2 (2.3×10^{12} charges/cm^2), corresponding to 4.5% of the surface Ti atoms or 2.2% of the surface oxygen atoms, assuming one charge per atom.

Table 3.1. Doping densities, flatband potentials with and without adsorbed N3 and photocurrent onset potentials for the four TiO_2 surfaces studied.

Surface	Doping Density	Flat Band Potential	Flat Band Potential N3	Photocurrent Onset
Anatase (101)	5.8×10^{19} cm^{-3}	- 0.40 V	- 0.47 V	- 0.2 V
Anatase (001)	1.5×10^{18} cm^{-3}	0.0 V	- 0.19 V	- 0.1 V
Rutile (100)	5.4×10^{18} cm^{-3}	- 0.15 V	- 0.17 V	0.1 V
Rutile (001)	2.0×10^{18} cm^{-3}	- 0.18 V	- 0.15 V	0.0 V

Table 3.1 also shows the potential for the onset of bandgap photocurrent for the four surfaces. All but the anatase (001) surface show a photocurrent onset 0.18 to 0.25 volts positive of the flatband potential, indicating that there is substantial carrier

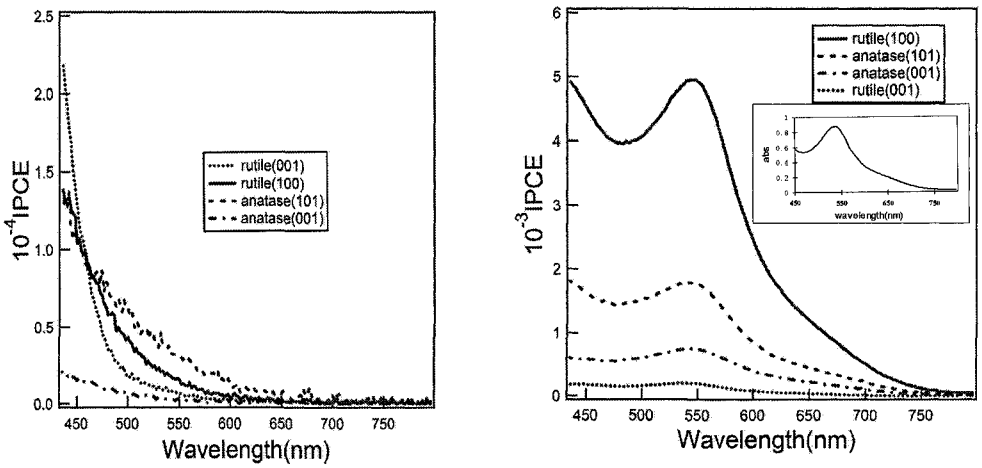

Figure 3.3. (a): Background photocurrent spectra for electrodes made from four different orientations and polymorphs of TiO_2. (b) Photocurrent spectra of the same four crystals in (a) but treated with a 0.21 mM N3 solution. Inset: UV-Vis spectrum of N3 in ethanol solution.

recombination near the flatband potential on these three surfaces. To establish the level of background currents in the wavelength region where the metal oxide will be dye sensitized, the wavelength dependence of the sub-bandgap photocurrent was investigated. Anatase (101) and rutile (100) displayed higher sub-bandgap photocurrents than anatase (001) and rutile (001) as shown in Figure 3.3(a). The anatase (001) electrode displayed the smallest sub-bandgap photocurrent over the entire wavelength range (436–796 nm) whereas the anatase (101) had a high sub-bandgap response that may be associated with the surface states detected in the Mott-Schottky plots. The photocurrent for the rutile (001) increases quickly for wavelengths shorter than 500 nm and is the highest among all four electrodes at a wavelength of 455 nm. The wavelengths corresponding to the band gap energies are 370 nm (3.0 ev) and 355 nm (3.2 eV) for rutile and anatase respectively and so a lower energy sub-bandgap increase for rutile is expected since it is approaching the band gap.

The photocurrent spectra for high surface coverages of N3 on anatase (101), anatase (001), rutile (100) and rutile (001) surfaces are shown in Figure 3.3(b). The sensitized photocurrents are much larger than the background currents measured in Figure 3.3(a). The inset shows the UV-Vis absorbance spectrum of an ethanol solution of N3 showing a peak at 538 nm. The photocurrent spectra have the same shape as the N3 solution absorption spectrum but the sensitization peak is shifted to the red by 10 nm to 548 nm. Previous work on single crystals of anatase (101) found the sensitization maximum to be at 525 nm[6]. The previous work was with much lower IPCE values, and presumably

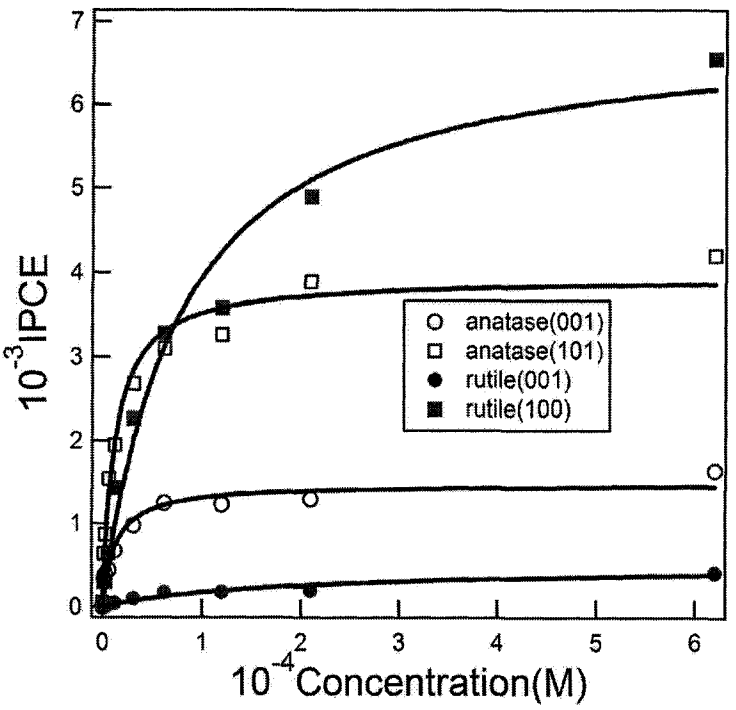

Figure 3.4. Isotherms for N3 adsorption onto the four crystal surfaces used in this study.

much lower coverages, since the UV cleaning procedure was not used.

The adsorption isotherms measured for N3 adsorbed on the four oxide surfaces are shown in Figure 3.4. The measured IPCE values on some crystals varied with the position of the light spot on the crystal surface, but the variation is within a factor of two. This variation may be due to regions of different surface roughness or to doping level variations across the surface and is especially noticeable on the natural anatase crystals where these parameters are not well controlled. The isotherms on each individual crystal were measured on areas that consistently gave higher IPCEs. The N3 concentration range from 1.5 μM up to 0.62 mM was investigated. The adsorption time was varied in order to establish that equilibrium was obtained between the ethanol solution of N3 and the adsorbed N3 during the dye adsorption step. It was found that at lower concentrations (less than 0.12 mM) the IPCE reaches a plateau at immersion times of 60 minutes or longer. At higher concentrations, the adsorption is faster and steady state is reached after immersion for 30 minutes. Therefore isotherms were measured using a 60 minute dipping time at the lower concentrations and 30 minutes for the higher concentrations. All four isotherms showed a steep increase in coverage at small concentrations (<62 μM) and reached a plateau at higher concentrations (>62 μM). Since the measurement is IPCE and not directly surface concentration we assume that the IPCE is proportional to the amount of adsorbed dye, an assumption that is probably valid in this case since, as discussed below, we have close to the theoretical IPCE value for a monolayer on some surfaces. Also, since there was no dye in the electrolyte solution, a

true equilibrium was not established during the measurement of the photocurrent spectra. However, only a small amount of dye desorbs from the surface during the time needed to acquire a photocurrent spectrum[18].

The isotherms were fit using a simple Langmuir adsorption isotherm (eq. 1):

$$\theta = KC/(1 + KC) \qquad (1)$$

where θ is the fractional coverage, K is the adsorption coefficient (M^{-1}), and C is the molar concentration of N3 in solution. The fit of the isotherm to the adsorption data is perhaps a bit surprising since the basic assumptions of the Langmuir isotherm are not met in this system. However there are many examples of good Langmuir fits to adsorption data that do not satisfy the assumptions of the Langmuir model. We are not interpreting this fit beyond the use of the Langmuir constants to compare the strength of the interaction of N3 molecules with the various TiO_2 surfaces.

The fits of the isotherms were also used to determine the maximum achievable coverage, and thus maximum IPCE, for the various surfaces. The maximum IPCE of rutile (100) and anatase (101) were determined to be (0.65±0.14)% and (0.42±0.09)% respectively. Assuming that the quantum yield for charge injection from the excited sensitizer in to the TiO_2 and the electron collection efficiency are both unity, the IPCE for one monolayer of close packed N3 dye was predicted to be 0.27%[3] based on an area per N3 molecule of 180 $Å^2$. Our higher experimental values are probably due to some

surface roughness resulting in more dye in the beam. Additionally, an ordered chromophore may have a higher absorption than an isotropic dye due to the directionality of the transition dipole. Also the molecular size of N3 taken from the theoretical calculation[3] might not be correct, since according to a recent study, N3 molecules undergo significant structural adjustments upon binding to the TiO_2 surface[19]. In any case there is not much improvement possible in the light harvesting ability of N3 on these surfaces.

Anatase (001) and rutile (001) gave much smaller maximum IPCEs of (0.16±0.04)% and (0.04±0.009)%, respectively. There are several possible explanations for the low IPCE values on these two surfaces. One is that the dye coverage is low. The rutile (001) surface is terminated by four-fold Ti atoms that are demonstrated to be highly reactive[20]. The small IPCE may be because many binding sites are already reacted and blocked before exposure to the dye solution. These adsorbates, that are not as reactive towards the five fold Ti sites on the other surfaces, may be contaminants in laboratory air or the ethanol solvent. We performed an experiment to demonstrate this possibility. To minimize the exposure of the UV cleaned surface to other potential adsorbates, we added N3 to the electrolyte used for the UV cleaning treatment. The result was a doubling of the IPCE when compared to the usual subsequent dye treatment procedure. We must then conclude that the measured "isotherm" for the rutile (001) surface is not valid since, due to competitive adsorbtion, the dye was not in equilibrium with the surface. We are currently experimenting with a rutile crystal configured in an ATR configuration and that

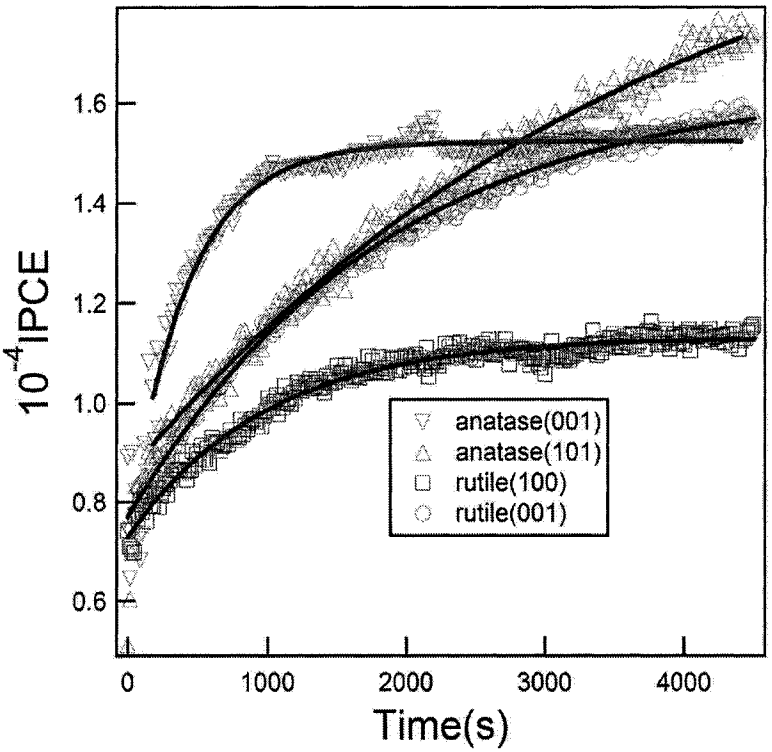

Figure 3.5. Kinetics for the adsorption of N3 to anatase (001), anatase (101), rutile (100) and rutile (001) electrodes. The curves were obtained continuously by recording the photocurrent at 548 nm after 0.1 mL of a 1.2×10^{-4} M solution of N3 was injected into 35 mL of acetonitrile electrolyte (resulting concentration 0.34 μM). The solid curves are fits using the expressions described in the text.

will allow us to measure dye coverages (via absorption spectra) and IPCE independently and be able to directly calculate absorbed photon current efficiencies (APCE) for the two rutile surfaces.

The kinetics of N3 adsorption onto the four crystal surfaces from the acetonitrile electrolyte solution was also studied. Although the isotherms were measured by adsorbing the N3 from ethanol solutions, the adsorption kinetics were measured by injecting N3 directly into the acetonitrile electrolyte that also contains the hydroquinone regenerator. The electrodes were UV treated and immersed in the electrolyte and the photocurrent at the dye sensitization maximum (548 nm) was continuously measured for 75 minutes after the injection as shown in Figure 3.5. In all cases there is a very fast initial adsorption occurring during the mixing time in the first few seconds after the dye is injected. Subsequent to this initial step the IPCE steadily increased in what we will call the second stage of adsorption. The adsorption kinetic parameters were obtained by fitting this second stage of the adsorption curves to a simple Langmuir kinetic model where:

$$R_{ads} = k_2(1-\theta)C \qquad (2)$$

$$R_{des} = k_1\theta \qquad (3)$$

So the net rate is:

$$R = R_{ads} - R_{des} = k_2(1-\theta)C - k_1\theta = d(N_0\theta)/dt \qquad (4)$$

After integration, the following equation was obtained:

$$\theta_t = \frac{k_2 C}{k_2 C + k_1}\left(1 - e^{\left[-\frac{k_2 C + k_1}{N_0} \bullet (t-B)\right]}\right) \qquad (5)$$

Where k_2 is the rate constant for adsorption, k_1 is the rate constant for desorption, θ is the fractional coverage, C is the concentration of N3 in solution (M), N_0 is N3 full coverage concentration on surface (9.2×10^{-11} mol/cm^{-2}), t is time and B is a time offset constant extrapolated to zero IPCE. The adsorption kinetics curves were fit to this equation, using the full coverage IPCE values, derived from the fits of the adsorption isotherms, to obtain the k_2 and k_1 values for all the surfaces (Table 3.2).

Table 3.2. Adsorption and desorption rate constants (k_2 and k_1, respectively) derived from the adsorption kinetics.

surface	k_1(mol·cm^{-2}·s^{-1})	k_2(mol·cm^{-2}·s^{-1}·M^{-1})	k_2/k_1(M^{-1})
Anatase(101)	$(3.9\pm1.0)\times10^{-14}$	$(3.6\pm1.1)\times10^{-9}$	9.2×10^{4}
Anatase(001)	$(3.4\pm1.3)\times10^{-13}$	$(9.0\pm2.0)\times10^{-8}$	2.6×10^{5}
Rutile(100)	$(1.5\pm0.6)\times10^{-13}$	$(6.5\pm2.1)\times10^{-8}$	4.3×10^{5}
Rutile(001)	$(4.1\pm0.7)\times10^{-14}$	$(4.4\pm0.6)\times10^{-8}$	1.1×10^{6}

From these data, one can see that k_2/k_1 ratio was not proportional to the full coverage IPCE values of each electrode. The rutile (001) surface gave the smallest IPCE among

all four electrodes, but the k_2/k_1 was the highest, indicating that the strength of binding between the dye and the rutile (001) surface was probably the strongest however as was discussed above much of the surface may be blocked by chemisorbed solvent or impurities. For the other electrodes, where the binding strength was lower, the dye molecules might also be able to better rearrange on the surface so that additional incoming dye molecules can find binding sites, yielding a higher IPCE. We have to point out that to collect the isotherms, the electrodes were dipped in solutions containing only dye, whereas for this kinetic study the electrodes were in a solution containing electrolyte and hydroquinone, species that could possibly compete with the dye for adsorption sites[7].

The fact that the adsorption kinetics can be fit with a Langmuir model, even though the N3 molecules can bind through multiple carboxylate linkages, is perhaps a bit surprising. The very fast initial adsorption, where the IPCE is already at 50% to 70% of its maximum value, is not fit by the function derived for the slower final step however one cannot lose site of the assumption that IPCE is proportional to the dye coverage. One explanation is that all of the dye is quickly adsorbed but there is a population of dye molecules on the surface that is not injecting electrons effectively perhaps because only one carboxylate linkage has been made. The slow step then represents the reorganization of the dye on the surface into a more efficiently injecting form perhaps with more carboxylate linkages. Hara et al have previously postulated that the injection efficiency of a dye is related to the number of carboxylate linkages however the redox potential of

their dye series was also changing with the number of carboxylates[21]. Conversely the fast step could indicate that the first adsorption step, where only one carboxylate is bound, is very fast and that the dye linked with a single carboxylate is effective at electron injection. The following slow step would then be related to a reorganization of the dyes on the surface to accommodate more dye molecules perhaps in a more ordered structure as was proposed earlier[4]. The ATR experiment described above will also be able to discriminate between these two models.

The rate of electron transfer from the excited dye molecules to the TiO_2 has been measured to be extremely fast on the nanocrystalline anatase electrodes and since the overall quantum efficiencies are very high in these systems the recombination must be relatively low[22-24]. Information about carrier recombination on our crystal surfaces can be obtained from the bias dependence of the sensitized photocurrent. Therefore we measured the N3 sensitized photocurrent dependence on applied voltage for all the TiO_2 surfaces. Figure 3.6 shows normalized photocurrent/voltage curves measured with an N3 coverage obtained by adsorption from a dye concentration of 130 μM that will produce saturation or near saturation coverage. The difference between the flat band potential (with adsorbed N3) and photocurrent onset for anatase (101) is about 0.3 V while for the other three electrodes it is about 0.1 V. The anatase (101) electrode displayed the most negative photocurrent onset potential and the most positive saturation potential. The slopes of photocurrent voltage curves for the two rutile surfaces are quite similar and are steeper than the anatase (101), indicating that there were more significant recombination

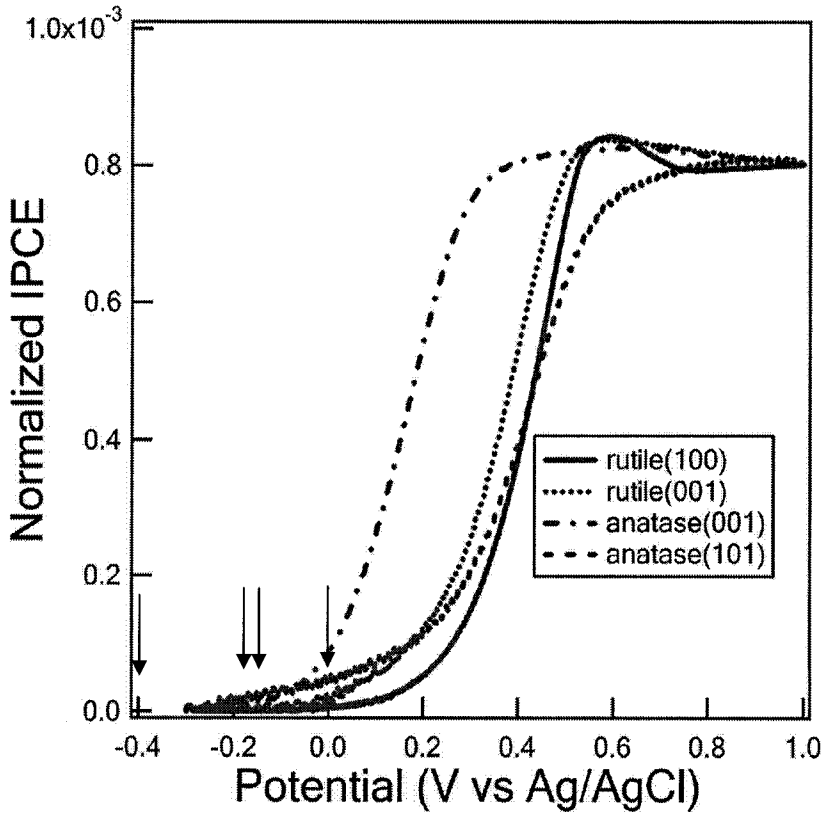

Figure 3.6. Normalized N3 dye sensitized photocurrent/voltage curves. A diode laser at 532 nm with a power of 2.25 mW was the light source. Potentials are relative to Ag/AgCl electrode in acetonitrile solution saturated with TMAC. The arrows indicate the flat band potentials of anatase (101), rutile (001), rutile (100) and anatase (001) from left to right.

of the injected electrons. The photocurrent of the other three electrodes all reached a plateau region indicating that the collection of the injected electrons was in equilibrium with any recombination in this potential region whereas that for anatase (101) the photocurrent is still slightly increasing with increasing potential. The fact that there was still recombination on the anatase (101) surface even at the plateau region is in agreement with the Mott-Schottky analysis that verified anatase (101) has more surface states however it contrasts with the high IPCE for this surface. The presence of traps due to impurities in the natural crystal, that are not present in the nanocrystalline thin films, may account for the non-ideality of the anatase (101) crystal.

N3 molecules covalently bind to the unsaturated Ti atoms via the peripheral carboxylate groups. N3 has four pendant carboxylate groups that are capable of binding to the TiO_2 surface, two on each of the bipyridine ligands. It is most likely that N3 binds to the surface with at least two of these carboxylate groups. There are three possible binding configurations for bidentate binding of N3 where the carboxyl groups are spaced 6.2 Å, 9.8 Å, or 10.0 Å apart, as shown in Figure 3.7(b). The Ti binding sites corresponding to the unsaturated Ti atoms on the different surfaces are schematically shown in Figure 3.7(a). Shklover et al[4] has reported the bind of N3 dye with anatase (101) surface based on a simple one-dimensional tight-binding model and we will discuss the N3 binding on the same basis. The five coordinate Ti-Ti distances on a rutile (100) surface are 5.9 Å, 9.7 Å and 10.0 Å, distances that match perfectly with the spacings of N3 carboxylates on the same bipyridine ligand. For anatase (101), the N3 dye would

(a)

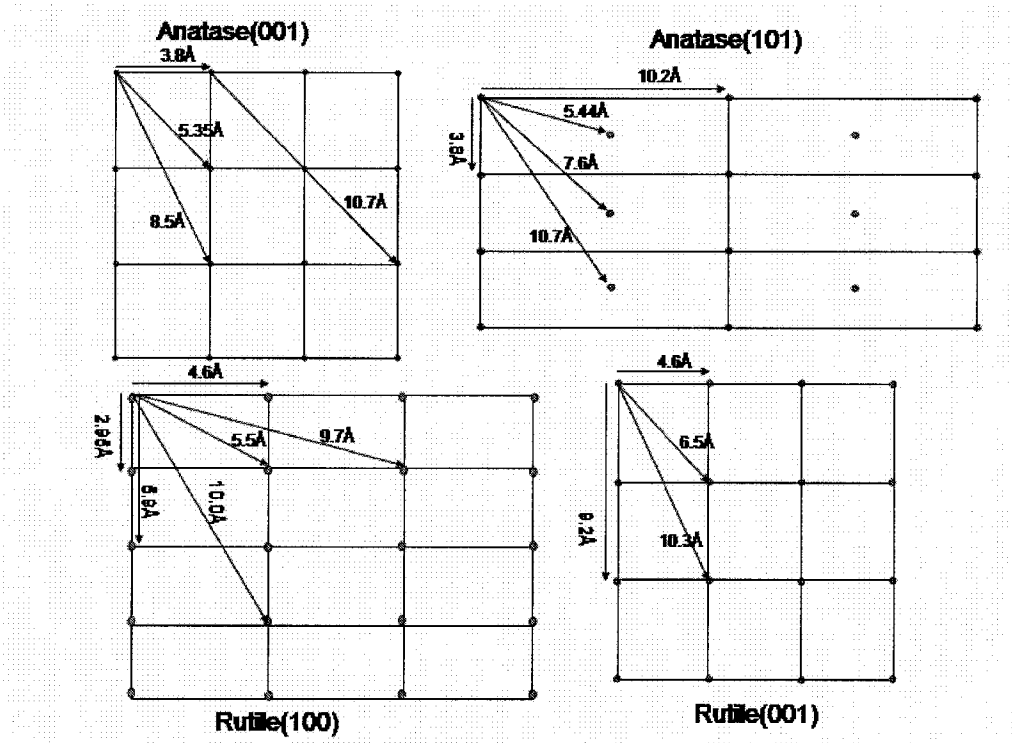

(b)

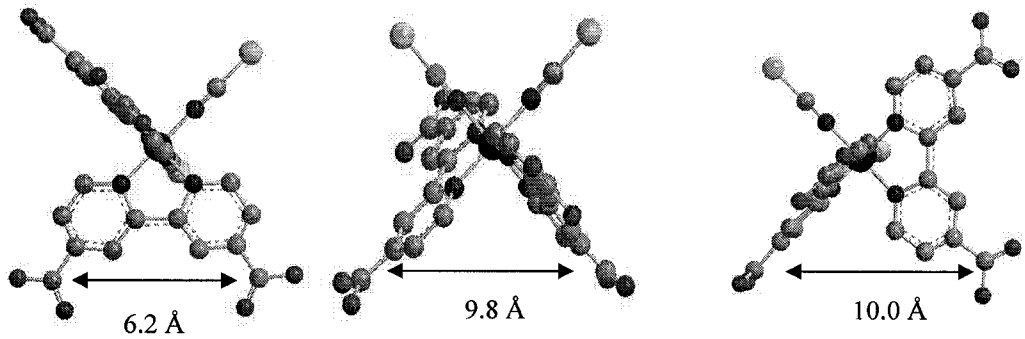

Figure 3.7. Structural models of the four low index TiO_2 surfaces and possible bidentate binding combinations for carboxylate groups from N3. (a) The distances between Ti binding sites. (b) Possible carboxyl group combinations for bidentate chelating binding of N3 to the surfaces[4].

appear most likely to bind across the 10.2 Å and 10.7 Å Ti-Ti distances, corresponding to two carboxylates on different bipyridine ligands[4, 6]. The anatase (001) surface appears to have fewer possible binding possibilities with only one Ti-Ti distance of 10.7 Å. The chelating bidentate binding of N3 appears to be necessary to stabilize the dye bonding to the surface via the chelate effect and so variations in IPCE could be related to the ability of the dye to bind with two carboxylate groups. The K value derived from the Langmuir fitting of the isotherms for rutile (100) (~1.3×10^5 M^{-1}) is much higher than for anatase (101) and anatase (001) (~8×10^4 M^{-1}), whereas rutile (001) is the smallest (~5×10^3 M^{-1}). The binding strength of rutile (100) and the two anatase surfaces agree with results of our adsorption kinetic study. The value for rutile (001) is anomalous, probably because of the high reactivity of rutile (001) surface where a slow rate of displacing impurities on the surface greatly reduces K. At the higher concentrations the dyes start to compete for binding sites making it difficult for N3 molecules to attach with multiple binding sites. Isotherms for both anatase electrode surfaces reached a plateau at the studied concentration ranges whereas the IPCEs of the two rutile surfaces were still increasing even at the solubility limit of N3 in ethanol.

Dye-sensitized solar cells need to be both efficient and stable for many years. The efficiency is influenced by the obtainable dye coverage since the nanocrystalline layer can be thinner if more dye is available for light absorption. We find higher yields for N3 sensitization are obtained on anatase (101) and rutile (100) surfaces. The predominant face of the nanocrystalline anatase films has been shown to be (101)[4, 25]

whereas the efficient nanocrystalline rutile cell was shown to have a predominantly (110) orientation[26]. Our results suggest that anatase (001) and rutile (001) would not be favorable orientations in a cell due to lower yields obtained on these surfaces. Whether the low yields are due to low dye coverages or to recombination has not yet been definitively determined.

3.5 Conclusion

We have studied the dye sensitization of N3, the most extensively used nanocrystalline TiO_2 sensitizer, on 4 different atomically flat TiO_2 single crystal surfaces. The surfaces were prepared by polishing, annealing and a UV photooxidation treatment to ensure their atomic flatness and cleanliness and that reproducible dye adsorption could be achieved. IPCE values for N3 sensitization vary significantly between the different polymorphs and crystal orientations, 0.65% for rutile (100), 0.04% for the rutile (001), 0.42% for anatase (101) and 0.17% for anatase (001) surfaces. The high values for anatase (101) and rutile (100) correspond to about 100% APCE, indicating that these surfaces are not amenable to further improvements in their light harvesting ability using N3 dye. The adsorption kinetics was also studied. The adsorption rate constants for N3 onto the various surfaces were determined by fitting the kinetic data to a Langmuir kinetic model. Possible binding geometries for N3 to these various low index TiO_2 surfaces were proposed.

Acknowledgements

We thank C. Michael Elliott for donation of purified N3 dye and August Ferretti for the gift of a Nb doped TiO_2 crystal. This work was supported by the Department of Energy Office of Basic Energy Sciences under contract #DE-F603-96ER14625.

References:

1. Oregan, B. and Gratzel, M., *A Low-Cost, High-Efficiency Solar-Cell Based on Dye-Sensitized Colloidal TiO_2 Films.* Nature, 1991. **353**(6346): p. 737-740.

2. Nazeeruddin, M.K., Kay, A., Rodicio, I., Humphrybaker, R., Muller, E., Liska, P., Vlachopoulos, N., and Gratzel, M., *Conversion of Light to Electricity by Cis-X2bis(2,2'-Bipyridyl-4,4'-Dicarboxylate)Ruthenium(Ii) Charge-Transfer Sensitizers (X = Cl-, Br-, I-, Cn-, and Scn-) on Nanocrystalline TiO_2 Electrodes.* Journal of the American Chemical Society, 1993. **115**(14): p. 6382-6390.

3. Kavan, L., Gratzel, M., Gilbert, S.E., Klemenz, C., and Scheel, H.J., *Electrochemical and photoelectrochemical investigation of single-crystal anatase.* Journal of the American Chemical Society, 1996. **118**(28): p. 6716-6723.

4. Shklover, V., Ovchinnikov, Y.E., Braginsky, L.S., Zakeeruddin, S.M., and Gratzel, M., *Structure of organic/inorganic interface in assembled materials comprising molecular components. Crystal structure of the sensitizer bis (4,4 '-carboxy-2,2 '-bipyridine)(thiocyanato) ruthenium(II).* Chemistry of Materials, 1998. **10**(9): p. 2533-2541.

5. Fillinger, A. and Parkinson, B.A., *The adsorption behavior of a rutheninm-based sensitizing dye to nanocrystalline TiO_2 - Coverage effects on the external and internal sensitization quantum yields.* Journal of the Electrochemical Society, 1999. **146**(12): p. 4559-4564.

6. Fillinger, A., Soltz, D., and Parkinson, B.A., *Dye sensitization of natural anatase crystals with a ruthenium-based dye.* Journal of the Electrochemical Society, 2002. **149**(9): p. A1146-A1156.

7. Ryan, M.A., Fitzgerald, E.C., and Spitler, M.T., *Internal-Reflection Flash-Photolysis Study of the Photochemistry of Eosin at TiO_2 Semiconductor Electrodes.* Journal of Physical Chemistry, 1989. **93**(16): p. 6150-6156.

8. Salvador, P., Garcia Gonzalez, M.L., and Munoz, F., *Catalytic Role of Lattice Defects In the Photoassisted Oxidation of Water at (001) n-TiO_2 Rutile.* J. Phys. Chem, 1992. **96**: p. 10349.

9. Yanagi, H., Chen, S., Lee, P.A., Nebesny, K.W., Armstrong, N.R., and Fujishima,

A., *Dye-Sensitizing Effect of TiOPc Thin Film on n-TiO_2 (001) Surface.* J. Phys. Chem, 1996. **100**: p. 5447.

10. Miki, T. and Yanagi, H., *Scanning Probe Microscopic Characterization of Surface-Modified n-TiO_2 Single-Crystal Electrodes.* Langmuir, 1998. **14**: p. 3405.

11. Taira, S., Miki, T., and Yanagi, H., *Dye-sensitization of n-TiO2 single-crystal electrodes with vapor-deposited oxometal phthalocyanines.* Applied Surface Science, 1999. **143**: p. 23.

12. Tsujiko, A., Kisumi, T., Magari, Y., Murakishi, K., and Nakato, Y., *Selective formation of nanoholes with (100)-face walls by photoetching of n-TiO_2 (rutile) electrodes, accompanied by increases in water-oxidation photocurrent.* J.Phys. Chem. B, 2000. **104**: p. 4873.

13. Kisumi, T., Tsujiko, A., Murakoshi, K., and Nakato, Y., *Crystal-face and illumination intensity dependences of the quantum efficiency of photoelectrochemical etching, in relation to those of water photooxidation, at n-TiO_2 (rutile) semiconductor electrodes.* Journal of Electroanalytical Chemistry, 2003. **545**: p. 99.

14. Ushiroda, S., Ruzycki, N., Lu, Y., Spitler, M.T., and Parkinson, B.A., *Dye sensitization of the anatase (101) crystal surface by a series of dicarboxylated thiacyanine dyes.* Journal of the American Chemical Society, 2005. **127**(14): p. 5158-5168.

15. Nakamura, R., Ohashi, N., Imanishi, A., Osawa, T., Matsumoto, Y., Koinuma, H., and Nakato, Y., *Crystal-face dependences of surface band edges and hole reactivity, revealed by preparetion of esentially atomically smooth and stable (110) and (100) n-TiO_2 (rutile) surfaces.* Journal of Physical Chemistry B, 2005. **109**: p. 1648.

16. Matsumura, M., Matsudaira, S., Tsubomura, H., Takata, M., and Yanagida, H., *Dye Sensitization and Surface-Structures of Semiconductor Electrodes.* Industrial & Engineering Chemistry Product Research and Development, 1980. **19**(3): p. 415-421.

17. Keis, K., Bauer, C., Boschloo, G., Hagfeldt, A., Westerark, K., Rensmo, H., and Siegbahn, H., *Nanostructured ZnO electrodes for dye-sensitized solar cell applications.* Journal of Photochemistry and Photobiology A: Chemistry, 2002. **148**: p. 57.

18. Lu, Y. and Parkinson, B.A., unpublished results.

19. Persson, P. and Lundqvist, M.J., *Calculated structural and electronic interactions of the ruthenium dye N3 with a titanium dioxide nanocrystal.* Journal of Physical Chemistry B, 2005. **109**(24): p. 11918-11924.

20. Muscat, J. and Harrison, N.M., *The physical and electronic structure of the rutile (001) surface.* Surface Science, 2000. **446**(1-2): p. 119-127.

21. Hara, K., Horiuchi, H., Katoh, R., Singh, L.P., Sugihara, H., Sayama, K., Murata, S., Tachiya, M., and Arakawa, H., *Effect of the ligand structure on the efficiency of electron injection from excited Ru-phenanthroline complexes to nanocrystalline TiO_2 films.* J. Phys. Chem. B, 2002. **106**: p. 374.

22. Hannappel, T., Burfeindt, B., Storck, W., and Willig, F., *Measurement of ultrafast photoinduced electron transfer from chemically anchored Ru-dye molecules into empty electronic states in a colloidal anatase TiO_2 film.* Journal of Physical Chemistry B, 1997. **101**(35): p. 6799-6802.

23. Asbury, J.B., Ellingson, R.J., Ghosh, H.N., Ferrere, S., Nozik, A.J., and Lian, T.Q., *Femtosecond IR study of excited-state relaxation and electron-injection dynamics of Ru(dcbpy)(2)(NCS)(2) in solution and on nanocrystalline TiO_2 and Al_2O_3 thin films.* Journal of Physical Chemistry B, 1999. **103**(16): p. 3110-3119.

24. Tachibana, Y., Nazeeruddin, M.K., Gratzel, M., Klug, D.R., and Durrant, J.R., *Electron injection kinetics for the nanocrystalline TiO_2 films sensitised with the dye (Bu4N)(2)Ru(dcbpyH)(2)(NCS)(2).* Chemical Physics, 2002. **285**(1): p. 127-132.

25. Spoto, G., Morterra, C., Marchese, L., Orio, L., and Zecchina, A., *The Morphology of TiO_2 Microcrystals and Their Adsorptive Properties Towards Co - a Hrtem and Ftir Study.* Vacuum, 1990. **41**(1-3): p. 37-39.

26. Park, N.G., Schlichthorl, G., van de Lagemaat, J., Cheong, H.M., Mascarenhas, A., and Frank, A.J., *Dye-sensitized TiO_2 solar cells: Structural and photoelectrochemical characterization of nanocrystalline electrodes formed from the hydrolysis of $TiCl_4$.* Journal of Physical Chemistry B, 1999. **103**(17): p. 3308-3314.

Preface to Chapter 4

The work in this chapter was published in the Journal of Physical Chemistry B 2006, 110, 25273-25278 as part of the special issue "Arthur J. Nosik Festschrift". Mark T. Spitler synthesized the dyes used in the experiments and was instrumental in data analysis and interpretation. All experimental data was collected by me.

Chapter 4: Photochronocoulometric Measurement of the Coverage of Surface Bound Dyes on Titanium Dioxide Crystal Surfaces

4.1 Abstract

Atomically flat terraced single-crystal anatase and rutile surfaces can be prepared allowing for the reproducible adsorption of covalently attached sensitizing dyes. Once reproducible surfaces and dye coverages are achieved, a photochronocoulometric technique is developed to measure the surface coverage of the dyes, an important parameter in determining the efficiency of sensitization. The surface-bound dyes are irreversibly oxidized by exposure to a light pulse with the n-type oxide semiconductor electrode held in depletion. A double-exponential decay of the subsequent photocurrent is then measured, where the integration of the faster decay is associated with the adsorbed dye coverage and the second much slower decay is attributed to trace regenerators, including water, in the nonaqueous electrolyte. The ruthenium-based N3 dye shows the expected linear dependence of the rate constant on light intensity whereas a dicarboxylated thiacyanine dye shows a square root dependence of its photooxidation rate on light intensity. The sublinear response of the thiacyanine dye is discussed in terms of the more complex surface chemistry that is known for this family of sensitizing dyes.

4.2 Introduction

Chronocoulometry and double potential step chronocoulometry[1,2] were developed to measure the surface concentration of adsorbed electroactive species in the presence of additional diffusing electroactive species. The technique was used to measure the coverage of many adsorbed metal complexes on Hg electrodes.[1,3] Mercury electrodes were favored because they provide a reproducible and renewable electrode surface necessary for the discrimination of background charge (charging currents) from charge due to adsorbed electroactive species. The technique was extended to semiconductor surfaces where the adsorption of I_3^- as a function of concentration onto WSe_2 surfaces was measured using light, rather than a potential step, to initiate the photooxidation of adsorbed I_3^-. WSe_2 was a useable substrate due to its atomically flat surface and the ability to renew the surface via cleavage of the 2D crystal resulting in reproducible surfaces and low capacitance backgrounds.[4]

We have been studying dye sensitization of oxide surface of low index faces of the anatase and rutile forms of TiO_2 by covalently attaching dyes to the surface.[5-7] To enable these studies methods to reproducibly prepare these oxide surfaces with clean and atomically flat surfaces were developed.[8] The structure and the dynamics of the photoinjected electron transfer processes of these dye covered surfaces are important for understanding and improving the operation of dye sensitized solar cells. Incident photon-to-current conversion efficiency (IPCE) values are measured as a function of dye concentration in the solution from which the covalent attachment is made. Adsorption isotherms for a particular dye/surface combination are then inferred using the assumption that the IPCE is proportional to the dye coverage.[5-7] Since the surface often contains

multiple forms of the dye (monomers, dimers and higher aggregates), it is difficult to determine if these species have different efficiencies for photocurrent generation. High absorbed photon-to-current conversion efficiencies (APCE) are the more important parameter for constructing efficient dye sensitized solar cells. To determine APCE values the amount of adsorbed dye and the extinction coefficient of the adsorbed dye are required.[1] The surface coverage of the adsorbed dye molecules onto the TiO_2 nanocrystalline thin films can be determined by desorbing the dye and measuring the optical absorbance of the solution due to the large amount of adsorbed dye.[6] Gratzel et al have measured the dye coverage on nanocrystalline anatase films by electrochemical oxidation of the dye and assumptions about the surface area of the nanocrystalline film.[9] Spitler and Calvin used the absorbance of the dye desorbed from multiple single crystal surfaces, however even using many expensive crystal plates resulted in a rather small absorbance in the solution.[10] Another method is to construct a single crystal ATR prism from the semiconductor of interest, where the absorbance of the adsorbed dye is multiplied by the number of internal reflections. The ATR approach is complicated by the optical absorption introduced by the dopants that are necessary for electrical conduction.[11] In the absence of a direct measurement of the absorbance of the dye on the surface, the surface coverage was inferred from the assumption that the plateau of the isotherm, determined with the previously mentioned assumption that IPCE is proportional to coverage, represented a complete monolayer. A geometric model of the dye packing on the surface is then used to calculate the dye coverage.[12] The absorbance of the monolayer was then calculated using the bulk extinction coefficients.

[1] In nanocrystalline solar cells the light harvesting efficiency is nearly 100% and so the absorbance value is not needed.

This method is not always accurate due to the possible preferential orientation of the dye on the surface and the anisotropy of light absorption by many polar dyes.[10]

A simple direct measurement of the dye coverage would be a great benefit for the development of dye-sensitized solar cells since it would allow accurate measurements of APCE values on dye monolayers. Herein we present a simple photoelectrochemical method for measuring the coverage of dyes covalently attached to low-index anatase and rutile surfaces. In our method, we expose a dye covered single crystal oxide semiconductor surface, held at a potential in the depletion region, to a light pulse that photoexcites the dye with subsequent election injection into the conduction band of the semiconductor. In the absence of a reducing agent (regenerator) in solution, the total photoinjected charge should be equal to the number of adsorbed dye molecules. Unlike conventional chronocoulometry there is no current due to diffusing molecules and the capacitance change, associated with the light pulse that is not absorbed by the semiconductor, is negligible and so no background double layer charging currents are produced.

4.3 Experimental Section

The rutile (100) single crystal was purchased from Commercial Crystal Laboratories, LTD. The anatase samples were natural anatase crystals that were mined in Hargvidda, Tyssedal in Norway. These bi-pyramidal crystals exhibited low-energy growth surfaces with the large wedge shaped (101) faces and (001) end caps. The (101) crystal faces were dark blue and the entire crystal was used. Atomically flat terraced surfaces for all polytypes and faces were prepared as described earlier.[8] Atomic Force

Microscopy (AFM) (Digital Instruments Nanoscope IIIA controller and a multimode SPM) was used to characterize the polished surfaces. Silicon tips from MikroMasch with a 40 N/m force constant and resonant frequency around 170 KHz were used.

The crystal was mounted to the electrode using epoxy (Dexter Epoxy Patch) with Ga/In eutectic applied to the back of the electrode for an ohmic contact. After the epoxy set, the electrode was sealed with silicone rubber (RTV) and allowed to dry for a few hours. Before photoelectrochemical experiments the crystal was polished with a soft polishing cloth using 20 nm colloidal silica (Buehler, inc) and cleaned with 0.2 M NaOH, followed by a MilliQ (18 MΩ) water rinse. The electrodes were then cleaned by illuminating at 0.6 V vs Ag/AgCl in 1 M HCl (for anatase) or 10 mM $NaClO_4$ (for rutile) for 5 minutes using an Oriel 150 W Xe lamp followed by an ethanol (Pharmaco, ACS grade) rinse. To allow the UV illumination to reach the sample surface a quartz electrochemical cell was used.

Cis-di(thiocyanato)-bis(2,2'-bipyridyl-4,4'-dicarboxylate) ruthenium(II) (usually referred to as N3) and Cis-di(chloro)-bis(2,2'-bipyridyl-4,4'-dicarboxylate) ruthenium(II) were obtained from Professor C. Michael Elliott. A 0.22 mM N3 dye solution and a 0.18 mM G7 dye solution (both dissolved in ethanol) were used to adsorb the dyes onto the cleaned crystal surfaces. These concentrations correspond to the plateau region of the respective isotherms and so represent the maximum obtainable dye coverage.[5,7] Chart 4 software (ADInstruments) was used to record the photocurrent signal from a RDE4 potentiostat (Pine Instrument Company) using a 532 nm diode laser as the light source with the beam expanded to illuminate the entire crystal surface. The cell was degassed

with N_2 gas before all measurements. The surface areas of the rutile (100) and anatase (101) electrodes were 0.20 cm^2 and 0.32 cm^2, respectively.

The transient photocurrent measurements were made in a three-electrode configuration with a platinum counter electrode and a Ag/AgCl reference electrode. Acetonitrile (Fisher, optima grade) electrolyte was used containing 10 mM tetrabutylammonium perchlorate (Fluka, electrochemical grade) as a supporting electrolyte.

4.4 Results and Discussion

A photoexcited dye adsorbed onto the surface of an n-type semiconductor under depletion will inject the photoexcited electron into the conduction band of the semiconductor resulting in a photocurrent. This process is described by the following equations:

$$M \xrightarrow{hv} M^* \qquad (1)$$

$$M^* \xrightarrow{fast} M^+ + e^-_{(semiconductor)} \qquad (2)$$

Many measurements of the timescale of dye sensitized electron injection into semiconducting nanocrystalline TiO_2 show that this process occurs on a subpicosecond timescale.[13-16] We expect that the injection should be fast on a single crystal TiO_2 surface as well. Therefore any measured transient photocurrent will be limited by the excitation rate of the adsorbed dye that is determined by the light intensity. If this photo

excitation process is a first order reaction, the following equations can be derived upon integration and differentiation:

$$[M] = [M]_0 e^{-\varepsilon L_p \Phi t} \quad (3)$$

$$I(t) = -\frac{d[M]}{dt} AF = \varepsilon L_p \Phi AF [M]_0 e^{-\varepsilon L_p \Phi t} \quad (4)$$

where ε is the absorption cross section of the dye in $cm^2\ mol^{-1}$, L_p is the photon flux in mol $cm^{-2}\ s^{-1}$, Φ is the photochemical yield for electron transfer, A is the surface area of the TiO_2 electrode in cm^2, F is the Faraday constant, and $[M]_0$ is the original surface concentration of the dye molecules in mol cm^{-2}.

N3 is a ruthenium-based dye that has been extensively studied as a sensitizer for nanocrystalline solar cells. We have previously studied the adsorption of N3 onto low index anatase and rutile crystal surfaces,[5,6] however we had no direct measurement of the surface coverage of the N3 dye. Therefore we decided to first apply photochronocoulometry to determine the coverage of adsorbed N3 on single crystal oxide surfaces. The structure, absorption and action spectrum (adsorbed onto single crystal rutile (100) surface) for N3 are shown in Figure 4.1. The photocurrent action spectrum showed a 10 nm red shift relative to its solution absorption spectrum. The electrochemistry of N3 in non-aqueous solutions has been studied by Bond et al.[17] At slow scan rates irreversible oxidations were observed at 0.45 and 0.83 volts vs the

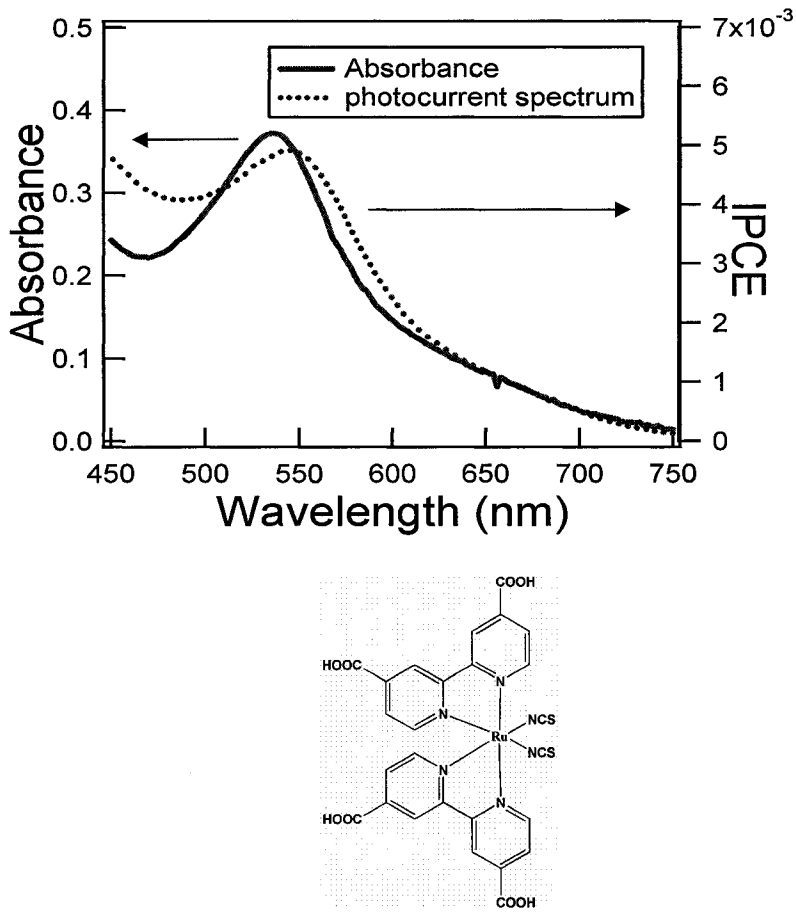

Figure 4.1. The molecular structure, solution absorption (solid line) and action spectrum adsorbed on rutile (100) surface (dashed line) for the N3 dye.

ferrocene/ferricenium couple in acetonitrile. The first oxidation was assigned to solution phase N3 while the second oxidation was assigned to the surface bound dye. Wang et al. studied the oxidation of N3 surface bound on mesoscopic TiO_2 and Al_2O_3 and found one oxidation at 0.38 volts vs ferrocene/ferricenium.[9] Therefore in the absence of N3 in solution we can expect an irreversible one-electron oxidation of surface bound N3.

A typical photochronoamperometric experiment was performed as follows: after UV cleaning of the TiO_2 crystal electrode, dye adsorption was accomplished by immersing into the dye solution. The electrode was then immediately transferred to the electrochemical cell and allowed to equilibrate in the dark under potential control at 0.6 V for 30 seconds. With the semiconductor in depletion in the dark there is almost no current flow across the blocking junction. The electrode was then exposed to 532 nm light from a diode laser that is very near the maximum sensitization wavelength. Immediately after illumination a transient photocurrent is measured due to electron injection from the adsorbed dye into the conduction band of the TiO_2. The measured photocurrent transients for N3 adsorbed onto rutile (001) and anatase(101) are shown in Figure 4.2a and 4.2b. The photocurrent transient can be fit by a double exponential decay (Figure 4.2c) that decays about 60 seconds to a constant value that persists for much longer times (this residual current will be discussed later). For the rutile (100) surface, the rate constant derived from the faster exponential decay shows a linear dependence with the light intensity, shown in Figure 3a, as is expected from equation 3. At higher laser intensities (>12 mW) the measured rate constant begins to be sublinear probably due to the very fast photocurrent transient and the limited frequency response and data

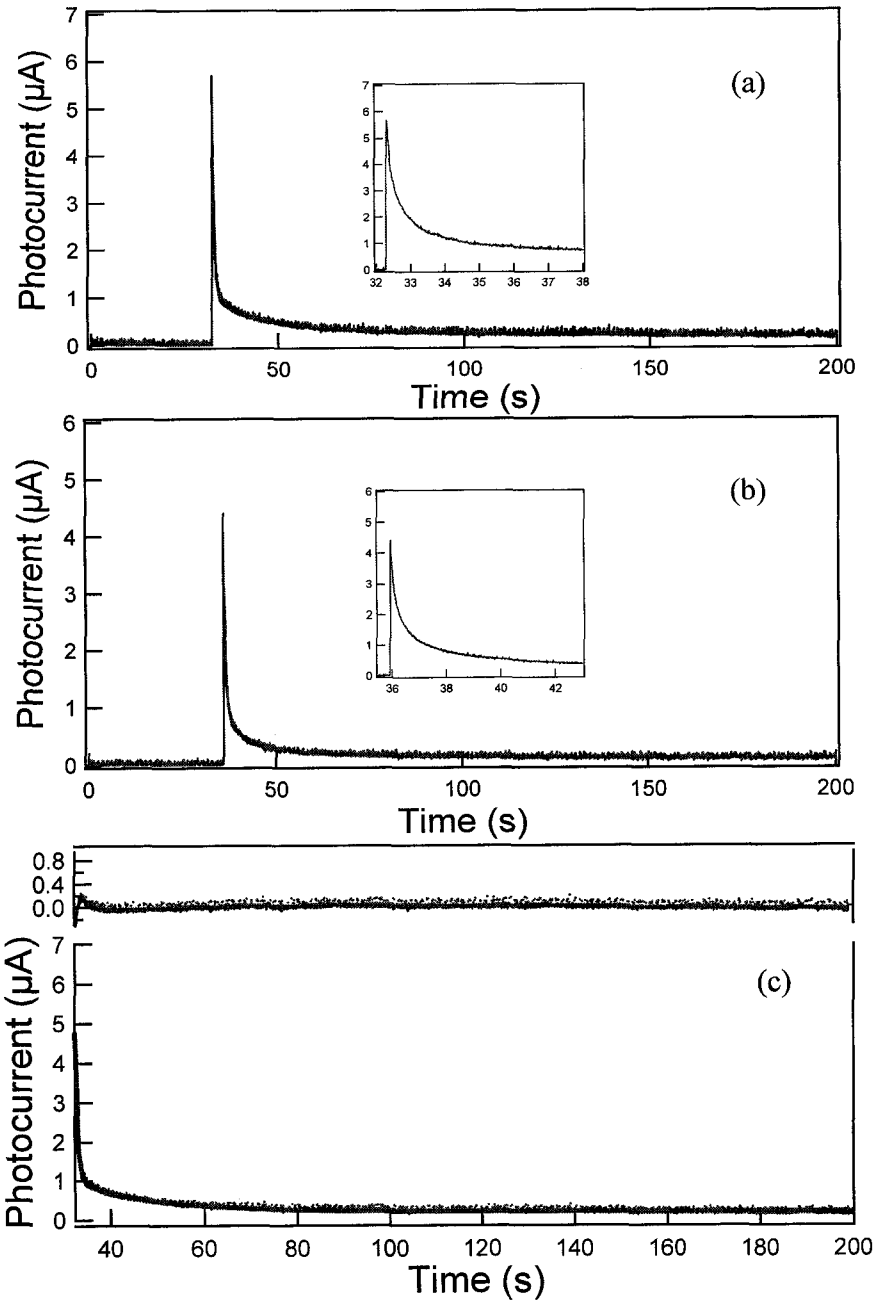

Figure 4.2. Transient photocurrent of N3 dye adsorbed onto (a), rutile (100) surface and (b), anatase (101) surface. The insets are zoom-ins. (c) shows the typical transient photocurrent (dots) and fit (solid line) and the residue after fit.

collection rate of the electronics used. The integrated current transient, or total charge from the fast decay (photochronocoulometric response), remains constant (2.0 ± 0.04 μC) at all laser powers as would be expected if the current is associated with the oxidation of a monolayer of adsorbed dye. Therefore, we use the integration of the fast current decay to determine the surface coverage of the adsorbed photoactive dye.

The transient photocurrent was also measured at different applied biases but at a constant light intensity. As long as the applied bias is above a threshold value, just positive of the flat band potential of the TiO_2 single crystal, the derived rate constant and the collected charge remained constant at 2.2 ± 0.2 s^{-1} and 11 ± 1.0 μC/cm^2, respectively.

The surface coverage calculated from the integrated charge of the fast decay component is 1.0×10^{-10} mol cm^{-2} or 0.6 molecule nm^{-2} for the rutile (100) surface. The anatase (101) surface behaves similarly to the rutile (100) surface, as shown in Figure 4.3b, where the surface coverage was calculated to be 8.1×10^{-11} mol cm^{-2} or 0.5 molecule nm^{-2}. These numbers closely match the monolayer surface coverage of a closed packed N3 dye with the single crystal TiO_2 surface[18] based on an area per N3 molecule of 1.8 nm^2.

The second slow current decay transient is problematic. In some cases the charge associated with the slow decay is up to 8 times the charge in the fast component. Blank experiments with no adsorbed dye produced no detectable sub-bandgap photocurrents on either anatase or rutile samples at the current scales used for the experiments with dye present. It is possible that SCN^- ions are released from oxidized N3 and act as regenerators of other adsorbed N3 molecules. However the additional charge from this process would only double that measured in the fast current decay. Nonetheless we

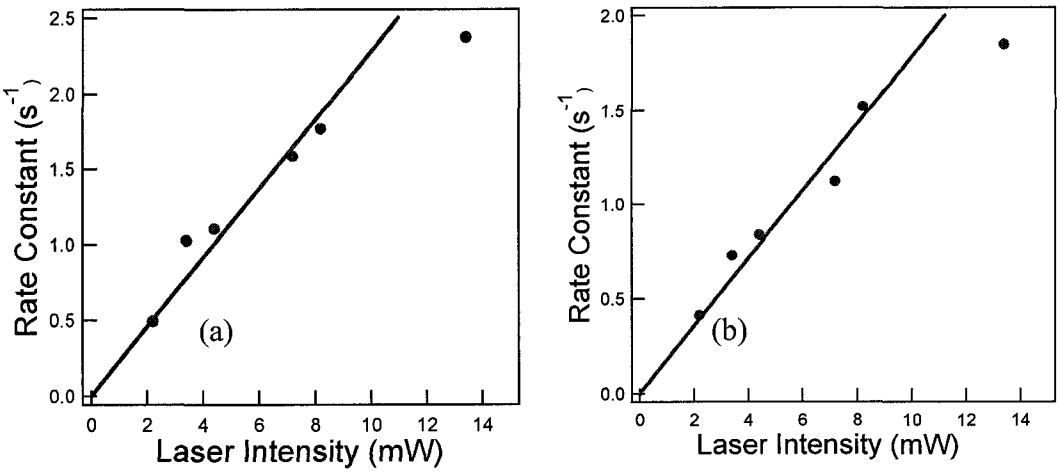

Figure 4.3. (a) The derived rate constant of the N3 dye photo-excitation at different laser intensities with (a), rutile (100) surface and (b), anatase (101) surface. Solid lines are from fitting.

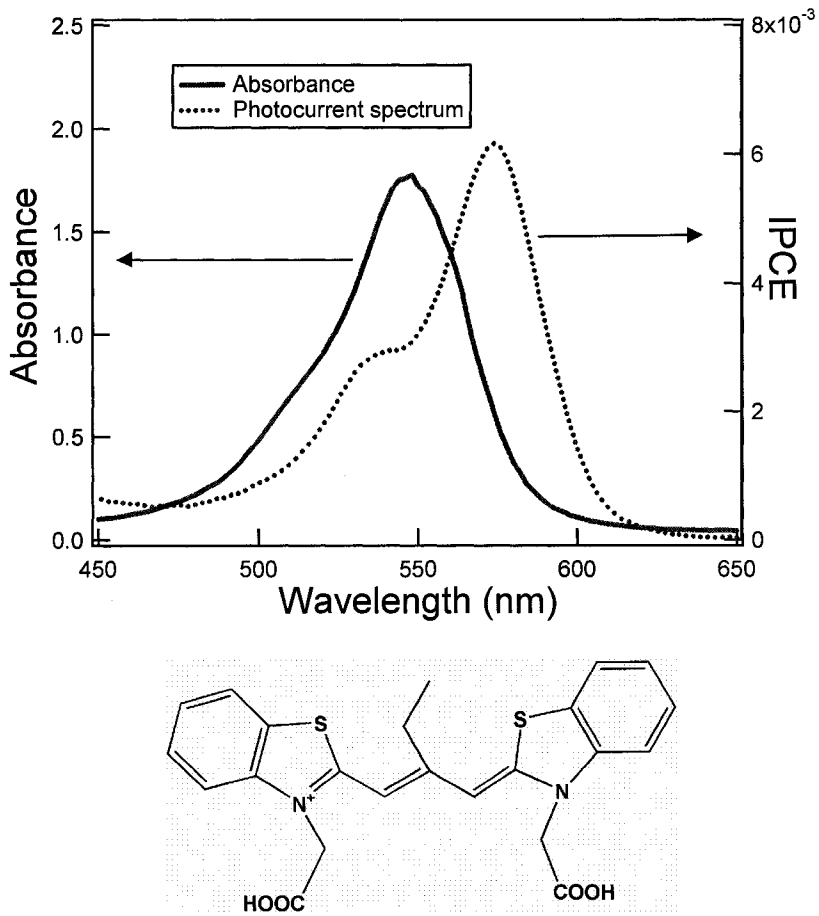

Figure 4.4. The molecular structure, solution absorption (solid line) and action spectrum (dashed line) of the G7 dye.

tested whether this process contributes to the charge in the second decay by measuring the photocurrent transient for the identical complex except with Cl^- ligands replacing the SCN^- in N3. The total integrated charge from the slow decay component was the same within experimental error for both ruthenium complexes. Another possibility for the slow decay would be the presence of small amounts of a reducing agent (regenerator) in the solution. Traces of hydroquinone, a regenerator used in previous sensitization experiments, adsorbed to the walls and frits of the electrochemical cell could contribute to this long decay. Therefore we cleaned the electrochemical cell in piranha solution prior to repeating the experiment. This resulted in a reduction of the charge in the second component by about 70%, presumably due to traces of hydroquinone still leaching from the walls and glass frits of the cell from previous sensitization measurements where hydroquinone was present in high concentrations (4.5 mM) as a regenerator. However even after consideration of both these mechanisms there is still an unaccounted-for charge that is up to 2.6 times larger than the charge in the fast component. The oxidized N3 dye adsorbed on nanocrystalline TiO_2 was reported to be stable for 75 min[18] and so any trace of reducing agent would be able to regenerate dye for at least this long. We attribute the persistent residual sensitization current to a regeneration by the small amount of water always present in acetonitrile that has been exposed to the atmosphere. The oxidized N3, or ruthenium containing decomposition products, have sufficient oxidation potential to oxidize water and even if there were only a few water oxidation sites the lateral charge transport observed for monolayers of N3 and related molecules on nanocrystalline TiO_2[9] would still allow for a small persistent regeneration of the photoactive dye.

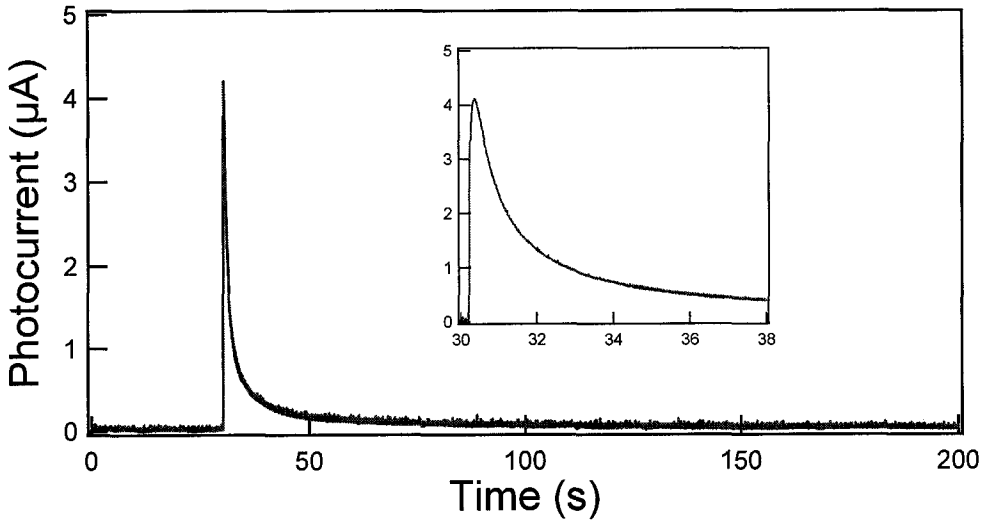

Figure 4.5. Transient photocurrent of the G7 dye adsorbed on rutile(100) surface. The inset shows a zoom-in of the graph.

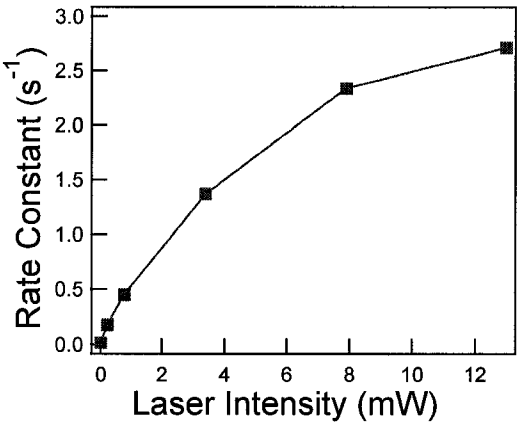

Figure 4.6. The derived rate constant of the photo-excitation of the G7 dye adsorbed on rutile (100) electrode at different laser intensities.

We also studied the photochronocoulometry of the single crystal rutile (100) surface with a dicaboxylated thiacyanine dye we call G7. The structure, absorption and action spectrum of G7 are shown in Figure 4.4. The sensitization of anatase (101) single crystal surfaces by this dye has already been reported.[7] The absorption spectrum peaks at 548 nm where only the monomer peak is present, whereas the photocurrent action spectrum is red-shifted by about 26 nm and also shows a sensitization peak associated with dimers. The structure of G7, with the ethyl group on the polyene bridge, prevents aggregation beyond the dimer.

Figure 4.5 shows the transient photocurrent generated from 532 nm laser illumination of G7 adsorbed onto a rutile (100) surface at an applied bias of 0.6 V. The photocurrent transient is similar to that measured for N3 and can also be fit with a double exponential decay however there are some distinct differences that will be discussed below. The monolayer coverage derived by integrating the fast decay component was 4.1 x 10^{-10} mol cm^{-2}. The integrated charge from the slow component was about twice that of the fast decay component (75-90 $\mu C/cm^2$). If the further oxidation occurs this accounts for about half of the charge from the slow decay component. The other half of the charge should be due to trace regenerator and water present in the solution as the case with the N3 study experiments discussed above.

The dependence of the transient current with laser intensity of G7 is shown in Figure 4.6. Interestingly the rate constant was proportional to the square root of the laser power rather than the expected linear dependence. The mechanistic explanation for the square root dependence on laser power is still unclear and needs further study. However

despite the lower than expected rate constant the charge associated with the fast decay component remained constant at 40 ± 3.0 $\mu C/cm^2$ at all laser intensities.

According to eq 3, the time constant for the decay of photocurrent should be proportional to the term $\varepsilon L_p \Phi [M]_o$. For comparable initial surface coverages ($[M]_o$), the decay of G7 should be faster than N3 since the ε for G7 is 5 times larger than N3 at the illumination wavelength (532 nm). Indeed, this faster decay is observed, as is evident in Figure 4.6 for the low intensity photolysis experiments. The surface area per molecule derived from the coulometry is 2.4 molecules nm^{-2} that is, like N3, nearly a close packed monolayer for this dye.

However, G7 has a much more complicated photochemistry than N3. Parton and Lenhard have reported that the oxidized dye radicals for these types of cyanine dyes can dimerize in solution after electrooxidation.[20] Thus the surface complement of oxidized G7 on TiO_2 should also be expected to dimerize. In addition, the electrochemical and absorption data for the dimer reveal that the dimer itself could sensitize photocurrent to the extent allowed by its internal photophysics.[20] The complexity of the G7 photochemistry is evident in the biphasic nature of the photochronocoulometric curve of Figure 4.6. The decline in photocurrent is preceded by a short 50-150 ms rise to the maximum, a feature that is not present in the N3 decay curves of Figure 4.5 where the maximum photocurrent is reached within the first several sampling intervals (10-20 ms). An analysis of the photocurrent decay in a photochronoamperometry experiments must therefore consider these following reactions:

$$2M^+ \rightarrow DH_2 \quad (5)$$

$$DH_2 \rightarrow D + 2H^+ \quad (6)$$

$$D + h\nu \rightarrow D^* \quad (7)$$

$$D^* \rightarrow D^+ + e^- \quad (8)$$

In reaction 5, the oxidized monomer dye dimerizes to produce the protonated dimer DH_2, which then subsequently releases two protons in reaction 6 to yield the dimer form D. Excitation of the dimer D may yield more photocurrent through reaction 8 and produce a singly oxidized dimer.

In the situation where D sensitizes photocurrent through reaction 8, a steady state approximation for M^+ in reactions 2 and 5 allows one to derive the following expression for the photocurrent:

$$I(t) = AF[\varepsilon(M)L_p\Phi[M]_o e^{-\varepsilon(M)Lp\Phi t} + 1/2[\varepsilon(M)/(\varepsilon(D) - \varepsilon(M))](\varepsilon(D)L_p\Phi[M]_o)\{e^{-\varepsilon(M)Lp\Phi t} - e^{-\varepsilon(D)Lp\Phi t}\}] \quad (9)$$

where Φ is the quantum yield for electron transfer for the excited sensitizers, assumed to be equal for M and D.

The first term in eq 9 is the same as eq 3 and represents the decay of the monomer form of the dye. The second term represents the contribution to the current from the dimer form of the dye as a sensitizer. It can be seen right away that the intensity dependence of the photocurrent of eq 9 will differ from that found for N3 in eq 3. However, the intensity dependence of the decay constant in eq 9 does not predict the observed behavior shown in Figure 4.6 where at higher light intensities, the slope of the photocurrent becomes sublinear. This behavior would be consistent with the action of a quenching agent produced through the photochemistry of eqs 5---8, a species that is produced in higher concentrations at higher light intensities. This species may be an energy transfer or electron transfer quencher, but the former is implied by the observation

that the integrated charge passed in the first fast decay is independent of light intensity: the first term in eq 9 is a function of light intensity.

A plausible species would be D^+, the radical dication form of the dimer since the dark oxidation of D is a two-electron process and the sensitization reaction 8 uses only one of the available electrons. It may also be that reaction 8 is negligible and the dimer itself then can serve as the quencher. With the available data, a definitive conclusion cannot be made for G7. A complete and thorough analysis of the complex photochemistry will require study of the dimer as a sensitizer as well as variations upon the structure of G7 that do not dimerize. These studies are currently underway.

4.5 Conclusion

Surface coverages of both the N3 dye and the thiacyanine dye G7 adsorbed onto atomically flat single crystal TiO_2 substrates was directly measured with the newly introduced photochronocoulometric method. This technique provides a simple method for the measurement of the amount of adsorbed dyes on semiconductor surfaces. The transient photocurrent can be fit with a double exponential decay function where the fast component is attributed to be the one electron oxidation of the dye. By varying the applied bias and laser intensity, the charge generated by the 1-electron oxidation process, and associated with the first decay, stayed constant whereas the rate constant displayed a linear relationship on laser power (for N3 dye) and square root of laser power (for G7 dye). Monolayer coverages of 1.0×10^{-10} mol cm^{-2} and 8.1×10^{-11} mol cm^{-2} for the N3 dye were measured for rutile (100) and anatase (101), respectively. For the smaller molecule G7, the surface coverage is 4.1×10^{-10} mol cm^{-2} on the rutile (100) surface.

Residual photocurrents were attributed to trace amounts of reducing agents, including water, that can regenerate the reduced dye at a slow rate. The example of G7 shows that complex photochemistry can be encountered on sensitized solids, however the coulometric approach offers another tool with which to study that photochemistry.

Acknowledgements

We thank C. Michael Elliott for donation of purified N3 dye and the dichloro N3 dye and for helpful discussions. This work was supported by the Department of Energy Office of Basic Energy Sciences under contract #DE-FG03-96ER14625

References:

1 Anson, F. C.; Christie, J. H.; Osteryoung, R. A., A Study of Adsorption of Cadmium(2) on Mercury from Thiocyanate Solutions by Double Potential-Step Chronocoulometry *Journal of Electroanalytical Chemistry* **1967**, *13*, 343.

2 Christie, J. H.; Osteryoung R. A.; Anson, F. C. Application of Double Potential-Step Chronocoulometry to Study of Reactant Adsorption Theory *Journal of Electroanalytical Chemistry* **1967**, *13*, 236.

3 Anson, F. C., Patterns of Ionic and Molecular Adsorption at Electrodes *Accounts of Chemical Research* **1975**, *8*, 400.

4 Turner, J. A.; Parkinson, B. A., The Application of Chronocoulometry to the Study of Adsorption at the Semiconductor Electrolyte Interface *Journal of Electroanalytical Chemistry* **1983**, *150*, 611.

5 Lu, Y.; Choi, D.J.; Nelson, J.; Yang, O.; Parkinson, B. A., Adsorption, Desorption and Sensitization of low Index Anatase and Rutile Surfaces by the Ruthenium *Journal of the Electrochemical Society,* **2006**, *153*, E131.

6 a. Fillinger, A.; Parkinson, B. A. The adsorption behavior of a rutheninm-based sensitizing dye to nanocrystalline TiO_2 - Coverage effects on the external and internal sensitization quantum yields *Journal of the Electrochemical Society* **1999**, *146*, 4559.
b. Fillinger A., Soltz, D. and Parkinson, B. A., Dye sensitization of natural anatase crystals with a ruthenium-based dye *Journal of the Electrochemical Society*, 149(9), A1146, (2002)

7 Ushiroda, S.; Ruzycki, N.; Lu, Y.; Spitler, M. T.; Parkinson, B. A. Dye sensitization of the anatase (101) crystal surface by a series of dicarboxylated thiacyanine dyes *Journal of the American Chemical Society* **2005**, *127*, 5158

8 Lu, Y.; Jaeckel, B.; Parkinson, B. A. Preparation and Characterization of Terraced Surfaces of Low-Index Faces of Anatase, Rutile, and Brookite *Langmuir* **2006**, *22*, 4472

9 Wang, Q.; Zakeeruddin, S. M.; Nazeeruddin, M. K.; Humphry-Baker, R.; Gratzel, M. Molecular wiring of nanocrystals: NCS-Enhanced cross-surface charge transfer in self-assembled Ru-complex monolayer on mesoscopic oxide films *Journal of the American Chemical Society* **2006**, *128*, 4446.

10 Spitler, M. T.; Calvin, M. Electron-Transfer at Sensitized TiO_2 Electrodes *Journal of Chemical Physics* **1977**, *66*, 4294.

11 Ryan, M. A.; Fitzgerald, E. C.; Spitler, M. T. Internal-Reflection Flash-Photolysis Study of the Photochemistry of Eosin at TiO_2 Semiconductor Electrodes *Journal of Physical Chemistry* **1989**, *93*, 6150.

12 Takeda, N.; Parkinson, B. A. Adsorption morphology, light absorption, and Sensitization yields for squaraine dyes on SnS_2 surfaces *Journal of the American Chemical Society* **2003**, *125*, 5559.

13 Bitterling, K.; Willig, F. Charge Carrier Dynamics in the Picosecond Time Domain in Photoelectrochemical Cells *Journal of Electroanalytical Chemistry* **1986**, *204*, 211.

14 Asbury, J. B.; Ellingson, R. J.; Ghosh, H. N.; Ferrere, S.; Nozik, A. J.; Lian, T. Q. Femtosecond IR study of excited-state relaxation and electron-injection dynamics of Ru(dcbpy)(2)(NCS)(2) in solution and on nanocrystalline TiO_2 and Al_2O_3 thin films *the Journal of Physical Chemistry B* **1999**, *103*, 3110.

15 Haque, S. A.; Palomares, E.; Cho, B. M.; Green, A. N. M.; Hirata, N.; Klug, D. R.; Durrant, J. R. Charge separation versus recombination in dye-sensitized nanocrystalline solar cells: the minimization of kinetic redundancy *Journal of the American Chemical Society* **2005**, *127*, 3456.

16 Ellingson, R. J.; Asbury, J. B.; Ferrere, S.; Ghosh, H. N.; Sprague, J. R.; Lian, T.; Nozik, A. J. Dynamics of Electron Injection in Nanocrystalline Titanium Dioxide Films Sensitized with [Ru(4,4'-dicarboxy-2,2'-bipyridine) 2 (NCS) 2] by Infrared Transient Absorption *the Journal of Physical Chemistry B* **1998**, *102*, 6455.

17 Bond, A. M.; Deacon, G. B.; Howitt, J.; MacFarlane, D. R.; Spiccia, L.; and Wolfbaur, G., Voltammetric determination of the reversible redox potential for the oxidation of the highly surface active polypyridyl ruthenium photovoltaic sensitizer cis-Ru-(II)(dcbpy)(2)(NCS)(2) *Journal of the Electrochemical Society* 1999, 146, 648

18 Kavan, L.; Gratzel, M.; Gilbert, S. E.; Klemenz, C.; Scheel, H. J. Electrochemical and photoelectrochemical investigation of single-crystal anatase *Journal of the American Chemical Society* **1996**, *118*, 6716.

19 Wang, P.; Wenger, B.; Humphry-Baker, R.; Moser, J.-E.; Teuscher, J.; Kantlehner, W.; Mezger, J.; Stoyanov, E. V.; Zakeeruddin, S. M.; Gratzel, M. Charge Separation and Efficient Light Energy Conversion in Sensitized Mesoscopic Solar Cells Based on Binary Ionic Liquids *Journal of the American Chemical Society* **2005**, *127*, 6850.

20 Parton, R. L.; Lenhard, J. R. Dimerization Reactions of Cyanine Radical Dications *Journal of Organic Chemistry* **1990**, *55*, 49.

Preface to Chapter 5

This chapter has been submitted for publication in Langmuir. Mark T. Spitler helped with the derivation of the equations and discussion of the results. All experimental data was obtained by me.

Chapter 5: Regenerator Dependent Photo-Induced Desorption of a Dicarboxylated Cyanine Dye from the Surface of Single Crystal Rutile

5.1 Abstract

The desorption starting at various surface coverages of a dicarboxylated thiacyanine dye from the surface of a single crystal rutile was studied. It was found that if hydroquinone was used as a regenerator the dye was desorbed when illuminated whereas no desorption was found under the same conditions when KI was used as the regenerator. Intermitant illumination experiments suggest that the oxidized regenerator (quinone) competes for dye adsorption sites. By comparing the photocurrent decay at both dye monomer sensitization maximum and the dimer sensitization maximum, a rearrangement of monomer into dimer was observed. A kinetic model for the photocurrent decay as a function of desorption time was derived and the desorption rate constants were obtained by fitting the experimental data to the model. The importance of stable surface bonding and appropriate choice of regenerator when constructing dye-sensitized solar cells is discussed.

5.2 Introduction

Dye-sensitized solar cells (DSSC) have attracted increasing interest due to the urgency of developing inexpensive solar energy converters.[1] The most efficient sensitizing dyes so far are a series of very stable Ru based complexes.[2, 3] There have been extensive efforts to discover inexpensive stable organic dye sensitizers to substitute for the ruthenium complexes due to the scarcity of the metal and the higher extinction coefficients of the organic dyes.[4-7] An efficient sensitizer should have strong electronic coupling to the semiconductor and be strongly bound to the semiconductor surface.

Dyes with the possibility of binding to the oxide surface with multiple covalent linkages are the most useful for dye sensitized solar cells. This is a result of the "chelate effect" where the dissociation of a single binding site will not result in desorption of the dye molecule and the possibility that two site binding can be reestablished either at the original or an adjacent binding site. Desorption of a chelated dye will only occur in the relatively unlikely event of dissociation of the second binding group before reattachment of the first group.

At low coverages there is little competition for binding sites on the surfaces and most dye molecules will be able to attach by more than one carboxylate group. However at high dye coverages it is likely that many dyes will be attached by only one group, due to the lack of nearby binding sites. These "one legged dyes" should be more susceptible to desorption. The binding of the ruthenium complex dye N3 upon adsorption onto TiO_2 surfaces is complicated due to the number of carboxylate groups of the molecule[8-10] and the possible existence of dye aggregates[11]. We have reported studies of dye/TiO_2

interfacial structures by using atomically flat TiO_2 single crystal surfaces sensitized by structurally more simple organic dye molecules,[12] since we believe the use of atomically flat single crystals will make the binding mechanism more easily understood. However, the desorption kinetics of the covalently bound dyes from the TiO_2 surface and whether the aggregates and monomers are interconverting on the surface has not been studied .

Since high dye coverages are needed to optimize the performance of dye sensitized solar cells, desorption of the sensitizing dyes after adsorption onto TiO_2 surfaces needs to be minimized. Herein we report studies of the desorption and rearrangement of a dicarboxylated cyanine dye covalently bound to an atomically flat single crystal rutile surface and the effect of the identity of the regenerator on the desorption process.

5.3 Experimental

Rutile crystals with a (100) orientation were purchased from Commercial Crystal Laboratories, LTD. Atomically flat terraces were obtained as described earlier.[13] Atomic Force Microscopy (AFM) (Digital Instruments Nanoscope IIIA controller and a multimode SPM) was used to verify that the polished surfaces were flat and showed characteristic terraces. Silicon AFM tips from MikroMasch with a 40 N/m force constant and resonant frequency around 170 KHz were used.

The rutile (100) crystal was mounted as an electrode using epoxy (Dexter Epoxy Patch) with Ga/In eutectic applied to the back of the crystal for an ohmic contact. After the epoxy set, the back and edges of the electrode were sealed with silicone rubber (RTV) and allowed to dry for a few hours. Prior to photoelectrochemical experiments the crystal

was polished with a soft polishing cloth using 20 nm colloidal silica (Buehler, inc) and cleaned with 0.2 M NaOH, followed by a MilliQ (18 MΩ) water rinse. The electrodes were then cleaned with photooxidation by illuminating at 0.6 V vs Ag/AgCl in 10 mM $NaClO_4$ for 5 minutes using an Oriel 150 W Xe lamp followed by an ethanol (Pharmaco, ACS grade) rinse. To allow more UV illumination to reach the sample surface a quartz electrochemical cell was used.

A dicarboxylated thiacyanine dye (G15, structure shown in Figure 1) was dissolved in ethanol to make a series of different solutions with varying concentrations that were used to adsorb the dyes to the cleaned crystal surface. The apparatus for photocurrent spectra measurements was the same as reported previously.[10] The photocurrent as a function of time was collected at several fixed wavelengths (574 nm or 530 nm) using the same apparatus. A three-electrode configuration with a platinum counter electrode and a Ag/AgCl reference electrode was used in the electrochemical cell. Acetonitrile (Fisher, optima grade) containing 10 mM tetrabutylammonium perchlorate (Fluka, electrochemical grade) was used as a supporting electrolyte with 4.5 mM hydroquinone or 2 mM KI added as supersensitizer or regenerator. The experimental data (both absorption spectrum and photocurrent action spectra as a function of photon energy) were fit to a combined Gaussian and Lorentzian peak shape using Igor Pro software from WaveMetrics. Values for the relative position and intensity ratio of the main peak and shoulder for the dye monomer obtained from the solution spectrum were used to fit the photocurrent spectra. Values for the blue shifted aggregate peak and another aggregate peak, which is masked by the monomer peak, used in the fitting were taken from the literature.[14]

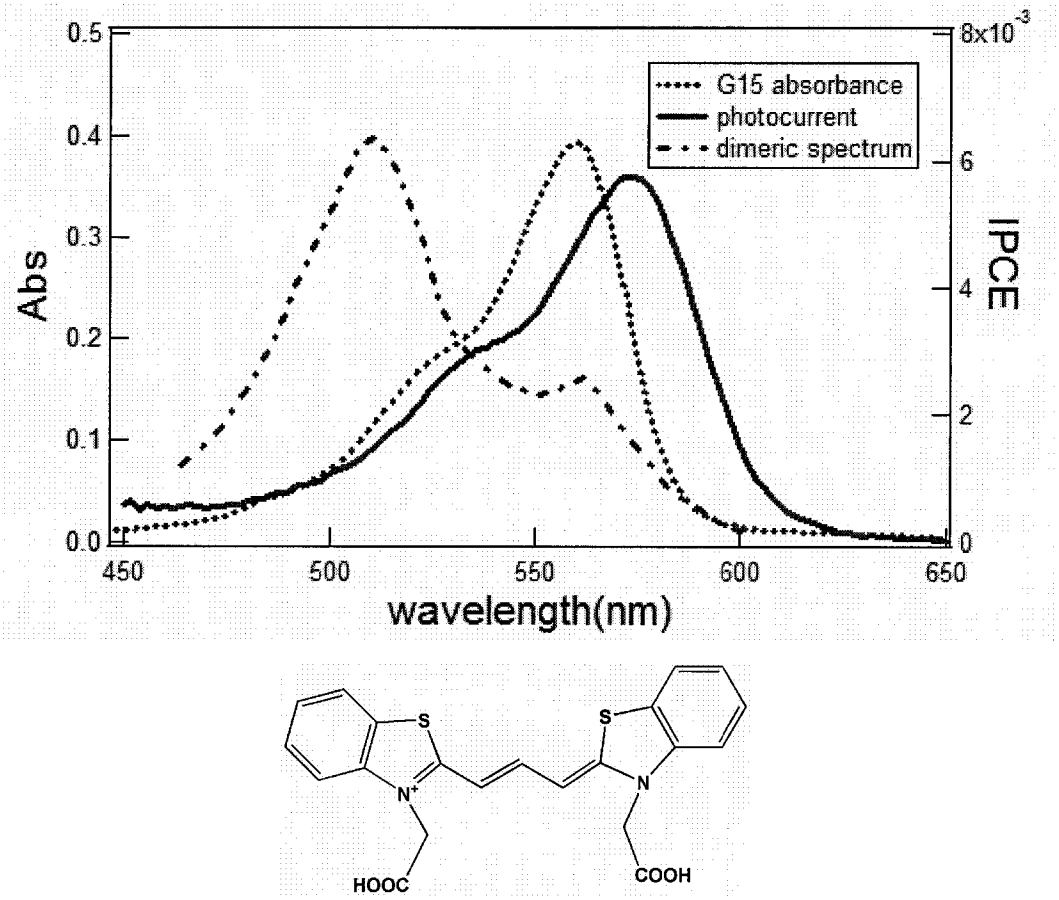

Figure 5.1. The molecular structure, solution absorption (dashed line) and action spectrum adsorbed on rutile (100) surface (solid line) of the G15 dye from an ethanol solution. The dashed-dotted line shows the dimeric spectrum taken from ref. 14.

5.4 Results

The molecular structure of G15, its solution absorption spectrum and photocurrent action spectrum adsorbed onto a rutile (100) surface are shown in Figure 5.1. The solution absorption peaks at 562 nm with a shoulder on the blue side of the main peak. When adsorbed onto a single crystal rutile (100) surface, the photocurrent action spectrum shows a monomer peak red-shifted about 12 nm together with a broadened blue-shifted dimer/aggregate peak at 549 nm. Given the role of dimers in this work, the spectrum of a pure dimeric trimethane thiacyanine dye in solution from reference 21 is provided in Figure 5.1. At its maximum at 530 nm, its extinction coefficient is 5 x 10^4 cm^2/mmole whereas the extinction coefficient of the monomer at its maximum is reported to be 1.5 x 10^5 cm^2/mmole.

Figure 5.2a shows photocurrent spectra from which the isotherm for G15 adsorbed onto a rutile (100) surface was obtained using hydroquinone as the regenerator (Figure 5.2b). The incident photon-to-current conversion efficiency (IPCE), which we assume is linearly proportional to the dye coverage, increases with the increase of G15 dye solution concentration (Figure 5.2a) and plateaus at higher concentrations. Figure 5.2b shows the fraction of monomer and dimer present on the surface, which were obtained from fitting the photocurrent action spectra in Figure 5.2a to the observed and calculated monomer and dimer spectra of trimethine cyanine dyes.[14] Although monomer is the predominant adsorbed species, there is still a significant amount of dimer present making it possible to study the desorption of both the monomer and dimer of the adsorbed G15 dye.

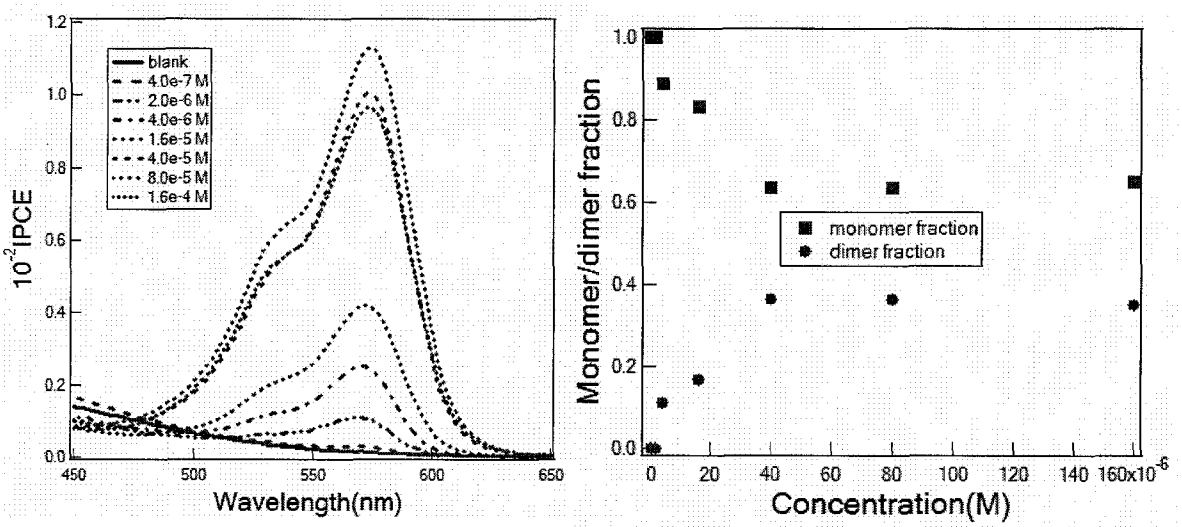

(a) (b)

Figure 5.2. (a)Increase of the sensitized photocurrent with increasing concentration of G15 adsorbed onto rutile (100) electrode and, (b) monomer and dimer fractions derived from fitting the photocurrent action spectra.

When KI was used as a reducing agent to regenerate the oxidized G15 dye molecules, the sensitized photocurrent is very stable with time suggesting that there is very little desorption of the dye, as shown in Figure 5.3 (dotted line). However when hydroquinone was used as the regenerator, a decrease in the photocurrent with time was observed. We interpret this as evidence that hydroquinone and/or the oxidation products of hydroquinone, such as a semiquinone, or more formally a quinone, compete for binding sites with the cyanine dye molecules.[15] There is precedent for this since Ryan et al.[14] have previously used hydroquinone as a regenerator for sensitizing rutile crystals and found out that it competes with dye adsorption. Also the extremely strong adsorption of a structurally similar molecule, catechol, onto TiO_2 surfaces has been studied extensively both experimentally and theoretically.[16-18] To determine if desorption of the G15 dye from the oxide surface was caused by the competitive adsorption of hydroquinone or the produced quinone, we performed an experiment where the sensitized photocurrent was monitored while periodically blocking the illumination. The solid line in Figure 5.3 shows that when the light beam was blocked the photocurrent went to zero and when illumination was restored the photocurrent returned to the previous value or in some cases even to a bit higher value rather than a value obtained from extrapolating the original decay trend (dashed line in Figure 5.3). The fact that no photocurrent decrease was observed when no quinone was being produced at the surface demonstrates that it is quinone that competitively binds to the oxide surface and replaces the adsorbed G15 dye molecules resulting in a photocurrent decrease. A possible explanation for the photocurrent being larger upon re-illumination would be that the APCE for a dye adsorbed by only one leg is lower than the APCE for a dye bound at two sites due to less

strong electronic coupling for electron injection. In the dark, when no quinone is being produced, one legged dyes have time to re-establish binding at two sites by finding an unoccupied site or by desorption of a quinone from an adjacent site due to the lower surface quinone concentration during the dark period. We also tested the time dependence of the desorption process at hydroquinone concentrations of 0.45 mM and 45 mM but no difference in the desorption rate was observed, providing further evidence that the dyes were replaced by photogenerated quinone that is produced at a constant rate regardless of the hydroquinone concentration.

Figure 5.4 shows the decay of the photcurrent for G15 excited at a wavelength of 574 nm and collected for 1800 seconds for four different surface concentrations of the dye. The observed current declines monotonically and we associate this decay with the desorption of the dye. At the monomer absorption maximum of 574 nm the spectra of Figure 5.2 shows the monomer absorption dominates at this wavelength compared to the dimer. The photocurrent decay data collected at 530 nm, where the dimer absorption is substantial, are shown in Figure 5.5. The striking feature of this data is the presence of an increase in the sensitized photocurrent at early times.

5.5 Discussion

The photocurrent decays at 530 nm and 574 nm can be modeled to gain insight into their differing behavior. A G15 covered TiO_2 surface contains dye dimers/aggregates and two different types of monomers: one that has only one bound carboxylate group and that is displaced easily; and the other that is less likely to be displaced by quinone that has both carboxylate groups bound. Dimers with three groups attached to the surface are

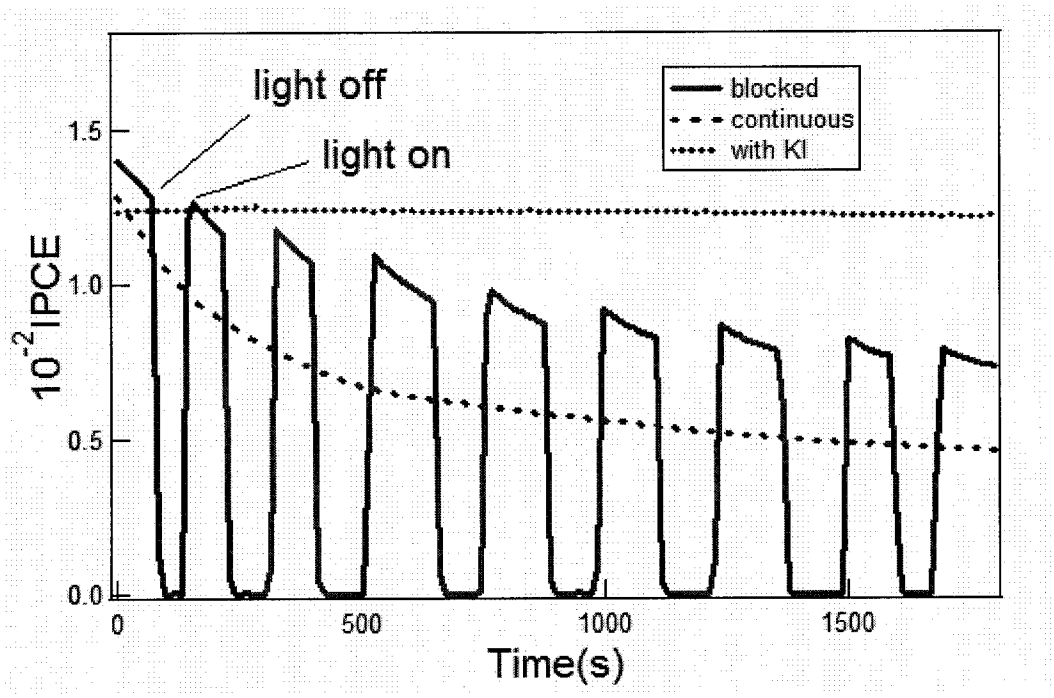

Figure 5.3. Photocurrent as a functiopn of time for G15 dye adsorbed onto a rutile (100) surface excited at 574 nm. The solid line represents an experiment where the light beam was manually blocked and unblocked as indicated on the graph. The dashed line represents a photocurrent decay plot under continuous illumination. The dotted line shows the photocurrent response with time when KI is used as the regenerator instead of hydroquinone.

not differentiated from dimmers with four attachments in our model. The surface fractional coverage of dye θ by these various forms of the dye can then be expressed as:

$$\theta = \theta_1 + \theta_2 + \theta_3 \qquad (1)$$

where θ_1 is the fractional coverage dyes with a single surface bond; θ_2 is the fractional coverage of monomers with two surface attachments and θ_3 is the fractional coverage of dimers.

This displacement phenomenon can be modeled and used to interpret the form and rate of the observed photocurrent decline. One first begins with the displacement of the monomeric dyes by the quinone on the surface. These attached monomeric dyes will be displaced and dissolve into the electrolyte once the titanium-carboxylate bonds dissociate according to the following reaction scheme:

$$D_T \underset{k_{-1}}{\overset{k_1}{\rightleftharpoons}} D_{ST} \xrightarrow{k_2} D_d$$

$$D_S \xrightarrow{k_2} D_d$$

where D_T and D_S refer to dyes originally bound with two carboxylate groups (θ_2) and those bound with one carboxylate group (θ_1), respectively. D_T becomes D_{ST} after losing one bond with rate k_1, and k_{-1} is the reattachment rate constant. D_{ST} and D_S are essentially the same but only D_{ST} portion of the one-legged dye is in equilibrium with D_T. After losing one more bond with a rate constant of k_2, these dyes dissolve into the

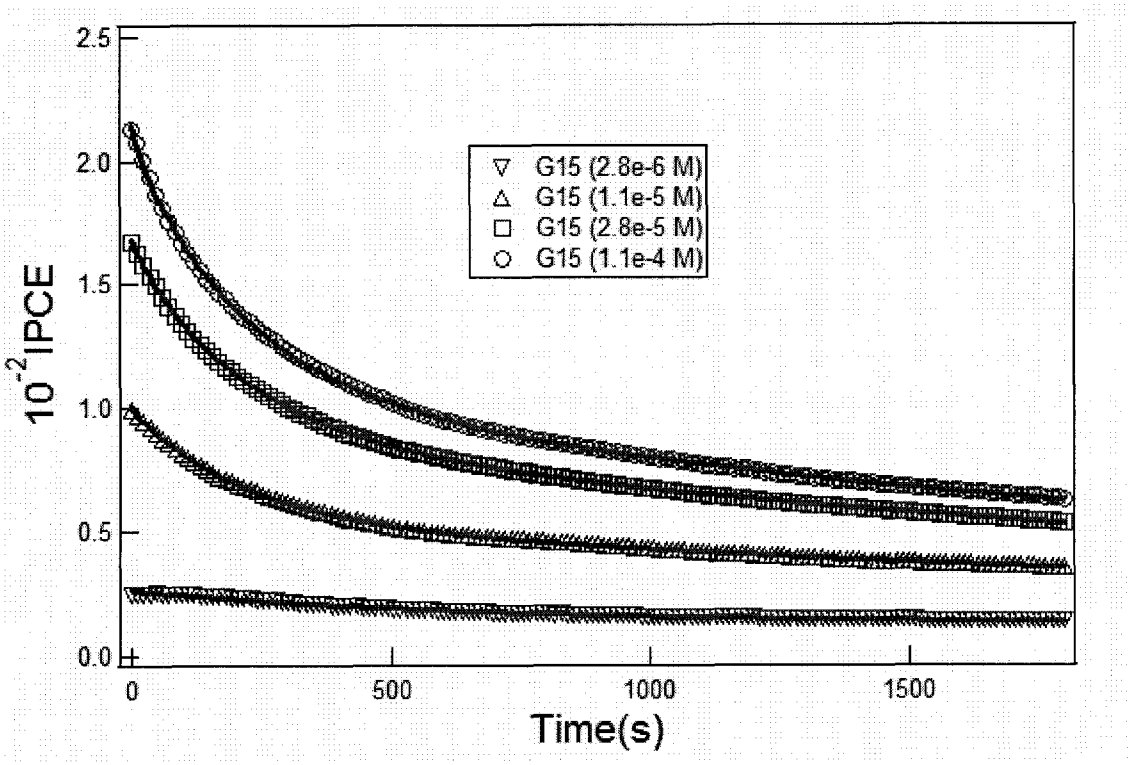

Figure 5.4. Sensitized photocurrent decay measurements for G15 dye adsorbed on a rutile (100) surface collected by illuminating at the monomer absorption maximum (574 nm). The decrease in photocurrent is due to monomer dye desorption. Solid lines are from fitting.

electrolyte (D_d). For dimers, the desorption process is more complicated. The dimer form of the adsorbed dye molecules is in equilibrium with monomers, which can then desorb as discussed above. Because the dimer fraction is small and in equilibrium with monomers, we incorporate monomers released from dimers into the desorption equations for D_T and D_{ST}, represented by the equilibrium constant K (k_1/k_{-1}) discussed later.

Since there is no dye dissolved in the electrolyte, under continuous illumination quinone will be constantly produced at the surface and therefore we assume the path from single carboxylate bound dyes to dissolved dyes is irreversible. If the desorption process for these dye molecules is assumed to be a first order reaction, then the following rate equations can be written (assuming fast equilibrium between D_T and D_{ST}):

$$-\frac{d[D_T]}{dt} = -\frac{d[D_{ST}]}{dt} = k_2[D_{ST}] = k_2\frac{k_1}{k_{-1}}[D_T] = k_2K[D_T] \tag{2}$$

$$-\frac{d[D_S]}{dt} = k_2[D_S] \tag{3}$$

where K is the equilibrium constant between D_T and D_{ST} (k_1/k_{-1}). After integration, we obtain the original monomer surface coverage as a function of time t (in seconds):

$$\theta(t) = \exp\left(\ln\theta_1^{\,0} - k_2 t\right) + \exp\left(\ln\theta_2^{0} - k_2 K t\right) \tag{4}$$

It is also possible for two monomers to rearrange themselves into a dimer according to

$$2 \text{ monomer} \xrightarrow{k_{md}} \text{dimer}$$

with a rate expression given by:

$$-\frac{d[C_m]}{dt} = k_{md}[C_m]^2 \qquad (5)$$

$$\theta_L = \theta_{[C_m]^0} - \theta_{[C_m]_t} = \theta_{[C_m]^0} - \frac{1}{\frac{1}{\theta_{C_m^0}} + k_{md} N_0 t} \qquad (6)$$

where equation (6) is obtained by integrating equation (5); k_{md} is the rate constant of dimer formation in $cm^2\ mol^{-1}\ s^{-1}$; $[C_m]^0$ is the original proportion of monomers that are able to reorganize into dimers; $[C_m]_t$ is the remaining proportion of monomer that will reorganize into dimer at time t; θ_L is the amount of monomer lost due to dimerization and N_0 is the full monolayer coverage on the surface (1.4×10^{-10} mol/cm^2) determined using the photocoulometric measurement reported previously.[19] Therefore, equation (4) should be corrected to:

$$\theta(t) = \exp\left(\ln \theta_1^{\,0} - k_2 t\right) + \exp\left(\ln \theta_2^{0} - k_2 K t\right) - \theta_L \qquad (7)$$

Equation (8) is obtained after integration of equation (5) and plugging equation (6) back into equation (7):

$$\theta(t) = \exp\left(\ln \theta_1^{\,0} - k_2 t\right) + \exp\left(\ln \theta_2^{0} - k_2 K t\right) - \left(\theta_{C_m{}^0} - \frac{1}{\frac{1}{\theta_{C_m{}^0}} + k_{md} N_0 t} \right) \qquad (8)$$

where $\theta_{Cm}{}^0$ is the original fractional coverage of $C_m{}^0$.

We measured the dye desorption rate by following the sensitized photocurrent at a particular wavelength as a function of time in an electrolyte containing no dye. Assuming the sensitized photocurrent is proportional to dye surface coverage, we obtained photocurrent as a function of time in equation (9) by multiplying by constants to convert coverage per unit time to photocurrent density the same way as reported previously.[19]

$$J(t) = \varepsilon_m(\lambda) L_P \Phi_S A F N_0 \left[\exp\left(\ln \theta_1^{\,0} - k_2 t\right) + \exp\left(\ln \theta_2^{0} - k_2 K t\right) - \left(\theta_{C_m{}^0} - \frac{1}{\frac{1}{\theta_{C_m{}^0}} + k_{md} N_0 t} \right) \right] \qquad (9)$$

In the above equation, $\varepsilon_m(\lambda)$ is the monomer light absorption cross section for the dye at wavelength λ, L_p is the photon flux in mol cm^{-2} s^{-1}, Φ_s is the photochemical yield for electron transfer from a single monomer, A is the illuminated surface area of the TiO_2 electrode in cm^2 and F is the Faraday constant.

The monomer and dimer forms of the dye overlap over the entire spectral range of their absorption. Therefore there are contributions from both monomer and dimer to the photocurrent generation and the expression of the total surface coverage will contain another term θ_3, the fractional coverage of dimers as shown in equation (1). Taking into

account the original dimer fraction on the surface, the time dependent dimer coverage will then be:

$$\theta_3 = \theta_{[C_d]^0} + \theta_L = \theta_{[C_d]^0} + \theta_{[C_m]^0} - \theta_{[C_m]_t} \tag{10}$$

where $\theta_{[Cd]}{}^0$ is the original fractional coverage of dimers on the surface before any rearrangement occurs and θ_L is the same as defined in equation (6).

By plugging equation (6) into equation (10) and adding θ_3 to equation (9) and converting coverage to photocurrent, the overall currrent at any wavelength can be seen to be:

$$J(t) = \varepsilon_m(\lambda) L_P \Phi_S AF \left\{ \left[\exp\left(\ln \theta_1{}^0 - k_2 t\right) + \exp\left(\ln \theta_2^0 - k_2 Kt\right) - \left(\theta_{C_m{}^0} - \frac{1}{\frac{1}{\theta_{C_m{}^0}} + k_{md} N_0 t} \right) \right] + \frac{\varepsilon_d(\lambda)\Phi_d}{\varepsilon_m(\lambda)\Phi_S} \left(\theta_3{}^0 + \theta_{C_m{}^0} - \frac{1}{\frac{1}{\theta_{C_m{}^0}} + k_{md} N_0 t} \right) \right\} \tag{11}$$

where $\varepsilon_d(\lambda)$ is the absorption cross section at λ of the dimer in $cm^2\ mol^{-1}$; Φ_d is the photochemical yield for dimer electron transfer. As discussed earlier, the first three terms in equation (11) decrease with time and describe the desorption of monomers. But the rearrangement of monomers into dimers increases the dimer coverage. At excitation wavelengths where the dimer extinction is greater than the monomer, this increase in dimer coverage should result in a net increase in current upon illumination. This is indeed what is observed and appears to be the only reasonable explanation for an increase in photocurrent while dye desorption is occurring.

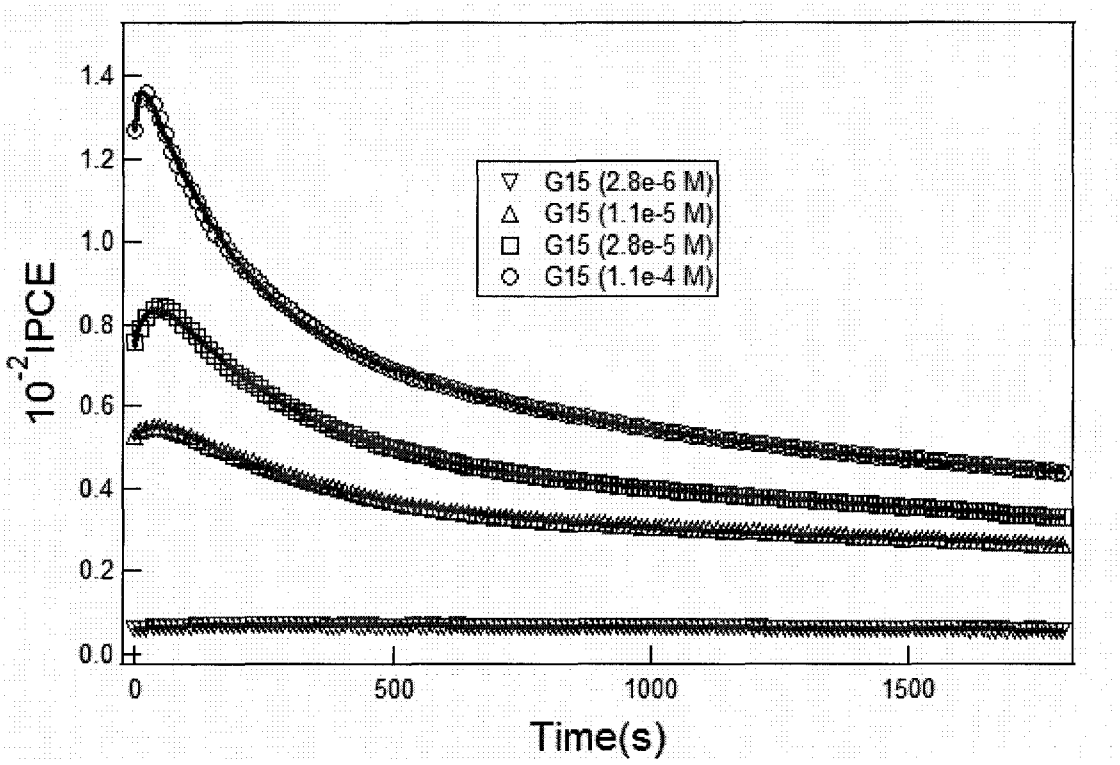

Figure 5.5. Sensitized photocurrent decay measurements for G15 dye adsorbed on a rutile (100) surface collected by illuminating at the dimer absorption maximum (530 nm). The change in photocurrent is from a combined effect of both dimer formation and monomer desorption. Solid lines are from fitting.

A fitting of the decay curves of the photocurrent at 530 nm and 574 nm to Equation (11) should yield the same values for the kinetic and thermodynamic constants in Equation (11). By fitting the desorption data using a $\varepsilon_d/\varepsilon_m$ ratio of 0.30 at monomer absorption maximum and 3.235 at dimer absorption maximum, we obtained the equilibrium constant K and desorption rate constant k_2 as shown in Table 5.1. We assume the Φ_d/Φ_s ratio is eaual to 1 in our fits. At the smallest concentration (2.8×10^{-6} M), the photocurrent can only be successfully fit by a single exponential function. We interpret this to indicate that at small coverages most of the dyes can get two legs down so there are virtually no dyes on the surface that are bound with only one carboxylate group. Since the coverage is very small, the rearrangement from monomers into dimers should also be negligible. In such a case we are only able to derive values for the product of K and k_2. At higher surface concentrations, the rate constants K and k_2 remain constant within experimental error.

Table 5.1: Monomer desorption coefficients and rate constant of monomer to dimer reorganization of G15 with Rutile (100)

Concentration(M)	**K**	**$k_2(s^{-1})$**	**k_{md} ($cm^2 \cdot mol^{-1} \cdot s^{-1}$)**
2.8×10^{-6}	$1.4 \times 10^{-3}/k_2$	$1.4 \times 10^{-3}/K$	N/A
1.1×10^{-5}	0.10	4.6×10^{-3}	4.8×10^{7}
2.8×10^{-5}	0.16	5.2×10^{-3}	2.6×10^{8}
1.1×10^{-4}	0.15	5.3×10^{-3}	3.5×10^{8}

It can be seen from Figure 5.5 that the rearrangement is very fast compared to the monomer desorption resulting in an initial photocurrent increase due to dimer formation on the electrode surface. Later, when most of the dimer formation is complete, monomer desorption is responsible for the decrease in photocurrent which decays with a multi-exponential dependence. Because of the contribution of dimer and the continuous transformation of dimer into monomers, the desorption behavior is more complicated at this wavelength and the error in the determination of the rate constants is probably larger. By comparing the action spectra obtained within the first 3 min of the desorption experiment and after the desorption progressed for 30 min, an increase in the dimer/monomer ratio was measured, providing additional evidence that the initial increase in photocurrent is a result of the dimerization of dye molecules on the surface.

Khazraji et al. reported that the dimer electron injection yield is lower than that of a monomer in a merocyanine dye-sensitized solar cell.[20] In other studies, aggregated dyes were also found to decrease the solar energy conversion performance.[21] It was suggested that there are quenching processes due to energy transfer or charge transfer reactions between the aggregated dye molecules and/or between monomers and aggregated molecules. In our case the monomers and aggregates are both strongly bound to the surface and due to the fast injection expected from the excited states aggregation should not greatly affect the quantum yields in our case and we then assume their quantum yield ratio to be 1 as mentioned previously.

We have previously studied the sensitization of single crystal oxide surfaces with the ruthenium based dye N3. N3 binds to the surface very strongly and no desorption was observed within the experimental time frame used herein even when hydroquinone

was used as the regenerator.[10,22] The G15 dye studied herein yields initially higher IPCE values than those measured for N3 on the same crystal surface (rutile (100)) probably due to the higher extinction coefficient of the G15 dye (1.0×10^5 M^{-1} cm^{-1} vs 1.42×10^4 M^{-1} cm^{-1} for N3). However if hydroquinone is used as a regenerator the desorption of the G15 dye occurs and the binding sites are rapidly occupied by quinone and more than half of the originally adsorbed dyes are lost in about 20 minutes, demonstrating the vital importance of choosing the right regenerator for optimal performance of a dye cell. To fabricate a more efficient organic dye-sensitized TiO_2 solar cell, a cheap sensitizer needs to be developed that binds as strongly as the N3 dye together with the use of an appropriate regenerator.

5.6 Conclusion

We have studied the desorption behavior of the dicarboxylated thiacyanine dye G15 covalently bound to single crystal rutile (100) surface. Upon adsorption, both G15 monomer and dimer exist on the surface and a rearrangement of the G15 dye from monomer to dimer was observed. If iodide is used as a regenerator no dye desorption is observed when the surface is illuminated however if hydroquinone was used as the regenerator its photooxidation product (quinone) displaces adsorbed dyes. A mechanism that takes into account the various forms of the dye present on the surface was developed. By fitting the experimental data with the proposed mechanism, desorption and dimer formation rate constants were successfully derived. Studies of desorption kinetics shed light onto the binding of dye sensitizers to the TiO_2 surface and the rearrangement of dye molecules on the surface.

References:

1. Oregan, B. and Gratzel, M., *A Low-Cost, High-Efficiency Solar-Cell Based on Dye-Sensitized Colloidal TiO_2 Films.* Nature, 1991. 353(6346): p. 737-740.

2. Nazeeruddin, M.K., Pechy, P., Renouard, T., Zakeeruddin, S.M., Humphry-Baker, R., Comte, P., Liska, P., Cevey, L., Costa, E., Shklover, V., Spiccia, L., Deacon, G.B., Bignozzi, C.A., and Gratzel, M., *Engineering of efficient panchromatic sensitizers for nanocrystalline TiO_2-based solar cells.* Journal of the American Chemical Society, 2001. 123(8): p. 1613-1624.

3. Nazeeruddin, M.K., Humphry-Baker, R., Liska, P., and Gratzel, M., *Investigation of sensitizer adsorption and the influence of protons on current and voltage of a dye-sensitized nanocrystalline TiO_2 solar cell.* The Journal of Physical Chemistry B, 2003. 107(34): p. 8981-8987.

4. Horiuchi, T., Miura, H., and Uchida, S., *Highly-efficient metal-free organic dyes for dye-sensitized solar cells.* Chemical Communications, 2003(24): p. 3036-3037.

5. Horiuchi, T., Miura, H., Sumioka, K., and Uchida, S., *High Efficiency of Dye-Sensitized Solar Cells Based on Metal-Free Indoline Dyes.* Journal of the American Chemical Society, 2004. 126(39): p. 12218-12219.

6. Thomas, K.R.J., Lin, J.T., Hsu, Y.C., and Ho, K.C., *Organic dyes containing thienylfluorene conjugation for solar cells.* Chemical Communications, 2005(32): p. 4098-4100.

7. Hara, K., Wang, Z.S., Sato, T., Furube, A., Katoh, R., Sugihara, H., Dan-Oh, Y., Kasada, C., Shinpo, A., and Suga, S., *Oligothiophene-containing coumarin dyes for efficient dye-sensitized solar cells.* The Journal of Physical Chemistry B, 2005. 109(32): p. 15476-15482.

8. Shklover, V., Ovchinnikov, Y.E., Braginsky, L.S., Zakeeruddin, S.M., and Gratzel, M., *Structure of organic/inorganic interface in assembled materials comprising molecular components. Crystal structure of the sensitizer bis (4,4 '-carboxy-2,2 '-bipyridine)(thiocyanato) ruthenium(II).* Chemistry of Materials, 1998. 10(9): p. 2533-2541.

9. Fillinger, A. and Parkinson, B.A., *The adsorption behavior of a rutheninm-based sensitizing dye to nanocrystalline TiO_2 - Coverage effects on the external and internal sensitization quantum yields.* Journal of the Electrochemical Society, 1999. 146(12): p. 4559-4564.

10. Lu, Y., Choi, D., Nelson, J., Yang, O., and Parkinson, B.A., *Adsorption, Desorption and Sensitization of low Index Anatase and Rutile Surfaces by the*

Ruthenium Complex Dye N3. Journal of the Electrochemical Society, 2006. 153(8): p. E131-E137.

11. Neale, N.R., Kopidakis, N., vandeLagemaat, J., Gratzel, M., and Frank, A.J., *Effect of a Coadsorbent on the Performance of Dye-Sensitized TiO_2 Solar Cells: Shielding versus Band-Edge Movement.* The Journal of Physical Chemistry B, 2005. 109(49): p. 23183-23189.

12. Ushiroda, S., Ruzycki, N., Lu, Y., Spitler, M.T., and Parkinson, B.A., *Dye sensitization of the anatase (101) crystal surface by a series of dicarboxylated thiacyanine dyes.* Journal of the American Chemical Society, 2005. 127(14): p. 5158-5168.

13. Lu, Y., Jaeckel, B., and Parkinson, B.A., *Preparation and Characterization of Terraced Surfaces of Low-Index Faces of Anatase, Rutile, and Brookite.* Langmuir, 2006. 22(10): p. 4472-4475.

14. West, W. and Pearce, S., *Dimeric State of Cyanine Dyes.* Journal of Physical Chemistry, 1965. 69(6): p. 1894-&.

15. Ryan, M.A., Fitzgerald, E.C., and Spitler, M.T., *Internal-Reflection Flash-Photolysis Study of the Photochemistry of Eosin at TiO_2 Semiconductor Electrodes.* Journal of Physical Chemistry, 1989. 93(16): p. 6150-6156.

16. Connor, P.A., Dobson, K.D., and McQuillan, A.J., *New Sol-Gel Attenuated Total-Reflection Infrared Spectroscopic Method for Analysis of Adsorption at Metal-Oxide Surfaces in Aqueous-Solutions - Chelation of TiO_2, ZrO_2, and Al_2O_3 Surfaces by Catechol, 8-Quinolinol, and Acetylacetone.* Langmuir, 1995. 11(11): p. 4193-4195.

17. Araujo, P.Z., Morando, P.J., and Blesa, M.A., *Interaction of catechol and gallic acid with titanium dioxide in aqueous suspensions. 1. Equilibrium studies.* Langmuir, 2005. 21(8): p. 3470-3474.

18. Redfern, P.C., Zapol, P., Curtiss, L.A., Rajh, T., and Thurnauer, M.C., *Computational studies of catechol and water interactions with titanium oxide nanoparticles.* The Journal of Physical Chemistry B, 2003. 107(41): p. 11419-11427.

19. Lu, Y., Spitler, M.T., and Parkinson, B.A., *Photochronocoulometric Measurement of the Coverage of Surface-Bound Dyes on Titanium Dioxide Crystal Surfaces.* The Journal of Physical Chemistry B, 2006. 110: p. 25273.

20. Khazraji, A.C., Hotchandani, S., Das, S., and Kamat, P.V., *Controlling dye (Merocyanine-540) aggregation on nanostructured TiO_2 films. An organized*

assembly approach for enhancing the efficiency of photosensitization. The Journal of Physical Chemistry B, 1999. 103(22): p. 4693-4700.

21. Hara, K., Dan-Oh, Y., Kasada, C., Ohga, Y., Shinpo, A., Suga, S., Sayama, K., and Arakawa, H., *Effect of additives on the photovoltaic performance of coumarin-dye-sensitized nanocrystalline TiO_2 solar cells.* Langmuir, 2004. 20(10): p. 4205-4210.

22. Fillinger, A., Soltz, D., and Parkinson, B.A., *Dye sensitization of natural anatase crystals with a ruthenium-based dye.* Journal of the Electrochemical Society, 2002. 149(9): p. A1146-A1156.

Chapter 6: Probing Cyanine Dyes Adsorbed onto Anatase(101) Surface with Atomic Force Microscopy

6.1 Introduction

Molecular self-assembly into supramolecular structures has drawn a lot of research interest recently due to their role in biology and molecular electronics. The ability to control the types of aggregation will open this area to further technological applications.

Cyanine dyes have a well demonstrated ability to form two types of aggregates: H and J aggregates. J aggregates are characterized by a sharp, narrow absorption band red-shifted compared to the monomer absorption band;[1-3] while H aggregates with a blue-shifted absorption band.[4] When the molecular long axes are tilted more than 54° from the line connecting the centers of the moledules, the aggregate is usually considered H—type and J-type aggregate has an angle of less than 54°. The spectroscopic properties and morphologies of some cyanine dye J-aggregates have been studied.[5-7] The morphological characterization was carried out with atomic force microscopy (AFM) by depositing the dye aggregates onto an atomically flat mica surface. These aggregates usually appear as long fibers or nanodisks. It was concluded that these nanostructures were formed in solution and the substrate did not contribute to the aggregate formation.[7, 8]

Cyanine dyes have been studied also as sensitizers in dye-sensitized solar cells and blue-shifted H aggregates are formed upon adsorbing onto a nanocrystalline surface.[9, 10] Chelating cyanine dyes that have two carboxylate groups were synthesized and H-aggregated dimer was formed upon adsorption onto nanocrystalline titanium dioxide (TiO_2).[11, 12] The photoelectrochemical properties of these adsorbed

dye molecules have been investigated extensively but the morphologies of these aggregates remain unknown.

TiO_2 has been of interest for both its photocatalytic properties and its function in solar energy conversion. There have been some theoretical studies[13, 14] of the adsorption of molecules and ordered structures of retinoate on the rutile TiO_2 (110) surface were revealed by scanning tunneling microscopy experiments[15].

In this study, we characterize the aggregate formation of a carboxylate-functionalized cyanine dye on atomically flat single crystal anatase TiO_2 (101) surfaces. Anatase (101) is the predominant face in nanocrystaline TiO_2 dye-sensitized solar cells.[16] Self-assembly of dye molecules on TiO_2 surfaces is of particular importance since the long-term stability of dye sensitized solar cell is affected directly by the binding strength between the surface and the dye molecules. The microscopic understanding of the dye cell interface may help us better understand the charge transfer mechanism of a dye-sensitized solar cell and eventually improve its performance.

6.2 Experimental Section

The anatase sample was a natural anatase crystal that was mined in Hargvidda, Tyssedal in Norway. The bi-pyramidal crystal exhibited low-energy growth surfaces with the large wedge shaped (101) faces and the (001) end caps. The (101) crystal faces were dark blue metallic and shiny and were cut along the (101) plane using a diamond saw. The crystal was polished and annealed to obtain atomically flat surfaces as described earlier.[17] Atomic force microscopy (AFM) (Digital Instruments Nanoscope IIIA controller and a multimode SPM) was used to characterize the polished surface.

Hi'Res® AFM tips from MikroMasch with a 3.5 N/m force constant and resonant frequency around 75 KHz were used. The anatase (101) crystal was mounted as an electrode and the photocurrent spectrum was recorded in the same way as described before.[18]

2, 2'-(diethylcarboxy)-9-ethyl-thiacarbocyanine bromide (G7) was obtained from Dr. Mark. T Spitler and was used without further purification. For photoelectrochemical and AFM study, the crystal was cleaned by illumination with Ultraviolet (UV) light for 5 minutes under 0.6 V applied bias in 1 M HCl electrolyte. Dyes were then adsorbed by dipping in a 30 μM G7 solution in ethanol. The crystal was then rinsed with ethanol to remove any physically adsorbed dye molecules before collecting photocurrent action spectrum in an acetonitrile electrolyte with 10 mM tetrabutylammonium perchlorare as a supporting electrolyte and 4.5 mM hydroquinone as the regenerator in a standard three electrode electrochemical cell. Before AFM study the crystal surface was dried with N_2. For liquid cell AFM studies, a 0.1 μM G7 solution in ethylene glycol was used. Scanning Probe Image Processor (SPIP) software was used for the height and size analysis of the AFM images.

6.3 Results

After polishing and annealing, a clean terraced surface of anatase (101) crystal was obtained, as is shown in Figure 6.1. The line profile indicates an average terrace height of about 0.36 nm, corresponding very well with the calculated value (0.35 nm) of a single unit-cell step height of anatase (101) surface. The terrace width varies over the different scanned areas, which is typical for a natural single crystal surface.

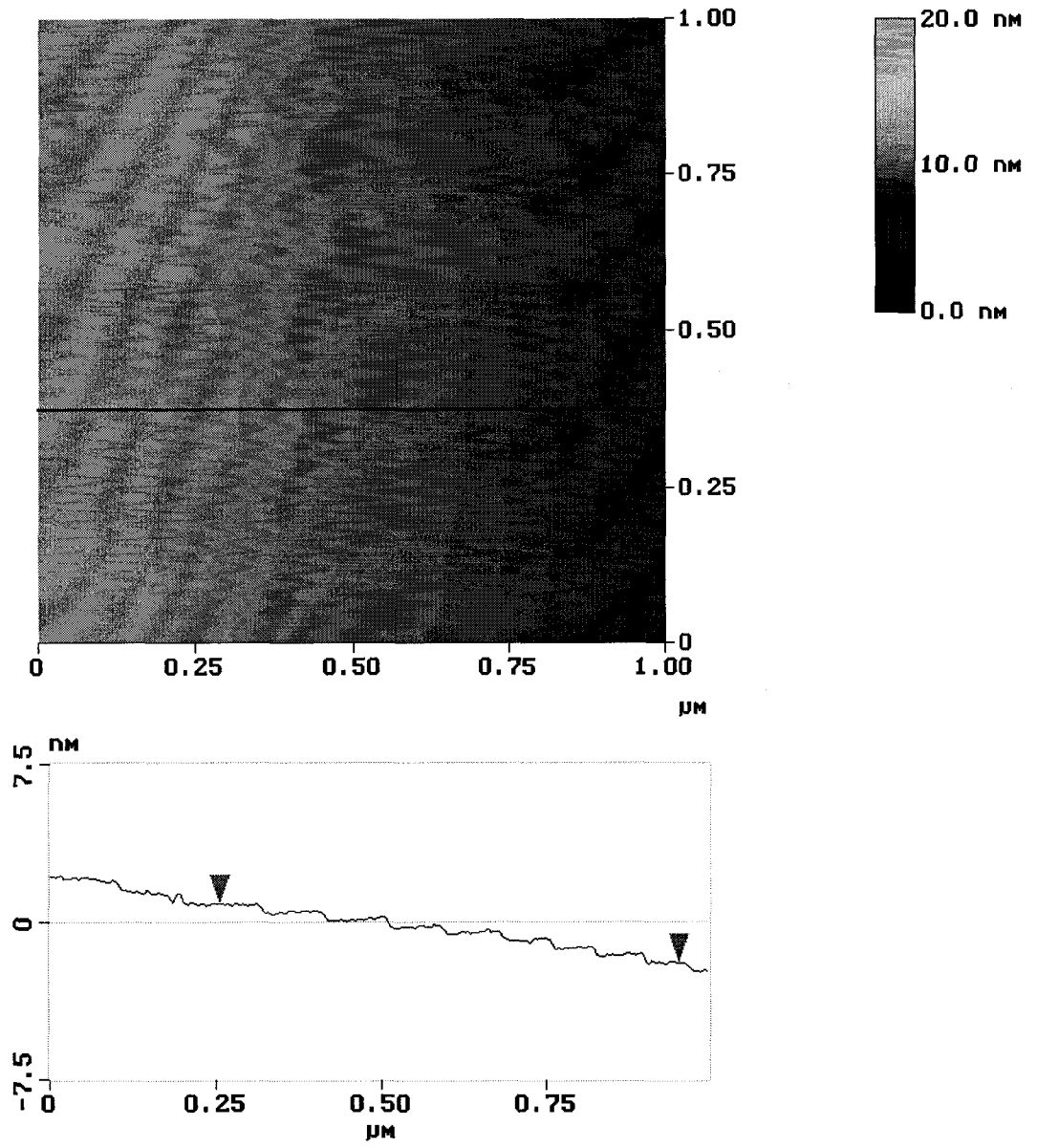

Figure 6.1. AFM image of anatase(101) surface showing the atomically flat terraces. The line profile corresponds to the line in the height image.

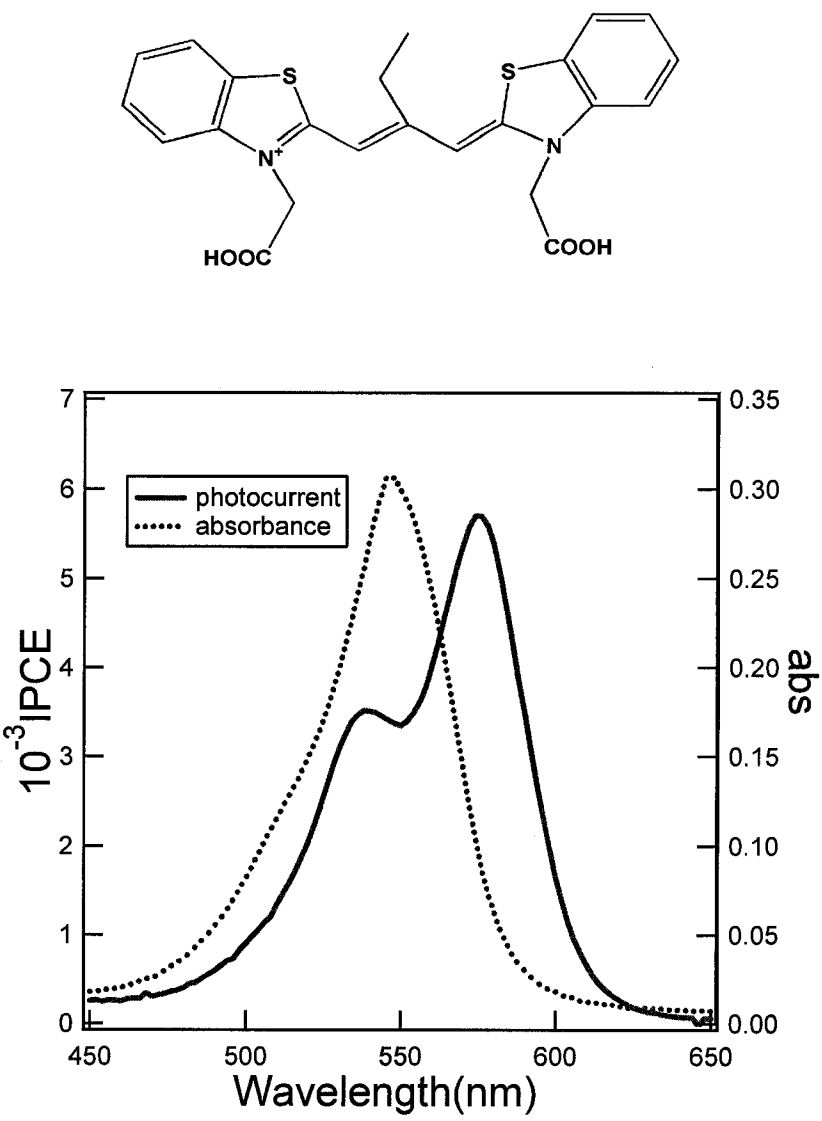

Figure 6.2. Top: Molecular structure of G7 dye. Bottom: Photocurrent spectrum of G7 dye with anatase(101) surface (red curve). The green curve shows the solution absorbance spectrum of G7 in ethanol.

After an UV cleaning of 5 minutes, the anatase (101) electrode was dipped into a 30 μM G7 solution for 10 minutes before photoelectrochemical studies. Figure 6.2 shows the molecular structure of G7 dye (the bromide counter anion is not shown) together with its photocurrent action spectrum adsorbed onto anatase (101) surface and solution absorption spectrum. The absorption spectrum shows a monomer peak around 546 nm, while the photocurrent spectrum shows both a red-shifted monomer peak around 576 nm and an H-aggregated dimer peak around 538 nm.[11, 19]

After G7 dye adsorption, the topography of the anatase (101) surface was studied with AFM. Small domains of dye molecules were found all over the surface, as seen in Figure 6.3. The line profile indicates the height variance on selected domains. The terraces can also be seen underneath the adsorbed dye molecules.

The height of the G7 dye domains was analyzed with SPIP software. The histogram is shown in Figure 6.4(a). The histogram shows a single Gaussian distribution centered at ~ 0.6 nm, corresponding to the height of a single layer of G7 molecules. Figure 6.4(b) shows the histogram of the sizes of the dye domains, which also fits a single Gaussian distribution centered around 30 nm. The effect of the tip on the domain sizes should be minimal since the radius of the Hi'Res® tips is about 1 nm, which is very small comparing to the domain size.

The polydispersity index (PI) is calculated (to better demonstrate the distributions of height and lateral size of the domains) according to the following equations:[7]

$$W(d) = \frac{\sum_i n_i d_i^2}{\sum_i n_i d_i}$$

$$N(d) = \frac{\sum_i n_i d_i}{\sum_i n_i}$$

where n_i is the number of domains of dyes and d_i is the dimension of height or lateral size of the domain i, W(d) is the weighted average and N(d) is the number average of height or lateral size. PI is calculated as W(d)/N(d). The PI values were calculated to be 1.14 and 1.15 for height and lateral size, respectively, which confirmed that both the height and lateral size displayed a narrow distribution.

To study the real time adsorption of G7 dyes onto anatase(101) surface, liquid cell AFM was carried out with a G7 concentration of 0.1 μM using ethylene glycol as a solvent. A control experiment with pure ethylene glycol revealed only clean terraces. After the injection of the dye solution, terraces with adsorbed G7 dye islands were clearly seen, as shown in Figure 6.5.

Figure 6.6 shows the histograms of height and size distributions of the adsorbed aggregates from Figure 6.5. Both of them demonstrate a simple Gaussian shape with the height centered at ~ 0.5 nm and the size at about 30 nm. PI analysis yielded a result of 1.08 and 1.15 for height and lateral size, respectively.

6.4 Discussion

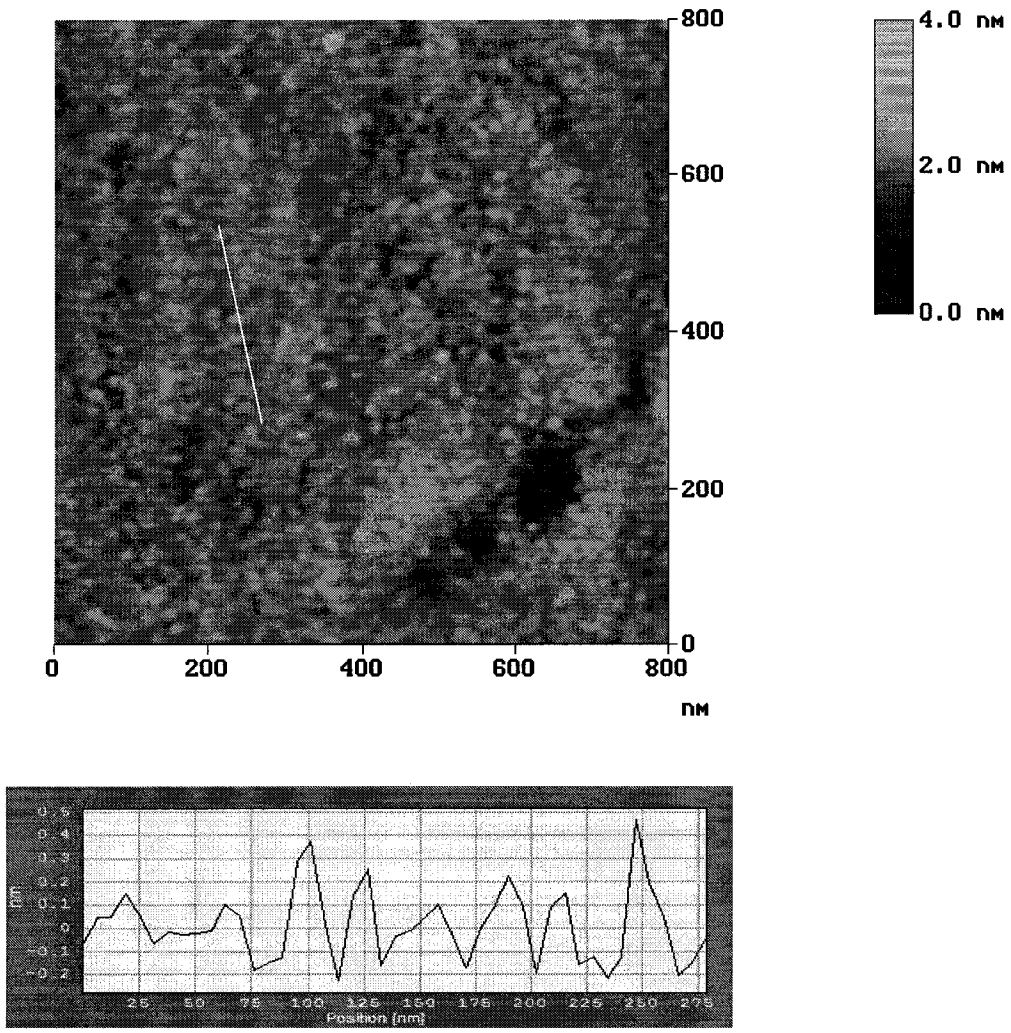

Figure 6.3. AFM image revealing anatase(101) surface with adsorbed G7 dye. The line in the height image corresponds to the line profile.

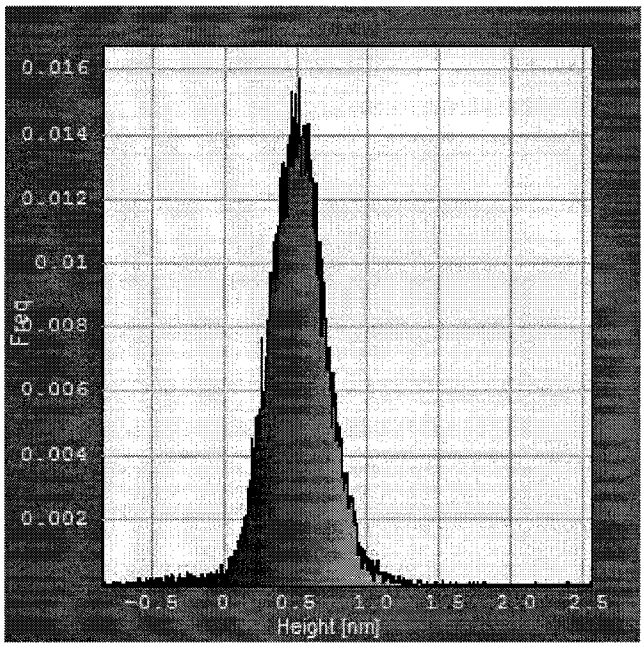

(a)

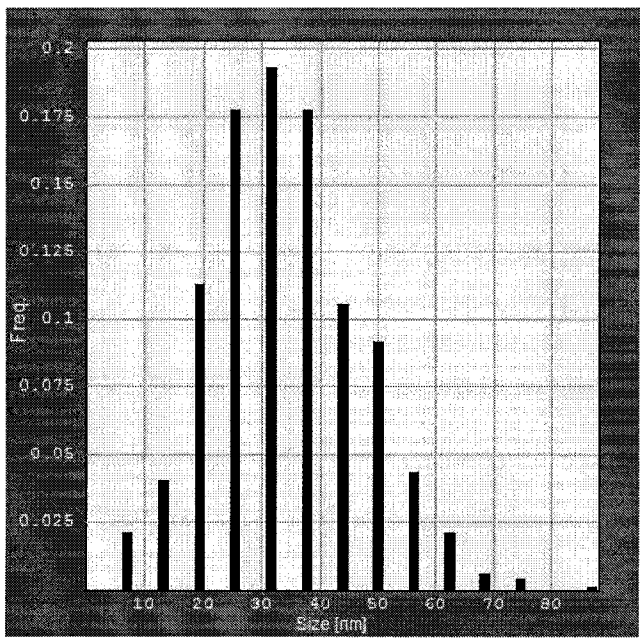

(b)

Figure 6.4. Height and size analysis of the AFM image from Figure 6.3.

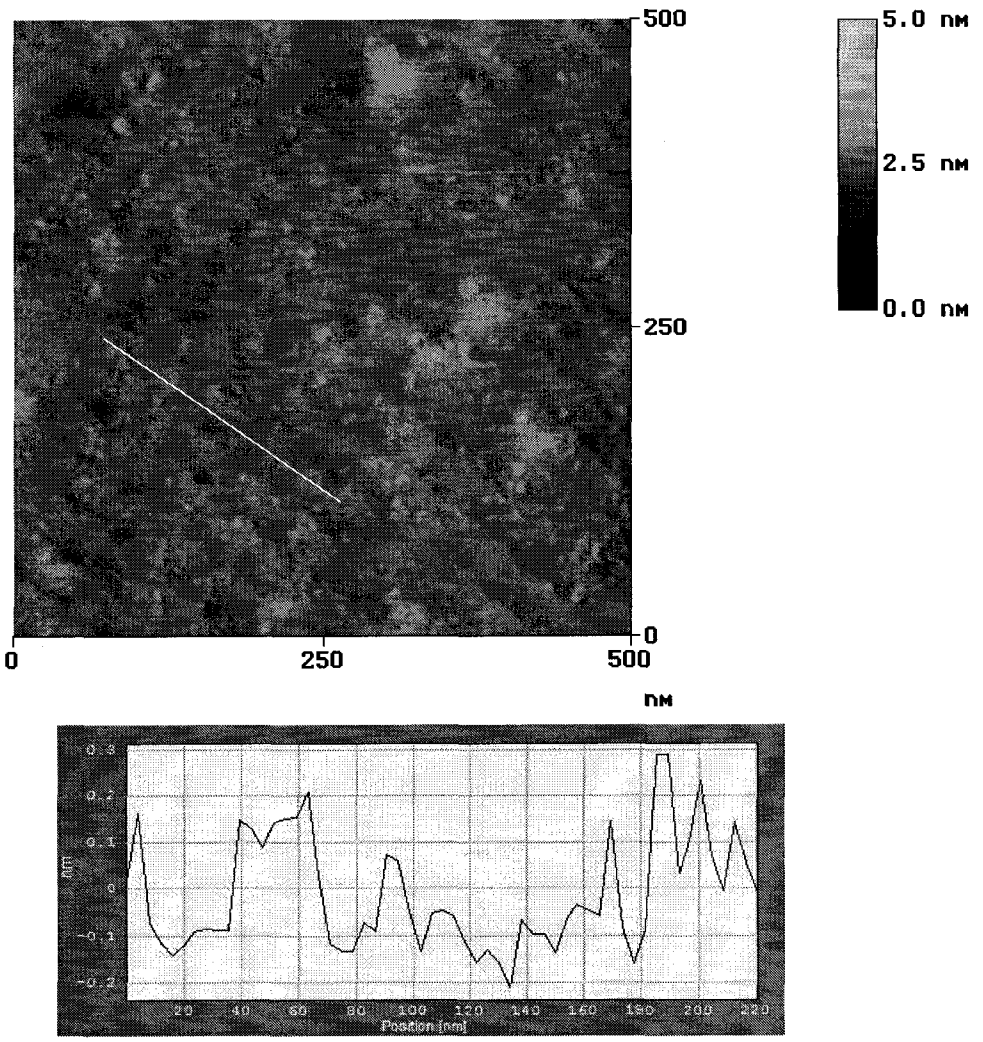

Figure 6.5. Liquid cell AFM image indicating adsorbed G7 dye from ethylene glycol solution.

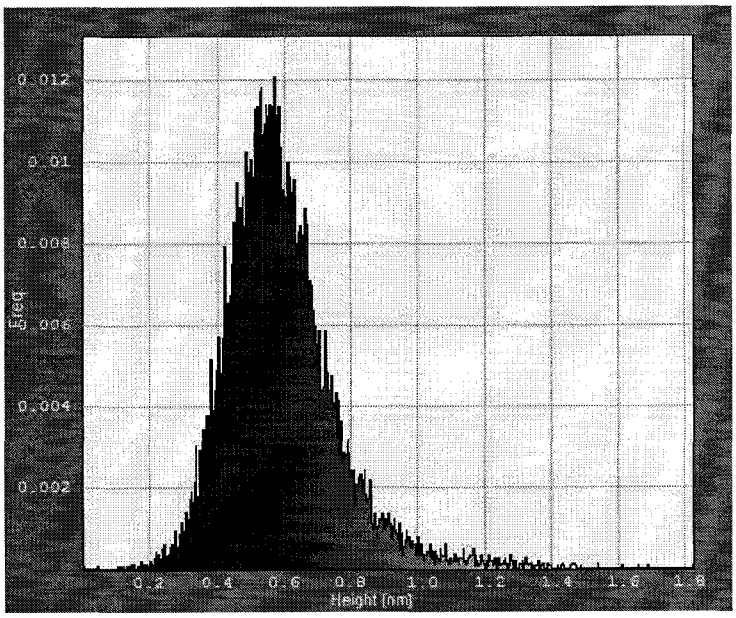

(a)

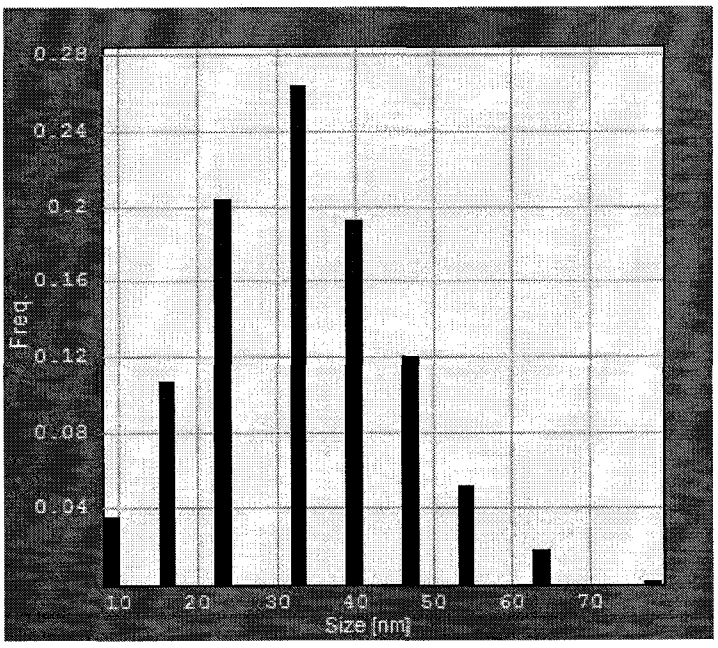

(b)

Figure 6.6. Height and size analysis of the AFM image from Figure 6.5.

Carboxylated cyanine dyes bind to TiO_2 surface through the oxygen-titanium bond.[11, 12] High resolution XPS and near-edge X-ray absorption spectroscopy indicated that both oxygen atoms of the same carboxylated group bind to the same Ti(5) sites.[20] For the G7 dye used here, it is believed that these dyes form dimers upon adsorption onto a TiO_2 surface and the ethyl group in the middle of the polyene chain prevents formation of extended aggregates.[11, 12, 18] The G7 dye on anatase(101) surface exhibited an average height of 0.5-0.6 nm, corresponding to the height of a single dye molecule. Based on a previously proposed model[18], taking the surface area occupied by one G7 molecule to be 0.9 nm^2, an average G7 domain (30 nm diameter as indicated by air AFM) contained about 1000 single G7 molecules or 500 dimers.

The size of the domains from the in situ AFM studies at a lower dye concentration corresponds to about the same number of molecules per domain. Currently we are unable to achieve high resolution sub-100 nm size image, but efforts are underway to achieve this.

The adsorption and stability of dye molecules onto TiO_2 surfaces are crucial to good performances of a dye-sensitized solar cell. The adsorbed dye domains observed here might be just physically clustered dye molecules since no significant aggregate peak was seen from its photocurrent action spectrum. Studies have shown that electron injection yield from aggregared dyes is lower than dye monomers due to intermolecular energy transfer.[10, 21] Spacers and surfactant molecules are incorporated as additives upon dye adsorption onto TiO_2 surfaces to minimize aggregation.[10] Therefore to fabricate a more efficient dye cell, dimerization or aggregation of the dye molecules upon adsorption need to be prevented.

6.5 Conclusion

We have successfully studied adsorbed carboxylated cyanine dye G7 on an atomically flat single crystal anatase (101) surface with both air AFM and liquid cell AFM. Narrowly distributed G7 aggregate domains that contain over 1000 dye molecules were revealed from the imaging. Further study may shed light on the dye/TiO_2 interfacial surface structure on an atomic level and such study is underway.

Acknowledgement

This work was supported by the Department of Energy Office of Basic Energy Sciences under contract #DE-F603-96ER14625.

References:

1. Jelley, E.E., *Spectral absorption and fluorescence of dyes in the molecular state.* Nature, 1936. **138**: p. 1009-1010.

2. Scheibe, G. and Rivas, A., *A new method in quantitive emission spectral analysis adaptable also as a micro method.* Angewandte Chemie, 1936. **49**: p. 0443-0446.

3. Scheibe, G., *Auxiliary valency as the cause of variability in the absorption spectra in solutions.* Angewandte Chemie, 1937. **50**: p. 0212-0219.

4. Wang, M.S., G. L. Armitage, B. A, J. Am. Chem. Soc., 2000. **122**: p. 9977.

5. Ono, S.S., Yao, H., Matsuoka, O., Kawabata, R., Kitamura, N., and Yamamoto, S., *Anisotropic growth of J aggregates of pseudoisocyanine dye at a mica/solution interface revealed by AFM and polarization absorption measurements.* Journal of Physical Chemistry B, 1999. **103**(33): p. 6909-6912.

6. Kuroda, S., Ito, H., Uchiyama, Y., Mori, T., Marumoto, K., and Hatta, I., *J-aggregate formation of 6-methyl-merocyanine dye in mixed Langmuir-Blodgett films with arachidic acid in a wide range of mixing ratio.* Japanese Journal of Applied Physics Part 1-Regular Papers Short Notes & Review Papers, 2002. **41**(10): p. 6223-6227.

7. Ozcelik, S., Demir, M.M., and Birkan, B., *Probing nanoscale domains of J-aggregates deposited on a mica surface.* Journal of Physical Chemistry B, 2004. **108**(15): p. 4679-4683.

8. Schwab, A.D., Smith, D.E., Rich, C.S., Young, E.R., Smith, W.F., and de Paula, J.C., *Porphyrin nanorods.* Journal of Physical Chemistry B, 2003. **107**(41): p. 11339-11345.

9. Nuesch, F., Moser, J.E., Shklover, V., and Gratzel, M., *Merocyanine aggregation in mesoporous networks.* Journal of the American Chemical Society, 1996. **118**(23): p. 5420-5431.

10. Khazraji, A.C., Hotchandani, S., Das, S., and Kamat, P.V., *Controlling dye (Merocyanine-540) aggregation on nanostructured TiO_2 films. An organized assembly approach for enhancing the efficiency of photosensitization.* Journal of Physical Chemistry B, 1999. **103**(22): p. 4693-4700.

11. Ehret, A., Stuhl, L., and Spitler, M.T., *Variation of carboxylate-functionalized cyanine dyes to produce efficient spectral sensitization of nanocrystalline solar cells.* Electrochimica Acta, 2000. **45**(28): p. 4553-4557.

12. Ehret, A., Stuhl, L., and Spitler, M.T., *Spectral sensitization of TiO_2 nanocrystalline electrodes with aggregated cyanine dyes.* Journal of Physical Chemistry B, 2001. **105**(41): p. 9960-9965.

13. Fahmi, A., Minot, C., Fourre, P., and Nortier, P., *A theoretical study of the adsorption of oxalic acid on TiO_2.* Surface Science, 1995. **343**(3): p. 261-272.

14. Kackell, P. and Terakura, K., *Dissociative adsorption of formic acid and diffusion of formats on the TiO_2(110) surface: the role of hydrogen.* Surface Science, 2000. **461**(1-3): p. 191-198.

15. Ishibashi, T.A., Uetsuka, H., and Onishi, H., *An ordered retinoate monolayer prepared on rutile TiO_2(110).* Journal of Physical Chemistry B, 2004. **108**(44): p. 17166-17170.

16. Shklover, V., Ovchinnikov, Y.E., Braginsky, L.S., Zakeeruddin, S.M., and Gratzel, M., *Structure of organic/inorganic interface in assembled materials comprising molecular components. Crystal structure of the sensitizer bis (4,4 '-carboxy-2,2 '-bipyridine)(thiocyanato) ruthenium(II).* Chemistry of Materials, 1998. **10**(9): p. 2533-2541.

17. Lu, Y., Jaeckel, B., and Parkinson, B.A., *Preparation and Characterization of Terraced Surfaces of Low-Index Faces of Anatase, Rutile, and Brookite.* Langmuir, 2006. **22**(10): p. 4472-4475.

18. Ushiroda, S., Ruzycki, N., Lu, Y., Spitler, M.T., and Parkinson, B.A., J. Am. Chem. Soc., 2005. **127**: p. 5158.

19. West, W. and Pierce, S., *DIMERIC STATE OF CYANINE DYES.* J. Phys. Chem. B, 1965. **69**: p. 1894.

20. Patthey, L., Rensmo, H., Persson, P., Westermark, K., Vayssieres, L., Stashans, A., Petersson, A., Bruhwiler, P.A., Siegbahn, H., Lunell, S., and Martensson, N., *Adsorption of bi-isonicotinic acid on rutile TiO_2(110).* Journal of Chemical Physics, 1999. **110**(12): p. 5913-5918.

21. Hara, K., Dan-Oh, Y., Kasada, C., Ohga, Y., Shinpo, A., Suga, S., Sayama, K., and Arakawa, H., *Effect of additives on the photovoltaic performance of coumarin-dye-sensitized nanocrystalline TiO_2 solar cells.* Langmuir, 2004. **20**(10): p. 4205-4210.

Chapter 7: Concluding Remarks and Future Work

In order to study the basic interface in dye-sensitized solar cells, low-index, atomically flat TiO_2 single crystal surfaces have been prepared using a simple polishing/annealing procedure[1]. The prepared surfaces have been characterized photoelectrochemically, microscopically and with low energy electron diffraction. Dye-sensitization of the oxide surfaces by both the N3 dye and a series of structurally related carboxylated thiacyanine dyes on these surfaces was reported.[2-4] The adsorption and desorption behavior of these dyes was studied extensively. Photocurrent action spectra at various dye concentrations for all the surfaces were obtained for all the dyes studied. Among the different low-index TiO_2 single crystal surfaces, rutile (100) was found to give the highest incident photon-to-current conversion efficiency (IPCE) for the N3 dye. This was attributed to a better match between the rutile (100) surface lattice structure and the possible N3 dye carboxylate-carboxylate group binding distances.

For dye-sensitized solar cells usually the absorbed photon-to-current conversion efficiency (APCE) is more important than IPCE since the APCE value determines the cell energy conversion efficiency and thus the total output power. By constructing an attenuated total reflectance (ATR) cell from single crystal TiO_2 (schematic shown in Figure 7.1), we will be able to simultaneously measure the light absorbance by the dye molecules

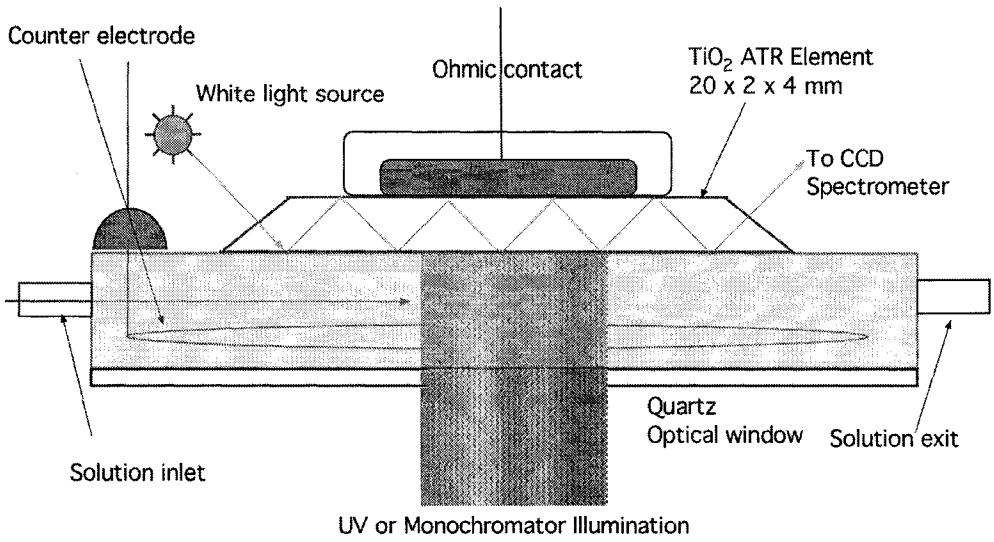

Figure 7.1 A schematic of the ATR cell built from single crystal TiO_2. A dye solution can be injected from the solution inlet and released from the solution exit. After dye adsorption onto the bottom side of the crystal, its absorbance can be measured by illumination with a white light source and the sum of 5 absorptions will be recorded with a CCD spectrometer. The IPCE will be obtained from electrochemical study by simultaneous monochromatic light illumination from the bottom. When the experiment is finished, the dyes can be cleaned off from the crystal surface through UV illumination from the bottom side.

adsorbed onto TiO_2 surfaces and their IPCE values. Therefore APCE values can be measured directly. This ATR experiment will also be able to measure the APCE difference, if any, between different types of surface adsorbed dyes such as monomers, dimers and higher aggregates. Preliminary results indicate that monomers and dimers have different APCE values when attached to the TiO_2 surface.

A simple photochronocoulometric method was developed to measure the surface coverage of dyes covalently attached to the TiO_2 substrates. The transient photocurrent can be fit with a double exponential decay function where the integration of the fast decay component corresponds to the surface coverage, given that each dye molecule is oxidized by one electron. The origin of the second slow decay component is complicated and was discussed in Chapter 4. Further experiments to elucidate the nature of this slow process are necessary.

The desorption of the G15 dye adsorbed onto a rutile (100) surface could be studied by monitoring the decay of the sensitized photocurrent at both the monomer absorption maximum (574 nm) and dimer absorption maximum (530 nm). Different desorption behavior for monomer and dimer is observed. A desorption mechanism is proposed where the reorganization of monomers into dimers is taken into account (Chapter five). Our mechanism is supported by the good match between the experimental results and the fit with the proposed mechanism. This result suggests that similar desorption studies for other cyanine dyes adsorbed onto different surfaces is worth studying, since we already know that the ability to form dimers varies dye to dye and surface to surface. Other results (Shin Ushiroda) have

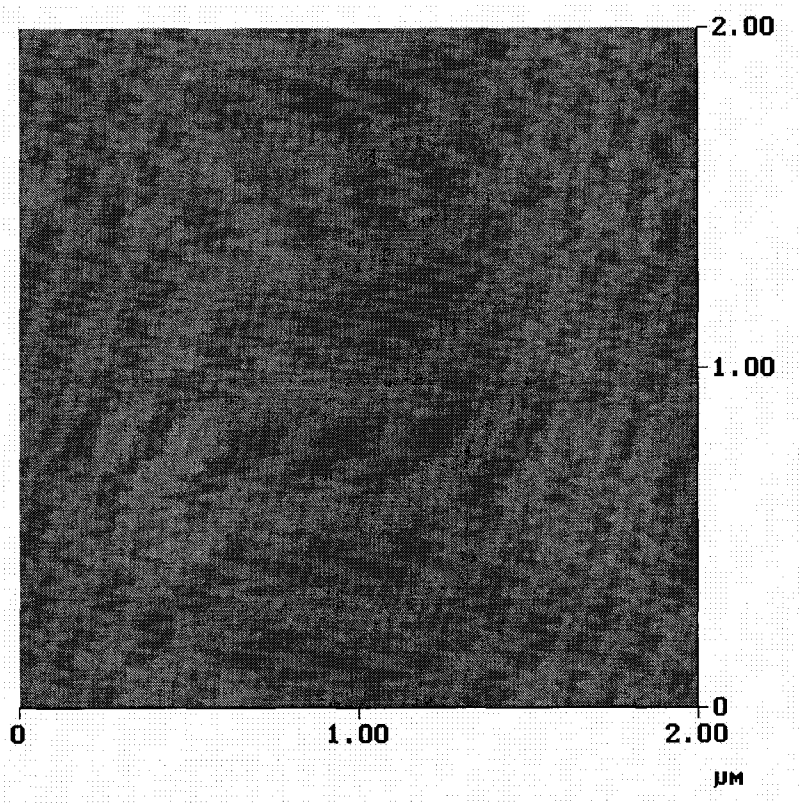

Figure 7.2 AFM image of as prepared sapphire single crystal surface showing the atomically flat terraces.

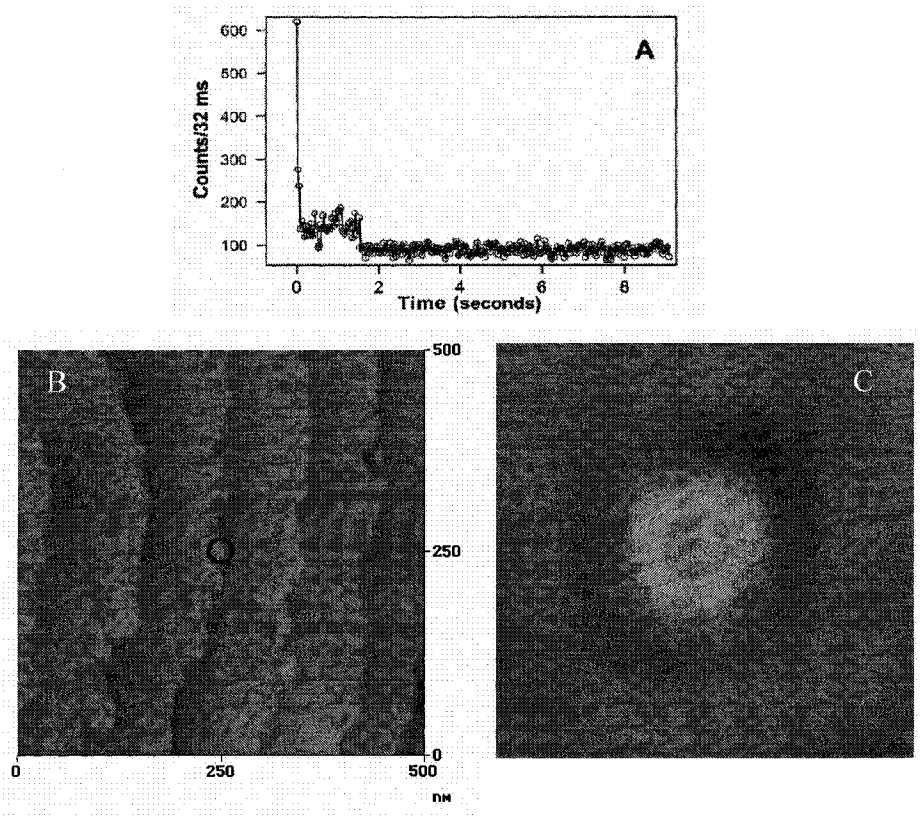

Figure 7.3 Projected results from the single molecule study. B and C are the simultaneously obtained AFM and fluorescence images, respectively. A shows the fluorescence signal as a function of time indicating the characteristics of a single dye molecule.

shown how to prepare surfaces with exclusively aggregated dyes by adding water to the electrolyte.

We have been attempting to resolve single dye molecules adsorbed onto atomically flat, well-terraced single crystal TiO_2 surfaces with atomic force microscopy (AFM). We hope to discover whether terrace, step, kink or defect sites are the preferred surface binding sites for the carboxylated dyes. This ultimate goal has not been obtained but domains of dye aggregates or islands have been observed, as reported in Chapter 6. The AFM images indicate that the dye molecules prefer to form islands of a defined size upon adsorption onto anatase (101) surfaces. More efforts are needed to resolve the interfacial structure of dye/semiconductor substrate with AFM either in a liquid media or under vacuum conditions.

It is important to understand whether there are preferred binding sites for dyes at low coverage or if there are adsorbed dye molecules that do not inject electrons from their excited states into the TiO_2. We are collaborating with the van Orden group on a study where potentially single surface adsorbed carboxylated thiocyanine dye molecule can be resolved. A very thin atomically flat, well terraced single crystal semiconductor surface will be prepared and dye molecules can be adsorbed from a dilute solution. With the use of the van Orden group's spatially correlated fluorescence/AFM, we will be able to collect fluorescence signal emitted by the adsorbed dye molecule simultaneously with the topographical AFM image. The ultimate goal is to probe single dye molecules adsorbed onto a TiO_2 single crystal surface. As a control system, we will use a well prepared, atomically flat sapphire single crystal substrate since due to its large band gap (8.1 eV), it is unlikely to quench the fluorescence emission due to electron injection. I

have obtained the atomically flat surface of sapphire single crystal using the same sample preparation method as reported in Chapter 2 and the AFM image is shown in Figure 7.2. The as-prepared surface reveals uniform terraces with an average terrace width of 40-50 nm. Figure 7.3 shows the projected experimental results. We expect to detect the fluorescence signal from single dye molecules adsorbed from a very dilute dye solution. An AFM image simultaneously obtained can spatially locate the site of the dye fluorescence. By comparing the two images the preferred binding sites of the dye molecules on the oxide surface can be inferred. The fluorescence as a function of time can also be obtained for the surface bound dye, as shown in Figure 7.3a and the bleaching rate can be determined. From this study we are hoping to find out the dye adsorption preference on the semiconductor surface, such as flat terraces, terrace edges or defect sites, as well as its fluorescence characteristics after adsorption onto the surface. On anatase or rutile it is expected that most dye molecules will have their fluorescence quenched by electron transfer. Detecting any dye fluorescence therefore would locate dye binding sites where photoexcited electron transfer is not efficient.

We believe if all the experiments mentioned here are all successfully conducted (and indeed we already have preliminary data), a much better understanding of the performance of dye-sensitized solar cells will be achieved, such as the dye/semiconductor interfacial structure, adsorption/desorption behavior of the dye molecules onto a TiO_2 surface and APCE differences in monomer/dimer/extended aggregates. All of these studies could also be extended to other semiconducting oxides such as ZnO and $SrTiO_3$, which are also studied as substrates for dye-sensitized solar cells.[5-7] Hopefully we will

be able to understand the dye/semiconductor interface sufficiently well in order to guide the fabrication of more efficient dye-sensitized solar cells.

Reference:

1. Lu, Y., Jaeckel, B., and Parkinson, B.A., *Preparation and Characterization of Terraced Surfaces of Low-Index Faces of Anatase, Rutile, and Brookite.* Langmuir, 2006. **22**(10): p. 4472-4475.
2. Fillinger, A., Soltz, D., and Parkinson, B.A., *Dye sensitization of natural anatase crystals with a ruthenium-based dye.* Journal of the Electrochemical Society, 2002. **149**(9): p. A1146-A1156.
3. Ushiroda, S., Ruzycki, N., Lu, Y., Spitler, M.T., and Parkinson, B.A., *Dye sensitization of the anatase (101) crystal surface by a series of dicarboxylated thiacyanine dyes.* Journal of the American Chemical Society, 2005. **127**(14): p. 5158-5168.
4. Lu, Y., Choi, D., Nelson, J., Yang, O., and Parkinson, B.A., *Adsorption, Desorption and Sensitization of low Index Anatase and Rutile Surfaces by the Ruthenium Complex Dye N3.* Journal of the Electrochemical Society, 2006. **153**(8): p. E131-E137.
5. Matsumura, M., Matsudaira, S., Tsubomura, H., Takata, M., and Yanagida, H., *Dye Sensitization and Surface-Structures of Semiconductor Electrodes.* Industrial & Engineering Chemistry Product Research and Development, 1980. **19**(3): p. 415-421.
6. Keis, K., Bauer, C., Boschloo, G., Hagfeldt, A., Westerark, K., Rensmo, H., and Siegbahn, H., *Nanostructured ZnO electrodes for dye-sensitized solar cell applications.* Journal of Photochemistry and Photobiology A: Chemistry, 2002. **148**: p. 57.
7. Sonntag, L.P. and Spitler, M.T., *Examination of the Energetic Threshold for Dye-Sensitized Photocurrent at $SrTiO_3$ Electrodes.* Journal of Physical Chemistry, 1985. **89**(8): p. 1453-1457.